Multisensory integration in spatial orientation

Maaike de Vrijer

ISBN 978-90-9024878-3
Cover photo: Auro, Jardin des Tuileries, Paris.

The research presented in this thesis was carried out at the Donders Institute for Brain, Cognition and Behaviour, Centre for Neuroscience of the Radboud University Nijmegen, the Netherlands.

Printed by Ipskamp Drukkers, Enschede, The Netherlands

Multisensory integration in spatial orientation

Een wetenschappelijke proeve op het gebied van de Sociale Wetenschappen

Proefschrift

ter verkrijging van de graad van doctor
aan de Radboud Universiteit Nijmegen
op gezag van de rector magnificus prof. mr. S.C.J.J. Kortmann
volgens besluit van het college van decanen
in het openbaar te verdedigen op woensdag 13 januari 2010
om 10.30 uur precies

door

Maaike de Vrijer

geboren op 18 juli 1979
te Wageningen

Promotores:	Prof. dr. C.C.A.M. Gielen
	Prof. dr. H. Bekkering
Copromotores:	Dr. J.A.M. Van Gisbergen
	Dr. W.P. Medendorp
Manuscriptcommissie:	Prof. dr. R.G.J. Meulenbroek (voorzitter)
	Prof. dr. J.B.J. Smeets (Vrije Universiteit Amsterdam)
	Prof. dr. H. Kingma (Academisch Ziekenhuis Maastricht)

Contents

Chapter 1

General introduction

All our movements, like walking, grasping an object, or throwing a ball, are affected by gravity and therefore require an awareness of gravitational direction at all times. How does our central nervous system achieve this awareness? The ability to know one's body orientation in space and being aware of the orientation of surrounding objects, usually referred to as spatial orientation, is the central theme of this thesis. This chapter provides some background information about the sensory organs that are involved in spatial orientation and describes the challenges faced by our brain during the processing of multisensory information. Along the way, we will refer to several related studies and explain some of the contemporary ideas about the neurocomputational strategies that play a role in spatial orientation.

SPATIAL ORIENTATION CUES

Our sense of spatial orientation originates from a variety of sensory cues. Visual information and inputs from the vestibular system are two important contributors, but somatosensory inputs, such as pressure sensors in the foot soles, muscle receptors, and receptors that sense the distribution of blood in the body may also provide useful information. In general, each sensory input has its own specific properties and limitations, as will be described in the following sections.

Vision

The importance of visual cues for spatial orientation becomes clear in situations when visual information is degraded, deceiving, or even missing. For example, in the dark or inside the cabin of a boat in stormy conditions, our sense of upright may become less secure or even fail. In the ship's cabin, visual cues that are normally very useful, like the ceiling, floor, and walls, deceive us because they are not anymore aligned to the Earth-vertical or horizontal.

In general, visual signals that support human spatial orientation can be divided into two groups: optostatic and optokinetic cues. Optostatic information comes from features that are known to be approximately vertical and horizontal, such as buildings, trees, the horizon, floors and ceilings. For example, if the image of a house on the retina is slightly tilted, this is most likely caused by a slight tilt of your own head, rather than that the house itself is tilted. The influence of optostatic cues on spatial orientation has been convincingly demonstrated by Asch and Witkin (1948), who showed that human observers, viewing a truly vertical rod within a roll-tilted square frame in otherwise total darkness, perceived the rod as being tilted in the opposite direction (see Figure 1.1A). This perceptual phenomenon, known as the rod-and-frame effect, shows that even very impoverished visual scenes, such as a simple visual frame, can have a distinct effect on the perceived direction of gravity.

Optokinetic cues are mainly important for the detection of low-frequency body translations and rotations, and arise as a result of our movements through space. Due to these movements, such as walking, cycling or riding a car, the visual scene moves on the retina, resulting in a so-called optic flow pattern, which is used by the brain for spatial orientation and navigation (Angelaki and Hess, 2005). The influence of such optokinetic cues is exploited in flight simulators, which make use of the fact that the brain interprets sustained large-field

optic flow as due to self-motion, a strategy that is very useful in most everyday situations. In these simulators, the optic flow field is generated artificially to evoke a strong sensation of self-motion while the participant actually remains completely still. Optokinetic cues may also encode rotational movements, as illustrated in Figure 1.1B. When facing a large roll-rotating pattern of random dots, human observers typically experience a slowly developing sensation of self-tilt in the direction opposite of the visual flow (Dichgans et al., 1972). Interestingly, patients with reduced vestibular function have been shown to be more susceptible to this so-called roll-optokinetic effect (Bronstein et al., 1996), which suggests that they rely more on visual orientation cues than healthy people.

Vestibular cues

Even though spatial orientation becomes more challenging when visual information is absent, it does not lead to a complete loss of spatial awareness. Other important spatial information is provided by the vestibular system, our 'sixth sense'. This sensory system, better known as the organ of balance, is located in our inner ear. Usually, people are not aware of its existence, but our vestibular system contributes to many important functions, not only spatial orientation, but also reflexive eye movements that support visual stabilization. Only when problems arise, such as vertigo, does the importance of the vestibular system become fully revealed.

Evolution

The significance of the vestibular system can be recognized from its early appearance in evolution. More than 600 million years ago, some aquatic animals developed a very primitive gravity-sensing organ, which enabled them to orient themselves with respect to gravity. This organ, a predecessor of the otoliths (see below), was no more than a fluid-filled cyst containing several calcareous particles with a higher density than the surrounding fluid. Attracted by gravity, the particles were distributed across the wall of the cyst, which was covered by specialized sensory cells that provided the animal with information about its spatial orientation. Later,

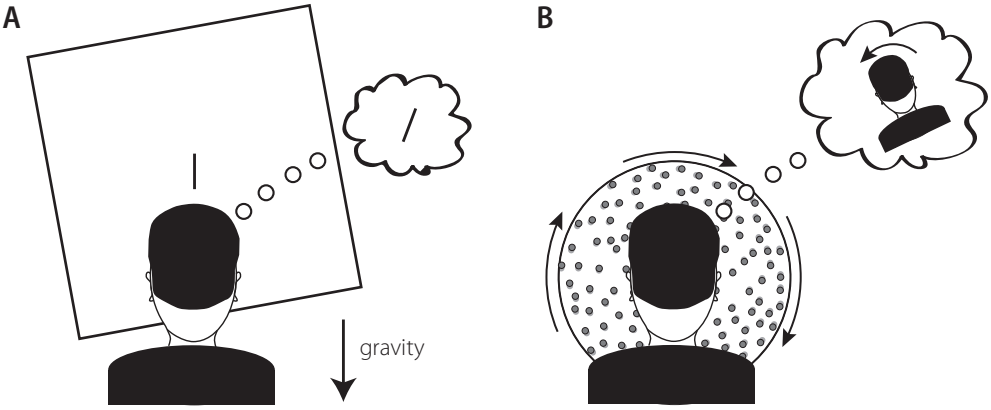

Figure 1.1 Optostatic and optokinetic influences on spatial orientation. A. Illustration of the rod-and-frame effect. An observer, viewing a large tilted frame, perceives the small earth-vertical rod as tilted in the opposite direction. B. Roll-optokinetic effect. When viewing a large rotating random dot pattern, participants typically feel tilted in the direction opposite of rotation and simultaneously experience continuous body rotation.

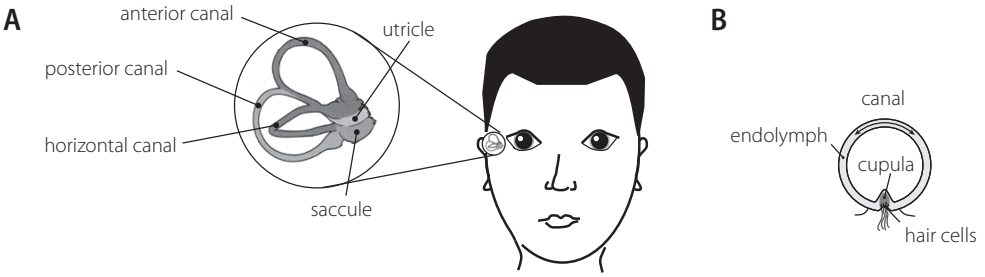

Figure 1.2 Schematic representation of the semicircular canals. A. The three canals (anterior, posterior, horizontal) form pairs with the canals at the other side of the head. B. Each canal is filled with endolymph which pushes against the cupula during rotational acceleration of the head.

this organ developed into what we now know as the vestibular labyrinth, reaching its peak of development about 100 million years ago, at the arrival of modern fish (Baloh and Honrubia, 2001). Nowadays, the vestibular system, which can be found in all higher vertebrates, consists of two parts: three roughly orthogonal semicircular canals, which sense rotations of the head (angular accelerations), and the otolith organs, utricle and saccule, which respond to linear accelerations, including gravity.

Semicircular canals

The three semicircular canals (horizontal, anterior and posterior), shown in Figure 1.2, are oriented orthogonally to each other. Each canal consists of a fluid-filled duct with a large expansion at its base, which contains hair cells that are similar those in the otoliths, as will be explained below. The hair bundles stick into a gelatinous mass, known as the cupula, which forms a partition ('swing door') in the semicircular duct. When the head is stationary, the fluid (endolymph) and the cupula remain still, and the afferent nerve fibers that innervate the hair cells discharge at rest rate. When the head starts to rotate in the plane of the canal, the fluid initially lags behind due to its inertia, and produces a force against the cupula. As a result, the hair bundles are displaced in the direction opposite to the head movement, which leads to an increase or decrease in the afferent firing rate depending on the direction of rotation. Since the canals on both sides of the head form pairs with hair cells that are oppositely polarized, a turn of the head simultaneously causes an increase of the firing rate at one side of the head, and a decrease at the other side. When the head keeps rotating at a constant

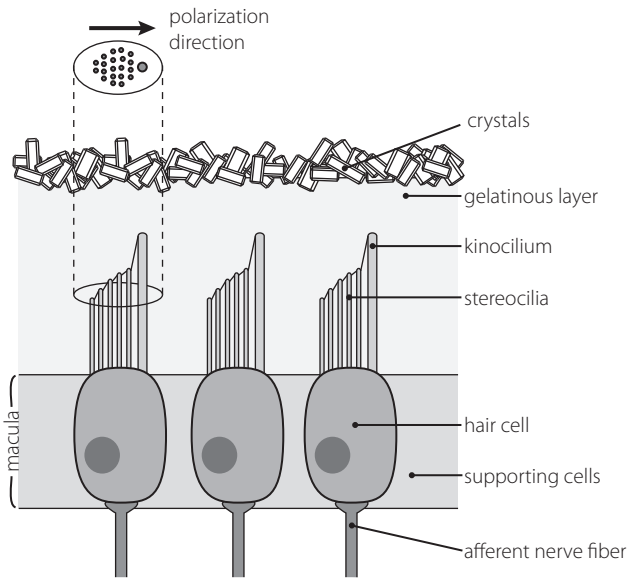

Figure 1.3 Schematic representation of otolith anatomy.

speed, the fluid will slowly catch up with the canal and the cupula will return to its initial position. This explains why the canals cannot detect constant angular velocity but are specifically sensitive to high-frequency rotations.

Otoliths

The utricle and saccule, positioned close to the canals, consist of a curved surface, the macula, in which a large number of receptor hair cells are embedded (see Figure 1.3). Each hair cell contains a bundle of 60-100 small hairs (stereocilia) and a single longer hair (kinocilium), which are all interconnected by small filaments. The hair cells are embedded in a gelatinous layer, which is covered by calcium carbonate crystals, better known as the otoliths, meaning 'ear stones' in Greek. The utricular macula is roughly oriented in the horizontal plane whereas the orientation of the saccular macula is mostly vertical, parallel to the mid-sagittal plane.

When the head is linearly accelerated or tilted with respect to gravity, the crystals are displaced due to their higher density, which results in deflection of the underlying hairs (see Figure 1.4). The response of the hair cell to these deflections depends on the direction of stimulation: When the stereocilia bend toward the kinocilium, the hair cell becomes depolarized, leading to an increased firing rate of the associated afferent nerve fiber. Conversely, when the stereocilia bend away from the kinocilium, the membrane potential is hyperpolarized, which reduces the firing rate of the afferent nerve cell. Hair cell displacement in the direction perpendicular to the optimal excitation direction does not lead to any changes in the afferent fiber. This organization leads to a sinusoidal relation between the firing rate of the otolith afferents and the tilt angle of the head (see Figure 1.4D), as Fernandez and Goldberg showed in their

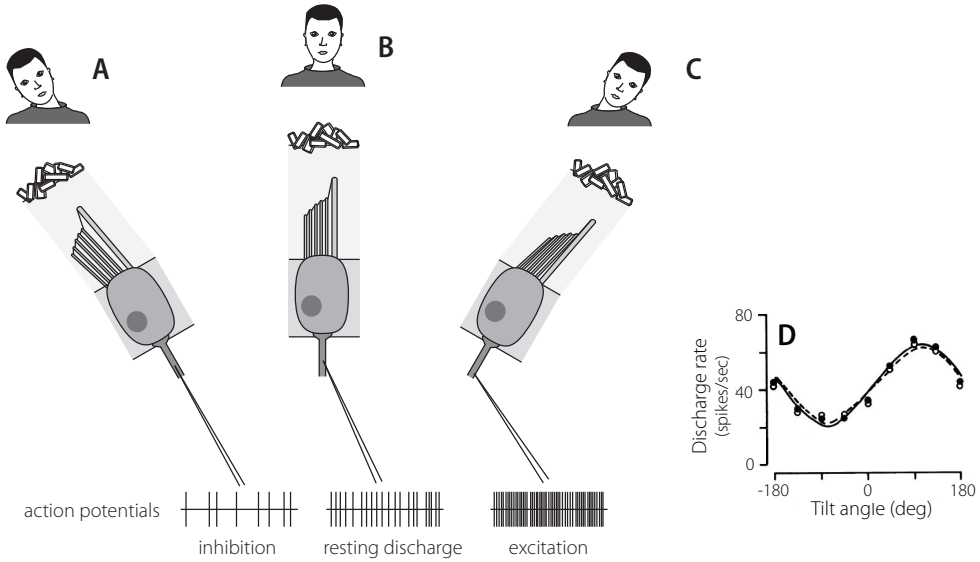

Figure 1.4 Response of hair cell to head tilt. In the upright condition (B), there is no displacement, causing no change in the resting discharge rate of the afferent nerve cell. During head tilt, hair cell cilia are bent, leading either to hyperpolarization (A) or depolarization (C), depending on the bending direction. As a result, the afferent nerve will be inhibited or excited, respectively. D: Firing rate of a utricular nerve fiber as a function of tilt angle. Adopted from Fernandez and Goldberg, 1976.

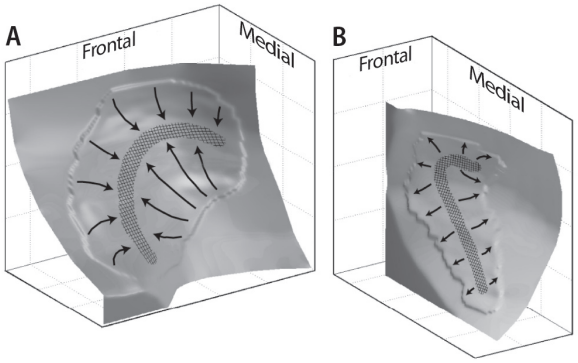

Figure 1.5 Three-dimensional curvature of utricle (A) and saccule (B). Arrows indicate local polarization direction of the hair cells. Adapted from Jaeger et al., 2002

landmark study on otolith neurons in the squirrel monkey (Fernandez and Goldberg, 1976). Importantly, the direction at which each cell is maximally depolarized, better known as its polarization direction, varies considerably across the macular surface (see Figure 1.5). As a result, each hair cell has its own tuning curve, depending on the specific orientation of the bundle of hairs. In other words, at a given tilt of the head, some otolith afferents discharge maximally, while others fire only moderately or even fall silent. Due to this organization, the organ as a whole is sensitive to accelerations and tilts in all directions (see section *Probabilistic tilt estimation*). Furthermore, otolith afferents can be divided into two classes, based on their spiking pattern. This classification distinguishes between afferents that have a relatively steady discharge rate (regular units) and afferents that show a more irregular rate of firing (irregular units). The regular units are more sensitive to static tilts, whereas the irregular units are particularly responsive to dynamic situations (Goldberg, 2000).

Altogether, the otoliths seem ideally suited for detecting the direction of gravity. However, one problem remains to be solved. As otolith hair cells respond to the sum of gravitational and linear acceleration (the gravito-inertial force or GIF), the brain must find out whether the otolith signal was caused by a tilt of the head, by a linear acceleration, or by some combination of both. One of the current theories suggests that the brain uses rotational information from the semicircular canals to disambiguate the otolith signal (Merfeld, 1995; Angelaki and Cullen, 2008). Neural correlates of otolith disambiguation, based on canal-otolith interaction, have been studied at various levels in the brain (Angelaki and Yakusheva, 2009).

Somatosensory cues

Apart from visual and vestibular cues, the brain can also use information from the somatosensory system. This system comprises a large variety of sensors, including mechanoreceptors in the skin and blood vessels, and proprioceptors. Somatosensory cues that assist in maintaining spatial orientation include information about muscle tension, joint reaction forces and the pressure distribution under the feet. Another contribution comes from the distribution of blood in our body, which is sensed by specialized receptors in the major blood vessels. Vaitl and colleagues studied the influence of these sensors by modifying the distribution of blood in the body through application of positive or negative pressure at the legs (Vaitl et al., 1997; Vaitl et al., 2002). It was shown that subjects in horizontal position perceived head-down tilt during positive pressure at the legs and head-up tilt if a negative pressure was applied, which suggests that information from the cardiovascular system has a distinct effect on the perception of body orientation.

PROCESSING OF MULTISENSORY INPUTS

When the brain can rely on various sources of sensory information in the estimation of body orientation, this raises the question how the various signals are weighted centrally. Mittelstaedt (1997) was the first to provide a thorough experimental analysis of this problem. To distinguish between the contributions of the otoliths and trunk-based somatosensory cues, he used a sled centrifuge. Subjects were placed right-ear-down on the sled, such that the radial distance *d* from the rotation axis of the centrifuge to the otoliths could be adjusted, as shown in Figure 1.6. Rotation at a constant velocity induced a centrifugal force on the body, which increased linearly with the distance from the centrifuge rotation axis. In the absence of any visual cues, the subjects were then asked to adjust their radial position on the centrifuge until they felt completely horizontal. The idea behind this approach was that, if body tilt estimation originated entirely from the otoliths, the subjects should align their binaural axis with the centrifuge rotation axis (*d*=0), because then the otoliths would not be affected by a centrifugal force (see Figure 1.6A). In case the sled was shifted toward the feet or in the opposite direction (toward the head), the otoliths would not be aligned with the rotation axis, so that a centrifugal force would act upon them and the subject would feel tilted head-upward or head-downward, respectively (see Figure 1.6 B, C).

However, instead of aligning the rotation axis with their otoliths, subjects actually set the centrifuge axis at approximately 20-30cm caudally (toward the feet) of their binaural axis. This result suggests that, in normal subjects, body tilt estimates are not solely based on otolithic inputs, but that input from other gravity-sensing systems in the trunk ('truncal graviceptors'), like the blood pressure receptors, must also be involved. Thus, when the subject is rotated around the binaural axis (*d*=0), the centrifugal force will not affect the otoliths, but does stimulate any truncal graviceptor(s), which leads to illusory body tilt (Figure 1.7A). Accordingly, in order to feel perfectly horizontal, the subject must move the sled to a position at which the centrifugal forces on the otoliths and the truncal graviceptors have equal but opposite effects, as shown in Figure 1.7B.

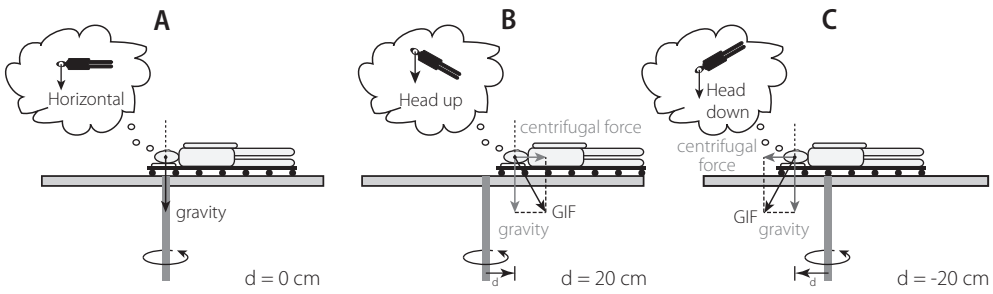

Figure 1.6 Illustration of Mittelstaedt's sled centrifuge experiment for the hypothetical case that only the otoliths are involved in the estimation of body tilt. A. The interaural axis is aligned with rotation axis so that the centrifugal force does not act upon the otoliths, which correctly sense the direction of gravity. B. When the body is shifted caudally, the gravito-inertial force (GIF) on the otoliths is shifted toward the feet, which is interpreted as head-up tilt. C. When the body is shifted cranially, the GIF rotates toward the head, which leads to illusory head-down tilt.

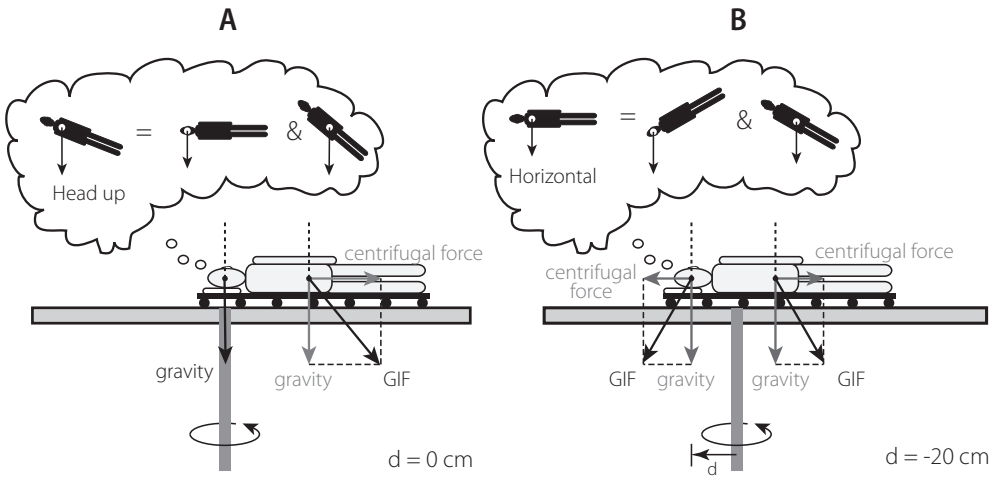

Figure 1.7 Illustration of body-tilt percept in Mittelstaedt's sled centrifuge experiment when both otoliths and graviceptors in the trunk are involved. A. The interaural axis is aligned with rotation axis. Otoliths are unaffected by the centrifugal force and correctly sense the direction of gravity (GIF directed downward), but the centrifugal force acts upon the truncal graviceptors, leading to illusory tilt. B. To feel perfectly horizontal, the rotation axis is adjusted in caudal direction (d≈-20cm). At this position, illusory tilt sensed by the otoliths and the truncal receptors is equal but in opposite direction, such that their effects are cancelled in the final body tilt estimate.

To localize the 'mass centroid' of these truncal graviceptors, Mittelstaedt also tested patients who had lost all vestibular function. Results showed that these subjects felt horizontal when the centrifuge rotation axis was located near the last ribs (*d*≈-45cm), which suggests that this is the location where the truncal graviceptors have their central point of application. To compute how the two inputs are centrally weighted, Mittelstaedt assumed that the final body tilt estimate (ρ_{total}) results from a linear combination of the vestibular estimate (ρ_{vest}) and the truncal estimate (ρ_{trunc}), according to $\rho total = w_{vest} \cdot \rho_{vest} + w_{trunc} \cdot \rho_{trunk}$. In this equation, the partial estimates ρ_{vest} and ρ_{trunc} are defined by the radial sled position (d). Based on the results from normal and vestibular-defective subjects, Mittelstaedt determined that the relative weights of the vestibular system (w_{vest}) and the truncal graviceptors ($w_{trunc}=1-w_{vest}$) in healthy subjects were ~0.4 versus ~0.6, respectively. This outcome underlines the importance of the truncal graviceptive system in the estimation of body orientation.

Testing spatial orientation

Human spatial orientation can be tested in various ways. Some experiments, like Mittelstaedt's 1997 study, test the ability to estimate one's body orientation in space, while others investigate the capacity to estimate the orientation of external (visual) objects with respect to gravity. In most of these studies, subjects are tilted in pitch (forward-backward) or in roll (sideways). In this thesis, all tests are concerned with tilts in the roll plane only.

The SVV-SBT paradox

Human subjects, who are roll-tilted to an unknown tilt angle in complete darkness, can provide fairly accurate estimates of their own body orientation (subjective body tilt, SBT)

across the entire tilt range (Mittelstaedt, 1983; Mast and Jarchow, 1996; Jarchow and Mast, 1999; Van Beuzekom et al., 2001). In contrast, when these subjects are asked to align a small luminous line with the direction of gravity (subjective visual vertical, SVV), a remarkable pattern of systematic errors arises, which is known as the *Aubert-* or *A-effect* (Aubert, 1861). More specifically, at tilt angles beyond ~60°, the final line setting usually deviates in the direction of the long body axis, as if participants underestimate their own tilt angle (Mittelstaedt, 1983). This poses an intriguing paradox: if the observer has an accurate estimate of his own body orientation in space, then why is it not used in determining the spatial orientation of the line? To try find an answer to this question, in this thesis, we will assess the specific computations and reference frame transformations that are required in the two tasks.

Reference frame transformations

As we saw, the brain has access to many kinds of sensory signals that may assist in spatial orientation. Combining these signals is complicated by the fact that the various sensors may encode information in different frames of reference. For example, the otoliths encode the orientation of the head in world-centered (gravitational) coordinates, whereas the eyes sense the orientation of the visual panorama with respect to the retina. To combine sensory information encoded in different reference frames, the central nervous system needs to perform reference frame transformations, as will become clear in the following example. Suppose one needs an estimate of trunk orientation with respect to gravity (trunk-in-space, T_S), as required in the SBT task. In this task, truncal graviceptors provide information that requires no additional reference frame transformation, as shown in Figure 1.8. Additionally, the brain may use information from the otoliths, encoding head orientation in space (H_S), but this requires supplementary information about head-on-trunk orientation (H_T), because the head may be tilted on the body ($T_S=H_S-H_T$). Panoramic cues, if present, can be incorporated similarly: Tilts of the visual scene on the retina ('space-on-eye', S_E), suggest that the eyes are tilted in the opposite direction ($E_S=-S_E$). To transform this signal into a trunk-in-space estimate, the brain requires information about eye-in-head orientation (E_H) and about head-on-trunk orientation (H_T), because $T_S=E_S-E_H-H_T$. As the eyes counterrotate in their orbits when the head is tilted, information about eye-in-head orientation is far from trivial. As a result of these computations, the brain can base its final estimate of trunk tilt on three separate estimates, originating from different sense organs with different properties. How these signals can be combined will be reviewed in the section *Optimal sensor integration: an example*.

In the SVV task, the brain can rely on the same sensory inputs as in the SBT task, but requires different reference frame transformations, as shown in Figure 1.9. To assess the spatial orientation of the visual line (L_S), as needed in the SVV task, the brain needs to know the retinal orientation of the line (L_E), together with an estimate of the orientation of the eyes in the head (E_H), and an estimate of head orientation in space, because $L_S=L_E+E_H+H_S$. Information about the head-in-space orientation is directly provided by the otoliths, but can also be based on trunk-in-space or eye-in-space information, which requires additional reference frame transformations.

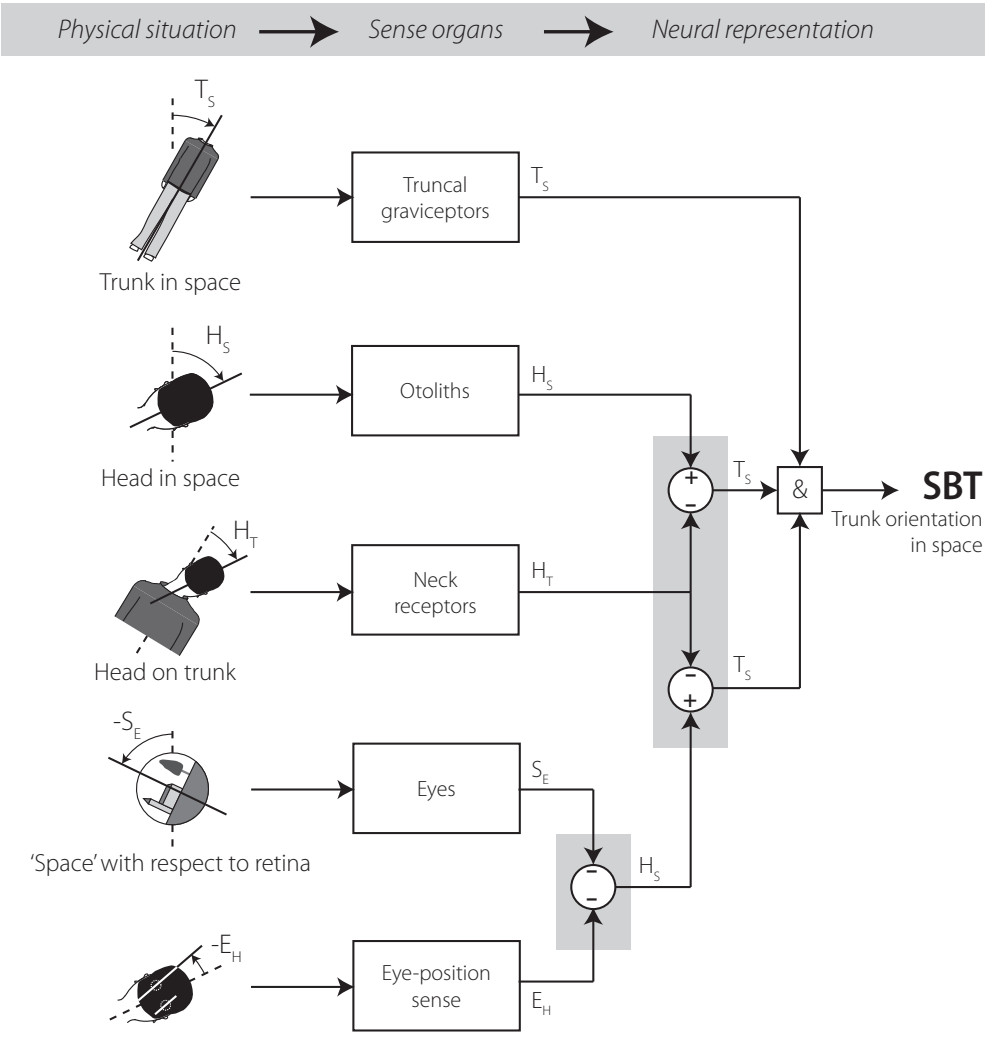

Figure 1.8 Reference frame transformations for the estimation of trunk orientation, as required in the SBT task. The brain has access to various sensory signals encoding head-in-space (H_S), trunk-in-space (T_S), head-on-trunk (H_T) and eye-in-head (E_H) orientation. Panoramic cues, encoding the orientation of space (gravity) on the retina (SE), can be used in normal situations, but are usually unavailable in SBT task. Reference frame transformations, indicated by shaded areas, are required to obtain multiple estimates of trunk orientation in space (T_S). Combination of these three signals is denoted by the "&"-block (see section "Optimal sensor integration: an example").

Optimal sensor integration: an example

The brain faces a further intriguing challenge in the processing of sensory signals: all its sensory inputs are contaminated by neural noise, which means that it can never be sure which physical situation caused the incoming neural signals. How then to make an estimate of the underlying state? The statistically optimal strategy for obtaining such an estimate based on multiple sensory inputs is known as optimal (Bayesian) sensor integration, which will now

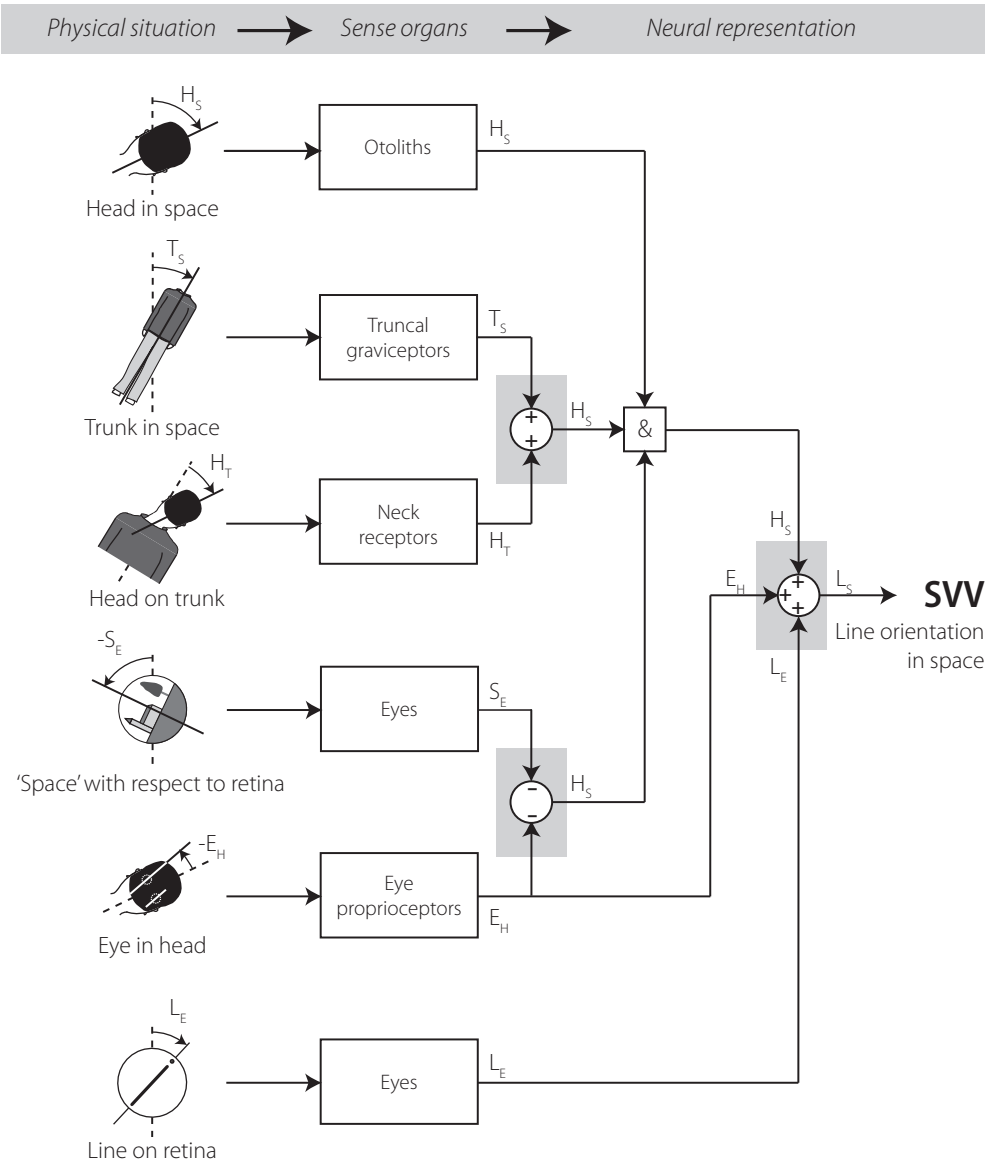

Figure 1.9 Reference frame transformations for the estimation of line orientation in space (L_S), as required in the SVV task. The brain has access to the same sensory signals as in the example of Figure 1.8, complemented by retinal line (L_E) orientation. Panoramic cues, encoding space (gravity) orientation on the retina (S_E), are usually not available in SVV task but are shown for completeness. Reference frame transformations, indicated by shaded areas, are required to obtain multiple estimates of head orientation in space (H_S). Integration of the three head-in-space signals is denoted by the "&"-block.

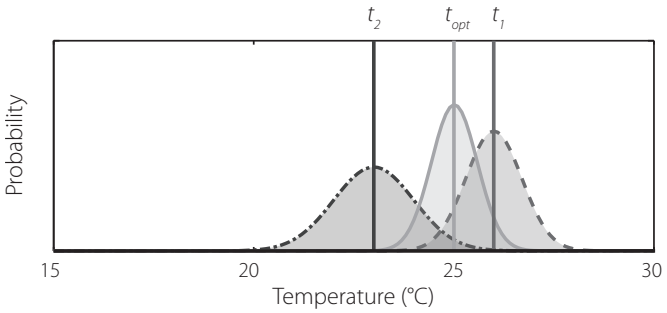

Figure 1.10 Schematic representation of optimal sensor integration. Dashed and dash-dotted curves represent probability distributions based on the two temperature measurements t_1 and t_2. Sensory noise (uncertainty) is indicated by the width of the curves. The optimal estimate of temperature (t_{opt}) is obtained by weighting each source by the inverse of its variance and contains less noise than the separate inputs.

be explained with an illustrative example.

Suppose weatherman Erwin Krol asked us to provide the best possible estimate of the temperature in Nijmegen on a particular day in July. Erwin gives us two thermometers, which are accurate but fairly imprecise[1]. However, our famous weatherman does provide information about the quality of the thermometers (noise levels of σ_1=0.7°C and σ_2=1°). As Erwin is in a hurry, he only allows us to make a single measurement with each thermometer, which results in thermometer 1 indicating a temperature of t_1=26°C, while thermometer 2 gives an indication of t_2=23°C. What should be our response to Erwin? According to statistical theory, the probability of a certain temperature (T) can be obtained with:

$$P(T|t_1,t_2) \sim P(t_1|T) \cdot P(t_2|T) \qquad \text{Eq. 1.1}$$

in which $P(t_1|T)$ and $P(t_2|T)$, the so-called likelihood functions, denote the separate probabilities of measuring values t_1 and t_2 with thermometers 1 and 2, given temperature T. A graphic illustration of this theory is shown in Figure 1.10, which shows the likelihood probability distributions, together with the optimal combined (posterior) probability distribution. The posterior distribution lies in-between the two other distributions, being slightly biased toward thermometer 1, which is the better of the two. Furthermore, the posterior distribution is more peaked, which implies that the final estimate is more precise than the estimates based on the two separate thermometers. In this example, the optimal temperature estimate (t_{opt}), reflected by the peak of the posterior distribution, is 25.0°C and should be reported to Erwin. Note that, instead of using only the best thermometer (#1), we used both of them to obtain a temperature estimate. This strategy is optimal because the second thermometer does provide useful information, even though it is less precise than the first thermometer. In fact, the final temperature estimate could be further improved by incorporating *a priori* information, such as a temperature record of the last 50 years, which could be implemented as a prior probability distribution.

1 *It is important to make a clear dissociation between accuracy, which is linked to systematic errors (bias), and precision, which involves variable errors (noise).*

Interestingly, in recent years, various behavioral studies have provided evidence for the notion that humans behave like optimal (Bayesian) observers (van Beers et al., 1999; Ernst and Banks, 2002; Niemeier et al., 2003; Körding and Wolpert, 2004). As we will see in the next section, similar principles can be applied to the estimation of head tilt from noisy otolith afferents.

Probabilistic tilt estimation

When we consider the firing rate of a single otolith nerve fiber, it is impossible to obtain an unambiguous, precise estimate of head tilt for two reasons. First, the neural signal is corrupted by noise, which means that, even if the subject is repeatedly tilted to exactly the same tilt angle, the neural signal may differ considerably between these situations (see Figure 1.11). Therefore, the central nervous system can never be certain which tilt angle caused the resulting firing rate. Second, even in the absence of noise, the sinusoidal relation between discharge rate and tilt angle means that the signal is ambiguous. For example, in the tuning curve in Figure 1.4B, a discharge rate of 30 spikes/s can be caused by either -135° or -45° tilt. In other words, it is impossible to distinguish between these angles based on just this one neuron. The only way to solve the latter problem is to incorporate a second cell with a different tuning curve, like cell 2 in Figure 1.11, which is tuned to a different tilt angle.

Due to the neural noise, the process of estimating head tilt requires a probabilistic approach. To reduce uncertainty, the information from all afferents should be combined, using the rules of optimal integration theory, as explained in the previous section. Let's consider the problem from the perspective of the brain: for simplicity, we only use information from the two cells shown in Figure 1.11. Suppose we obtained r_1=55 discharges from cell 1 and r_2 =35 discharges from cell 2 within a time frame of 1 s. What does this tell us about head tilt?

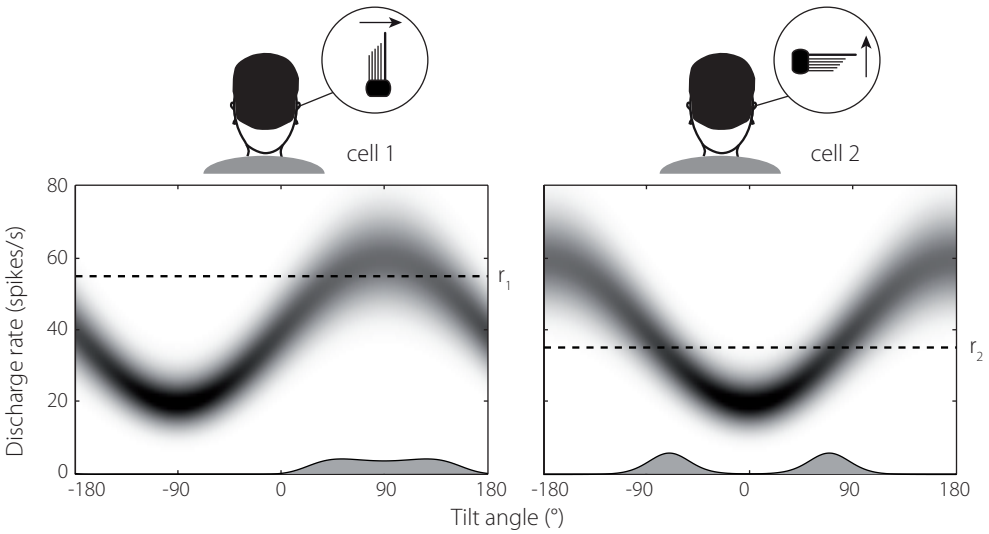

Figure 1.11 Tilt response curves of two otolith cells with different anatomical orientations. Cell 1, resembling a utricular unit, discharges maximally at 90° and is most sensitive to tilt changes around 0° and 180° (steepest slope). Cell 2, resembling a saccular unit, has a maximal discharge at 180° (upside down) and is most sensitive to tilt changes around -90 and 90°. Gray scale reflects probability. Cell discharge is assumed to be a Poisson process (which seems a valid assumption, see Goldberg 2000).

Given the tuning curves of cell 1 and 2, we can translate the firing rates into two tilt probability distributions, as shown in Figure 1.12A. According to Bayes' theory, the probability that tilt angle ρ led to response rates r_1 and r_2 ($P[\rho|r_1,r_2]$) is proportional to:

$$P[\rho|r_1,r_2]\sim P[r_1|\rho]\cdot P[r_2|\rho] \qquad \text{Eq. 1.2}$$

with likelihood functions $P[r_1|\rho]$ and $P[r_2|\rho]$ denoting the probability that tilt angle ρ caused r_1 and r_2 action potentials in cell 1 and 2, respectively. The likelihood function $P[r_1|\rho]$ can be modeled as a Poisson probability distribution, according to:

$$P[r_1|\rho]= e^{-\lambda}\cdot\lambda^k/k! \qquad \text{Eq. 1.3}$$

in which λ = tuning curve cell 1 = 20· sin(ρ)+40, and $k=r_1$. The same holds for cell 2, but then with λ = tuning curve cell 2 = 20· sin(ρ-90)+40 and $k=r_2$. Multiplying these distributions yields (after normalization) a new posterior distribution (Figure 1.12A), which represents the optimal tilt probability distribution, given these two inputs (r_1 and r_2).

Repeating this simulation ten times yields ten different sets of r_1 and r_2, which results in ten posterior distributions, as shown in Figure 1.12B. Clearly, each distribution is different, but, on average, the optimal estimates (peaks) scatter around 45°, the simulation angle that was actually used to generate r_1 and r_2.

Inhomogeneous population

What happens if we incorporate more hair cells in our simulations? To imitate the distribution of hair cells in the otoliths, with more hair cells in the utricle than in the saccule (Rosenhall, 1972, 1974), we use a simple model, containing 68 cells with various polarization directions. As shown in Figure 1.13A, the majority of cells is tuned to accelerations near the left-right

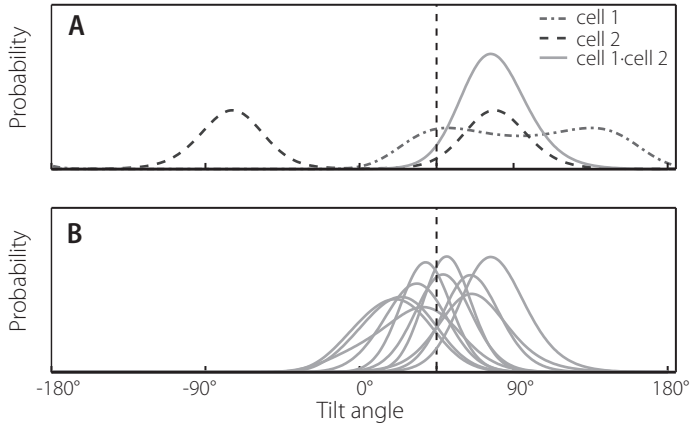

Figure 1.12 A. Tilt probability distribution functions based on cell 1 (dash-dotted line) and cell 2 (dashed line), and after optimal combination (solid line, posterior distribution). Note that tilt estimation based on single-cell data is ambiguous (two peaks), whereas combination leads to a single, unambiguous peaked distribution. Vertical dashed line shows the tilt angle that was used in the simulation (ρ=45°). B. Posterior distributions of 10 simulations. Probability functions vary due to neuronal noise (see main text).

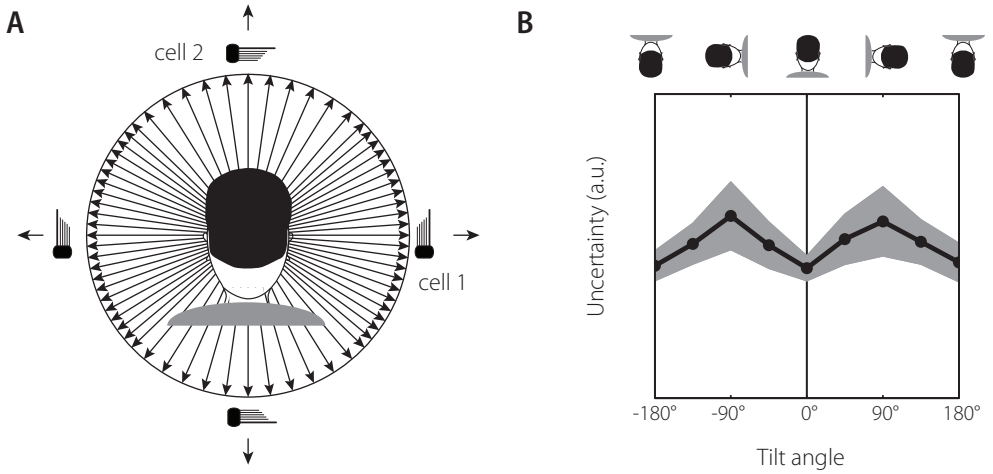

Figure 1.13 A. Simplified model of polarization directions of otolith hair cells in roll plane, imitating the distribution of utricular and saccular hair cell polarization directions (Jaeger and Haslwanter, 2004). B. Simulated perceptual uncertainty as a function of tilt angle. Curve reflects average width of posterior probability distributions given cell distribution in panel A. Gray band indicates ±SD.

direction, resembling utricular cells like cell 1 in Figure 1.11, whereas fewer cells are tuned to accelerations near the up-down direction, resembling saccular cells, like cell 2 in Figure 1.11.

Using the same approach as before, but now at a broad range of tilt angles, simulations show that perceptual uncertainty is higher around 90° than at upright (0°) or upside down (180°), as shown in Figure 1.13B. This observation, caused by the uneven distribution of hair cells, lends some credibility to a critical model assumption that was made in the studies of *Chapters 2*, *3* and *4*, that noise in the tilt signal becomes more pronounced at larger tilts.

OUTLINE OF THIS THESIS

This thesis aims at a better understanding of the neural strategies underlying spatial vision (using the SVV task) and the perception of one's body orientation in space (using the SBT task).

In *Chapter 2*, we investigate whether verticality judgments of visual motion, made by a tilted observer, have the same characteristics as when testing the perceived vertical of line orientation (SVV). Since visual motion and static visual contours are processed in different brain areas, this comparison may tell us something about how these visual signals are combined with the head-tilt signal. As we found virtually identical results, we conclude that the two tasks rely on a shared computational strategy. To explain these observations, we introduce a Bayesian observer model based on optimal observer theory. According to this model, the systematic SVV errors at large tilts reflect a negative side-effect of the brain's strategy to reduce noise in the head tilt signal. An essential aspect of this Bayesian observer model is that it predicts a trade-off between accuracy and precision levels in task performance. To test this model, we proceed in *Chapter 3* by providing a thorough investigation of SVV precision and accuracy levels, at a range of body-tilt angles, using a psychometric approach.

In *Chapter 4*, we focus on the separate contributions of gravity sensors in different parts of the body. To assess the relative contributions of trunk-based and head-based graviceptors, we use an extended Bayesian observer model that incorporates the subjective body tilt (SBT) task. We show that SVV and SBT performance, although markedly different, essentially follows the rules of optimal sensor integration.

Finally, *Chapter 5* investigates how roll-optokinetic stimulation affects the SVV and the SBT at different tilt angles. The question is whether the shift in the SVV simply reflects the change in perceived body tilt (SBT). Since eye torsion, evoked by the roll-optokinetic stimulus, could have an effect on the SVV but not on the SBT, we included a third task which aimed at testing this ocular-torsion effect in isolation.

Chapter 2

Shared computational mechanism for tilt compensation accounts for biased verticality percepts in motion and pattern vision

De Vrijer M, Medendorp WP, Van Gisbergen JAM (2008) *J Neurophysiology* 99: 915-930.

The topic of this study concerns the integration of visual motion and vestibular signals for spatial perception. One line of investigation in this broad field has concentrated on the visual contribution to the percept of egomotion and posture (Brandt et al., 1974; Wertheim, 1994; Lappe et al., 1999). This work showed that persistent large-field visual motion, initially perceived as motion in external space, induces a slowly developing percept of self-motion (vection). It is now widely accepted that large-field optic flow signals in the low-frequency range complement vestibular motion cues covering the high-frequency domain. This account is further supported by neurophysiological studies (Henn et al., 1974; Brandt et al., 1998) and has been incorporated in spatial-orientation models (Robinson, 1977; Merfeld, 1995; Zupan et al., 2002). Other studies have provided a better understanding of the brain areas involved in the integration of visual motion signals with nonvisual cues for the perception of self-motion (Bremmer et al., 2002; Page and Duffy, 2003; Angelaki and Hess, 2005; Müller et al., 2005; Gu et al., 2006, 2007; Fetsch et al., 2007). As a result, we now have a good understanding of how optic flow signals contribute to the percept of body posture and egomotion.

Much less is known about the opposite perspective: the involvement of postural information in the perception of visual object motion in space. To estimate the direction of visual motion in an earth-centric reference frame, visual signals coding the direction of motion on the retina must be combined with extraretinal signals coding eye position in space. Much previous work has investigated this issue for voluntary eye movements in head-restrained subjects. Studies on visual motion perception during smooth pursuit, for example, have shown that the brain can take extraretinal pursuit signals into account, despite certain imperfections in this integration process (Wertheim, 1994; Freeman et al., 2000; Souman et al., 2005).

Recently, neurophysiological studies have elucidated the major neural pathways involved in visuooculomotor integration during smooth pursuit (Newsome et al., 1988; Ilg et al., 2004; Lindner et al., 2006; Inaba et al., 2007; for reviews see Lisberger et al., 1987; Krauzlis, 2004). This work has identified brain areas with access to both visual-motion and gaze-motion signals. Thus with respect to this aspect of external motion perception, there is now at least a basic concept of how sensory and motor signals can merge into a coherent percept. We investigated to what extent laterally tilted subjects use vestibular information about body posture when estimating the direction of visual motion in external space. A further question was whether performance in this task involves the same intriguing misjudgments found in tests of line verticality. Numerous studies on the subjective line vertical have shown that human observers, tilted sideways in darkness, make substantial systematic errors when aligning a luminous line with the direction of gravity (for review see Mittelstaedt, 1983). Generally, at large tilts (60°) these errors suggest underestimation of head tilt and are known as the Aubert or A-effect, as first described by Aubert (1861). In the smallest tilt range (30°), errors are typically small, although errors of overestimation (the E-effect) have also been reported. Although line settings mostly suggest an underestimation of body tilt, systematic errors in the tilt signal cannot be held accountable since body tilt perception is almost veridical in these conditions (Mittelstaedt, 1983; Mast and Jarchow, 1996; Van Beuzekom and Van Gisbergen, 2000; Van Beuzekom et al., 2001; Kaptein and Van Gisbergen, 2004). Uncorrected eye torsion, causing errors in the opposite direction, cannot explain the A-effect either (Howard 1982). Instead, it has been suggested that these large systematic errors are the downside of a computational strategy to

improve verticality perception at small tilts (Eggert, 1998; Mittelstaedt, 1999).

Mittelstaedt (1983) proposed a model that implements this computational strategy by means of an internal bias signal, which serves to correct for the distortion caused by a putative imbalance in the tilt signal due to the unequal numbers of hair cells in the two otolith organs. This internal signal, called the idiotropic vector, is a head-fixed vector that is added vectorially to the estimated direction of gravity derived from the otoliths. Although the idiotropic contribution compensates for the distortion at small tilts, it worsens verticality perception at large tilts, where it accounts for the A-effect. Recently, it has been pointed out that the effect of the idiotropic component of Mittelstaedt's model is equivalent to the role of prior knowledge in the optimal evaluation of a noisy head tilt signal in a Bayesian framework (Eggert, 1998). Also MacNeilage et al. (2007) suggested that the A-effect in spatial perception could be explained from a Bayesian perspective, but this has never been tested explicitly.

In our experiments, subjects adjusted the direction of visual motion to the perceived vertical (*motion vertical*) at a range of different body tilts. For comparison, the same subjects were also tested in a classical luminous-line task (*line vertical*). We hypothesized that errors in the two tasks would be the same, indicating that these errors do not reflect errors in the neural processing of the visual cues themselves, but rather errors in the neural processing that yields the reference frame (gravity perception). We indeed found virtually identical performance in both tasks, with considerable systematic errors at the larger tilt angles, suggesting that there is a shared mechanism in the computation of the motion vertical and the line vertical. Simulations with two spatial-orientation models —Mittelstaedt's original idiotropic-vector model and a novel Bayesian model— show that the shared pattern of systematic errors probably reflects central handling of imperfections in the sensory tilt signal, before it is combined with signals from each visual subsystem.

METHODS

Subjects

Eight subjects (seven male, one female), aged between 23 and 62 yr (mean ± SD: 31 ± 13 yr), provided written informed consent to participate in the experiments. All subjects, including the three authors who were familiar with the purposes of the experiments, took part in the adjustment experiment (see following text). An additional control experiment involved four subjects (one author). All participants had normal or corrected-to-normal visual acuity and were free of known vestibular or other neurological disorders.

Setup

Subjects were seated in a computer-controlled vestibular chair with nested gimbals that allowed whole-body rotation about any axis in space. They were securely tightened in the chair using seat belts, adjustable shoulder and hip supports, a footrest, and Velcro straps to restrain feet and legs. The head was firmly fixated in a natural upright position for looking straight ahead, using a padded adjustable helmet. During the experiments, subjects were tilted in complete darkness by rotation about the nasooccipital (roll) axis to a stationary lateral tilt

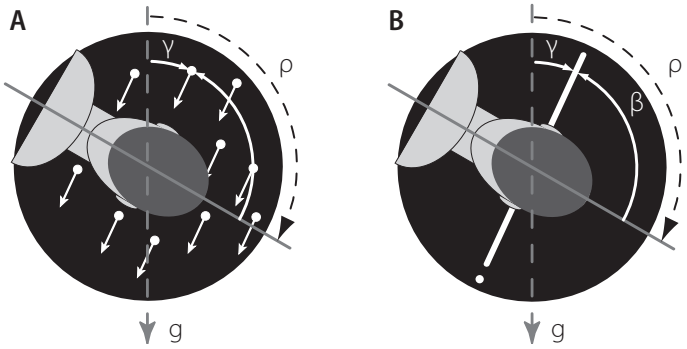

Figure 2.1 Schematic representation of the adjustment tasks. A. Motion task. Subject, shown in rear view, adjusted the motion direction of the random-dot-pattern to the perceived direction of gravity. Only 30% of the dots moved in coherent fashion (not shown). B. Line task. Subject aligned the orientation of the line to the perceived direction of gravity. Angular definitions: Rotation angle ρ, angle between longitudinal head axis and gravity. Compensation angle β, angle between line or motion setting and the longitudinal head axis. Alignment error γ, difference between rotation angle ρ and compensation angle β. The depicted response in both tasks shows undercompensation for tilt (β < ρ). In both figures (not drawn to scale), g represents the true direction of gravity.

position. The seat was adjusted so that the axis of rotation was aligned with the cyclopean eye. Chair orientation was measured using a digital position encoder with an angular resolution of 0.04° and was recorded on disk.

Visual stimuli for testing verticality percepts were presented on a chair-fixed Philips 15-inch LCD screen with a refresh rate of 60 Hz, mounted at eye level in the frontoparallel plane at a distance of 90 cm from the subject. Due to computational restrictions, movie frames were shown at an effective frame rate of 20 Hz. Visual stimuli were generated in Matlab (The MathWorks) using the Psychophysics Toolbox (Brainard, 1997; Pelli, 1997). To exclude visual cues about the direction of gravity, a mask with a circular aperture of 14° was mounted in front of the screen. As a further precaution against spurious tilt cues, stray light was reduced by a 2.7-log-unit neutral density filter, which kept background luminance of the screen to <0.001 cd/m^2. The intensity of test stimuli was 0.2 cd/m^2. Vision was always binocular and subjects were allowed to move their eyes freely at all times.

Starting from upright, subjects were roll-rotated in darkness to a tilt angle ρ, with right-ear-down rotations taken positive (see Figure 2.1). The chair rotated with a peak acceleration of 50°/s^2 to a constant velocity of 30°/s, which was reached within 1 s. After rotation to the tilt position had been completed, a 30-s waiting period followed to allow dissipation of putative canal effects. Then, the subjective motion vertical (Figure 2.1A) or the subjective line vertical (Figure 2.1B) was tested in a run of 12 sequential trials in the adjustment experiment or 66 trials in the control experiment (see following text). Next, subjects were rotated back to the upright position where they remained for 30 s, with the room lights on, until the next rotation started. Tests for positive and negative tilt angles were alternated regularly. Subjects never received feedback about their performance.

Adjustment tasks

We used an adjustment paradigm to determine both the motion vertical and the line vertical at tilt angles ranging from -120 to 120° at 20° intervals. Subjects performed these tasks, tested in random order, as follows.

Motion adjustment

In the motion-adjustment task (Figure 2.1A), subjects viewed a moving random-dot pattern with 0.3°-diameter dots. We used a random-dot pattern to ensure that the motion vertical was based on global motion mechanisms and to discourage the application of a line strategy based on single-dot trajectories (see *Global versus local motion* in *Results*). The pattern contained 50 dots on average, equivalent to a dot density of 0.3 dot/deg^2, of which 30% behaved as signal dots, moving coherently in steps of 0.3° at a speed of 6°/s (for a similar approach see Newsome and Paré, 1988). The other 70%, which were noise dots, shifted to a random location in the circular 14° aperture. At each movie frame, dots had a 30% chance of being treated as a signal dot (as in Newsome and Paré, 1988). As a result, signal dot life time was limited, with a 9% chance that a signal dot would survive two movie frames, a chance of 2.7% for surviving three subsequent frames, and so on. The subject's task was to adjust the direction of the noisy moving dot pattern toward the floor, parallel to the perceived direction of gravity, using a joystick.

Line adjustment

In the line-adjustment task (Figure 2.1B), subjects viewed a luminous line (length 12°, width 0.3°) that was polarized by a bright dot at one end. Subjects used a joystick to adjust the orientation of the line parallel to the perceived direction of gravity so that the dot pointed downward in space. The rotation axis of the line coincided with the subject's roll axis.

The time available for completing each adjustment was 10 s. Line and motion stimuli had random orientations at trial onset. Each combination of task and tilt angle involved 12 successive trials in a single run. In total, there were 26 combinations of tilt angle and task, each of which was tested once in random order in two experimental sessions of about 40 min each. Before testing began, subjects were given sufficient practice trials to get used to the tasks.

Control tasks

When it was found that performance in the line- and motion adjustment tasks was very similar, the question arose whether subjects had in fact performed the motion task by transforming it into a line task. If this scenario applied, the subject would have derived a percept of motion verticality by temporally integrating the extrapolated motion paths of individual signal dots. The similarity in results would be trivial if this strategy had actually been used. Therefore we designed a control experiment to rule out this possible confound. We used a forced-choice paradigm to quantify the motion vertical and line vertical psychometrically at a large tilt angle where the adjustment experiment had shown substantial systematic errors in the two tasks. In testing the subjective motion vertical, we compared two paradigms: 1) one was designed to impose reliance on a global motion percept for solving the task; and 2) the other enforced a single-dot strategy, which precluded spatial integration. We used the following tasks.

Global motion forced-choice task

As in the motion-adjustment experiment, subjects viewed a 30%-correlated random-dot pattern, but motion directions of signal dots were now drawn from a normal distribution with SD of 15° around a mean. Recall that in the motion-adjustment paradigm, all signal dots moved in the same direction. This modification, inspired by the previous work of Dakin et al. (2005), was introduced to deter reliance on local motion cues for solving the task. As a further measure, exposure duration was limited to 200 ms per trial, corresponding to four shifts of the random-dot pattern (five movie frames). Subjects indicated whether the motion direction of the pattern in space was clockwise (CW) or counterclockwise (CCW) from their perceived direction of gravity, by using a toggle switch within a 1.5-s-response interval after the stimulus.

Local motion forced-choice task

This task enforced a single-dot strategy to test whether this would degrade performance relative to the global motion task. The stimulus consisted of a single 0.3°-diameter dot, with the same motion statistics as the dots in the global motion forced-choice task. Thus the stimulus dot moved to a new position in each movie frame, with a 30% probability that it moved like a signal dot and with a 70% chance that it moved like a noise dot. Accordingly, if subjects had in fact used a single-dot strategy in the global motion forced-choice task, performance in both motion forced-choice tasks would be identical. The stimulus was shown for 200 ms, equivalent to four shifts of the single dot, followed by a 1.5-s-response period. Using a toggle switch, subjects indicated whether the motion direction of the dot was CW or CCW from their sense of gravity.

Line forced-choice task

In this task, subjects viewed the same luminous line as in the line-adjustment task but only for a brief period of 200 ms, followed by a 1.5-s-response period. Using a toggle switch, they had to indicate whether the presented line orientation was CW or CCW from the perceived direction of gravity. The objective behind this test was to verify whether the strong similarity between the global motion vertical and the line vertical, as revealed in the adjustment tasks, was retained in the altered conditions of the psychophysical experiments.

Care was taken to familiarize subjects with all tasks. The local motion task was first practiced at a 100% coherence level (with the single dot behaving as a signal dot). Stimulus coherence was then gradually reduced to the 30% level used in the actual experiment. The global motion and line tasks were practiced using the same characteristics as in the actual tests.

The three control tasks were performed at three different tilt angles: -100°, 100°, and 0° (upright). Psychometric data were collected using the method of constant stimuli, which is based on multiple presentations of test stimuli, in random order, in a predetermined range above and below the perceptual threshold (see Ehrenstein and Ehrenstein, 1999). We centered the test range on the subjective vertical estimated from the prior adjustment results. This value was determined from a third-order polynomial curve that characterized the best-fit relationship of the mean verticality settings in the adjustment tasks as a function of tilt angle.

In all three tasks we presented the same set of 11 directions, at 0, ±3, ±6, ±9, ±15, and ±25° relative to this value. Each stimulus direction was presented 12 times, yielding a set of 132 responses for each psychometric function. Data for each combination of task and tilt angle were collected in two 112-s runs of 66 forced-choice trials. In each subject, the 18 runs (3 tasks x 3 tilt angles x 2 runs) were tested in random order in two experimental sessions of about 45 min each.

Data analysis

Data analyses were performed off-line using Matlab software (Matlab 7.0, The MathWorks). Response error γ in the motion adjustment task was defined as the difference between the adjusted motion direction of the dot pattern and the actual direction of gravity (see Figure 2.1A). Likewise, the response error in the line-adjustment task was computed as the angular difference between the line setting and the true vertical (see Figure 2.1B). Compensation angle β was defined as the motion or line setting relative to the subject's vertical head axis. Response averages and their SDs were calculated using circular statistics (Batschelet 1981). Data points >3SDs from the mean, considered outliers, were excluded from further analysis. Differences in the results among different experimental conditions were considered statistically significant at $P<0.05$.

Psychometric data from the global motion forced-choice and the line forced-choice control experiments were analyzed in a standard manner. We calculated the proportion (P) of CW responses for each stimulus direction and fitted a cumulative Gaussian curve using the method of maximum likelihood (Wichmann and Hill, 2001). This curve is given by the following function

$$P(x) = \lambda + (1 - 2\lambda)\frac{1}{\sigma\sqrt{2\pi}}\int_{-\infty}^{x} e^{-(y-\mu)^2/2\sigma^2}dy \qquad \text{Eq. 2.1}$$

in which x represents global motion direction or line orientation of the stimulus and y is an integration variable that runs within the stimulus domain. The mean value of the cumulative Gaussian μ represents the subject's subjective vertical (motion or line); the slope of the curve σ reflects the noise in the subjective vertical, which serves as a measure of the subject's uncertainty. Parameter λ, the lapse rate, which accounts for stimulus-independent errors caused by subject lapses or mistakes, was restricted to small values ($0<\lambda<0.06$). Lapses may be due to a temporary lack of attention and cannot be attributed to stimulus properties (for details see Klein, 2001; Wichmann and Hill, 2001). The expected poor performance in the local motion forced-choice task made fitting a psychometric function to the respective data unfeasible. Therefore we compared these data to the global motion data by comparing the deviations of both data sets to the global motion–fit curve (see *Global versus local motion* in *Results*).

Modeling

As we will subsequently see in *Results*, our subjects made considerable errors at the larger tilt angles in both the motion task and the line task. Based on the assumption of a central mechanism that biases the internal representation of verticality toward the long body axis,

Mittelstaedt (1983) proposed a widely accepted model that can account for such errors in visual verticality perception. In the following, we will first briefly describe this model and then introduce an alternative framework that can explain biased verticality percepts with a different mechanism.

Mittelstaedt's idiotropic-vector model

Mittelstaedt (1983, 1986) suggested that systematic errors in verticality perception reflect a central mechanism that compensates for putative systematic errors in the tilt estimate derived from the otoliths. A schematic representation of his model is shown in Figure 2.2. The basic idea is that the brain reconstructs tilt angle ρ by combining the signals from the two otolith organs, utricle and saccule, which are arranged in two orthogonal planes. However, since these signals are mediated by unequal numbers of afferents (Rosenhall, 1972, 1974), combining them in the straightforward manner implemented in the model yields a distorted estimate of ρ (see Figure 2.2, *bottom left*). To minimize the effect of this distortion at small tilt angles, which are most frequently encountered in daily life, the model invokes an internal bias signal. This internal signal, called the idiotropic vector, is a head-fixed vector that is added vectorially to the estimated direction of gravity derived from the otoliths. The addition of the idiotropic vector biases the tilt estimate toward the head axis, thereby effectively canceling the distortion at small tilts (see Figure 2.2, *right*). The downside of this computational strategy, however, is to worsen performance at large tilts. In a sense, Mittelstaedt's concept echoes earlier ideas formulated in the seminal study by Aubert (1861), which interprets the subjective visual vertical as a compromise between the sensory input providing information about head tilt

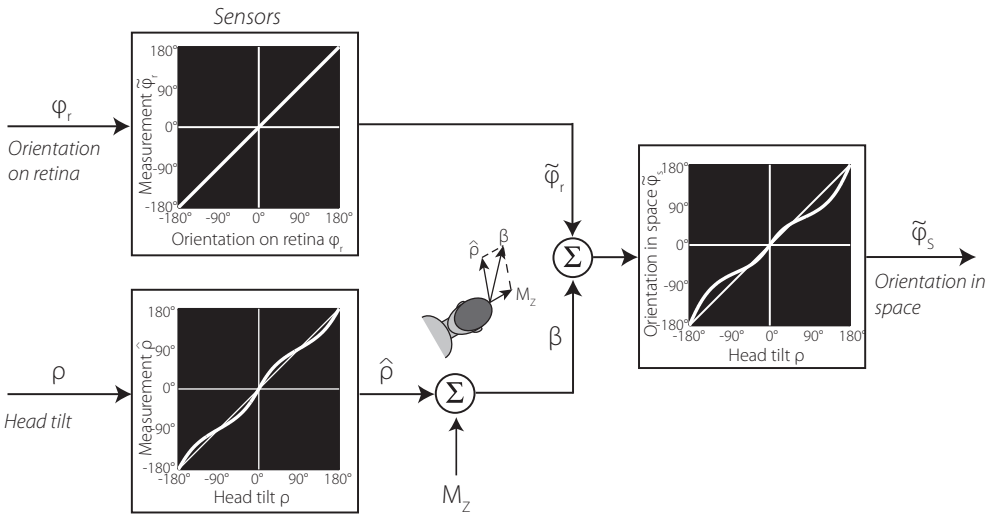

Figure 2.2 Schematic presentation of Mittelstaedt's idiotropic vector model. The model receives two inputs: orientation of the visual stimulus on the retina φ_r and head tilt ρ. The visual signal $\tilde{\varphi}_r$ is accurate, in contrast to the sensory tilt signal $\hat{\rho}$. Vectorial summation of $\hat{\rho}$ and the head-fixed idiotropic vector M_z yields compensatory tilt signal β (inset). Subsequently, the compensatory tilt signal and the visual signal are added ($\beta + \tilde{\varphi}_r$) to obtain the orientation of the visual stimulus in space $\tilde{\varphi}_s$, (see right panel).

and the vertical retinal meridian.

In the model, the internal representation of the roll-tilt angle, denoted as β, is specified as a function of ρ by the following relation

$$\beta(\rho) = \arctan\left(\frac{\hat{g}_y/N}{\hat{g}_z/N + M_Z}\right) = \arctan\left(\frac{\sin(\rho)/N}{S\cos(\rho)/N + M_Z}\right) \quad \text{Eq. 2.2}$$

In this equation, $\hat{g}_y = \sin(\rho)$ and $\hat{g}_z = S\cos(\rho)$ represent the neurally encoded gravity components along the head's *y*-axis and *z*-axis, as provided by utricle and saccule, respectively. *S* denotes the saccular gain (S<1), linked to the ratio of the number of saccular and utricular hair cells, and ρ is the physical tilt angle of the head. Furthermore, M_z is the *z*-component of the tilt-independent head-fixed idiotropic vector (*M*) and $N = \sqrt{\hat{g}_y^2 + \hat{g}_z^2}$ is a normalization factor to ensure that the internal representation of the gravity vector has a fixed length. Thus the model has two parameters to determine β: the size of the *M*-vector, an idiosyncratic value, and the normalized saccular gain *S*. In the model, it is assumed that the visual signal $\tilde{\varphi}_r$ is unbiased and can be simply added to the internal tilt representation to obtain the required output, i.e., the line orientation (or motion direction) in space $\tilde{\varphi}_s$. As a result, the systematic errors in the subjective vertical task merely reflect the bias in the internal tilt representation

$$\gamma(\rho) = \rho - \beta(\rho) \quad \text{Eq. 2.3}$$

which implies that, according to the model, systematic errors in the motion task and line task must be identical.

Furthermore, Mittelstaedt's model predicts that the noise in the internal tilt representation σ_β is inversely proportional to the length of the resultant vector, which is obtained by summation of the idiotropic vector and the normalized gravity vector (Mittelstaedt, 1983). Thus in analytical terms

$$\sigma_\beta(\rho) = \frac{C}{\sqrt{[\sin(\rho)/N]^2 + [S\cos(\rho)/N + M_Z]^2}} \quad \text{Eq. 2.4}$$

For the normal range of *S* and M_z parameter values, noise in the internal tilt signal increases with tilt angle, with *C* a proportionality constant, the third free parameter in the model. Qualitatively, Eq. 2.4 implies that subjects with a stronger idiotropic vector show reduced scatter at modest tilt angles but increased scatter at large tilts, compared with subjects with a smaller idiotropic vector. In the simulations, we assumed that the noise in the output error σ_γ depends not only on the noise in the internal tilt estimate σ_β, but also on the visual noise σ_v according to standard statistical rules for noise combination

$$\sigma_\gamma^2 = \sigma_\beta^2 + \sigma_v^2 \quad \text{Eq. 2.5}$$

in which visual noise for lines σ_{vl} and visual noise for motion σ_{vm} may be different, but independent of line orientation or direction of visual motion on the retina, ignoring the oblique effect (Löffler and Orbach, 2001; Luyat et al., 2001; Krukowski et al., 2003).

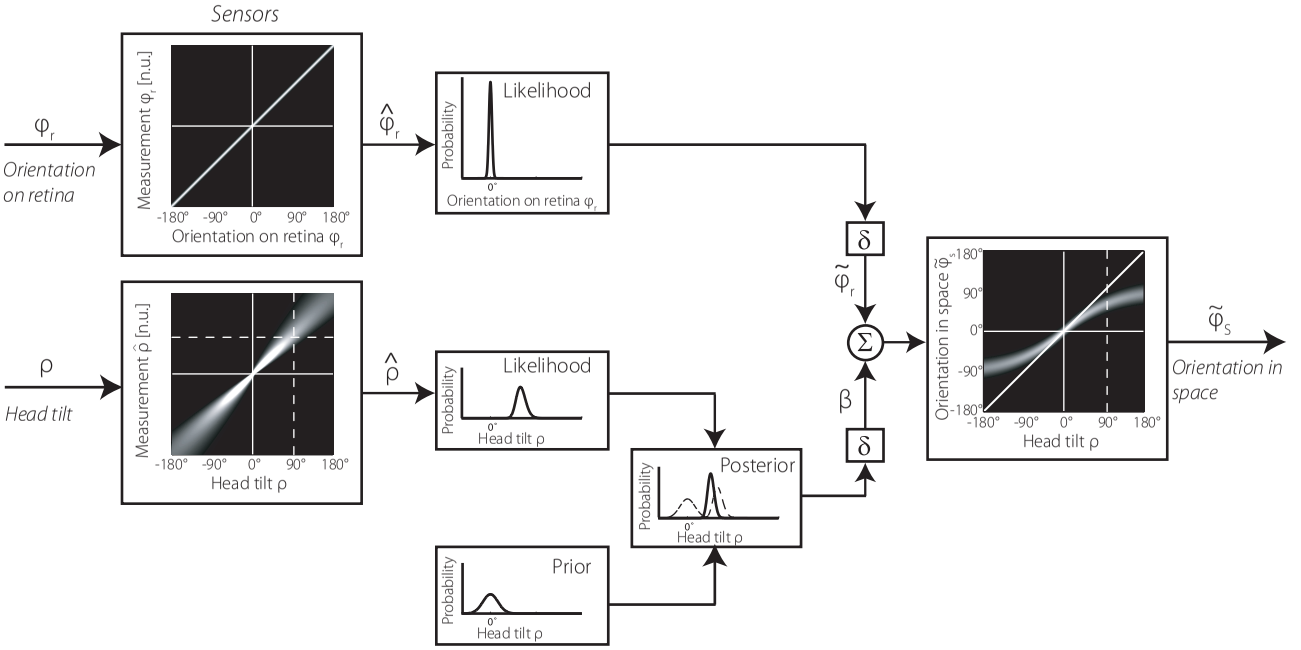

Figure 2.3 *Schematic presentation of the Bayesian observer model. Two inputs: visual orientation of the stimulus on the retina φ_r and head tilt ρ. The sensory tilt signal $\hat{\rho}$ is assumed accurate but contaminated by noise, which increases linearly with tilt angle (bottom left square panel). In the indicated example, the 90°-tilted observer receives the neural signal corresponding to the horizontal dotted line and computes the likelihood, $P(\hat{\rho} \mid \rho)$, of corresponding tilt angles. The likelihood is multiplied with the tilt angle's prior probability $P(\rho)$, which peaks at 0° tilt and does not depend on head-tilt angle. The resulting optimal posterior probability distribution of tilt angles $P(\rho \mid \hat{\rho})$ is biased with respect to the likelihood function. A decision rule δ is imposed to select the compensatory tilt angle β with maximum posterior probability (MAP). The visual system (top left panel) provides an unbiased visual signal $\hat{\varphi}_r$ with a noise level that does not depend on the orientation of the stimulus on the retina, illustrated here for $\hat{\varphi}_r = 0°$. Since the prior for visual orientation (not shown) is assumed to be flat, the observer selects the orientation $\tilde{\varphi}_r$ with maximum probability (decision rule δ). The world-centered orientation of the visual stimulus $\tilde{\varphi}_s$ is then obtained by a linear combination of the compensatory tilt signal and the visual orientation, $\beta + \tilde{\varphi}_r$. The three square panels show the probability densities of the sensory signals (left panels) and the output signal (right panel). The estimated visual orientation in the world $\tilde{\varphi}_s$ shows a clear bias with respect to the real orientation φ_s at the larger tilt angles. In the experiments, subjects adjust the orientation of the visual stimulus so that $\tilde{\varphi}_s = 0°$. Sensory signals are in neural units (n.u.)*

Bayesian model

Mittelstaedt's model assigns a major role to a deficiency in the accuracy of the sensory tilt signal to explain the response biases. In the following, we explore an alternative explanation, a so-called Bayesian model, which rather focuses on the precision of the tilt signal. Although the Bayesian account is similar to Mittelstaedt's vector-averaging model in various aspects (Eggert, 1998; MacNeilage et al., 2007), some of its basic assumptions are different, as we subsequently explain. In the literature, Bayesian models are used to deal with various sources of information to optimize performance in the context of optimal observer theory (e.g., Knill and Pouget, 2004; Körding and Wolpert, 2004). These frameworks have been applied successfully in studies reporting perceptual biases. For example, in visual speed perception, a Bayesian model has been used to explain the finding that subjects systematically underestimate object speed when stimulus contrast is reduced (Stocker and Simoncelli, 2006). Recently, Niemeier et al. (2003) provided evidence that optimal handling of noisy efference copy signals could account for the reduced ability to detect object motion during a saccade. In other words, as these examples show, an apparent shortcoming of the system may actually reflect optimal Bayesian processing.

We designed an optimal observer model, which is schematically illustrated in Figure 2.3, to test whether our results would fit a Bayesian framework. This model is designed to combine noisy signals in an optimal fashion, which means that it deals with probability distributions rather than with deterministic signals. Inputs to the model are head orientation in space ρ and the orientation of the visual line (or the direction of visual motion) with respect to the retina φ_r. These inputs are measured by the (noisy) sensors, which provide two sensory signals ($\hat{\rho}$ and $\hat{\varphi}_r$) to the observer. A major source for the sensory head tilt signal $\hat{\rho}$ are the otoliths, but other sensory systems, like somatosensory afferents (Bronstein, 1999) and the semicircular canals (Jaggi-Schwarz and Hess, 2003; Pavlou et al., 2003; Kaptein and Van Gisbergen, 2006), may contribute as well. The model assumes that the sensory tilt signal is veridical on average, but rather noisy in comparison with the sensory visual signal $\hat{\varphi}_r$. Thus computing the orientation of the line in space φ_s, simply by a straightforward combination of incoming sensory signals, would yield a noisy spatial percept. The key feature of Bayesian models is that, along with sensory information, *prior knowledge* is taken into account to obtain a statically optimal estimate. Application of this notion in the present model means that the observer uses prior knowledge about head tilt, implying that small tilts are most likely, to improve the internal tilt signal. This computational strategy comes at a price: although the reliance on prior knowledge has the beneficial effect of noise reduction at small tilts, this also causes systematic errors at larger tilts (further explanation is subsequently presented). Since Bayesian processing of the tilt signal applies to a stage before the computation of the line vertical and of the motion vertical, the model predicts the same tilt-dependent response bias in both tasks. A further interesting feature is that the model simultaneously makes quantitative predictions about both response bias and scatter. Before describing the mathematical structure of the model in detail, we will first list its assumptions and approximations.

Assumptions and approximations

First, sensory signals from the visual system and from the head-tilt detecting system are contaminated with independent Gaussian noise. Second, for the sake of simplicity, we ignored the oblique effect (Löffler and Orbach, 2001; Luyat et al., 2001; Krukowski et al., 2003) and assumed that visual noise is independent of line orientation or direction of visual motion on the retina. Third, errors due to imperfect compensation for ocular countertorsion (Curthoys, 1996) were ignored. Fourth, the model uses a priori information by assuming that the head is mostly oriented near upright, which is implemented by a Gaussian probability distribution that peaks at zero tilt. We purposely used Gaussians to find the analytical solutions of the model, but we are aware that they do not account for the periodic nature of spatial orientations. Space periodicity, however, can be neglected in the modeled tilt range (-120 to 120°), under the requisite that the width of the Gaussian distribution is kept at a moderate level.

Internal tilt representation

Guided by Figure 2.3, we now describe the sequential computational steps to obtain β, the central tilt signal that ultimately transforms retinal signals to spatial coordinates. We assume that the signal $\hat{\rho}$, provided by head-tilt sensors, is accurate but contaminated by noise. The noise parameters of the tilt signal will be subsequently specified (see Eq. 2.10). For a proper understanding of the model, it is of interest to look at this relation from two opposite perspectives. The forward perspective, indicated by the vertical dashed line in the *left bottom panel*, specifies the distribution of $\hat{\rho}$ signals that is produced at the various tilt angles. This is the viewpoint of the neurophysiologist who varies the head-tilt angle and records the sensory signal. The CNS, however, must adopt the inverse perspective. When it receives the sensory signal indicated by the horizontal dashed line, for example, the brain must find out which tilt angle may have been responsible. Because the tilt signal is noisy, this inverse problem has no unique solution, so a statistical approach is required. The Bayesian scheme applies knowledge of the forward ρ–$\hat{\rho}$ relationship to compute the probability that any particular tilt angle produced the incoming sensory signal. The result of this computation, the likelihood function $P(\hat{\rho} \mid \rho)$, is based exclusively on the sensory evidence $\hat{\rho}$. Note that the likelihood is a function of tilt angle ρ and that more sensory noise yields a broader distribution and thus an increased uncertainty about which tilt angle may have caused the sensory signal. To optimize the tilt estimate, the observer should take into account which tilt angles are likely on an a priori basis, as expressed by the prior distribution $P(\rho)$, which is shown in the middle part of Figure 2.3. The resulting probability of any particular tilt angle, given the combination of sensory evidence and prior knowledge, is termed the *posterior* probability distribution $P(\rho \mid \hat{\rho})$, which follows from the product of likelihood and prior

$$P(\rho \mid \hat{\rho}) = \frac{P(\hat{\rho} \mid \rho) \cdot P(\rho)}{P(\hat{\rho})} \qquad \text{Eq. 2.6}$$

where the probability $P(\hat{\rho})$ in the denominator serves a normalization purpose. Note that the posterior peaks in between the prior and the likelihood (compare panels in Figure 2.3). The exact location of the peak depends on the relative widths of the prior and the likelihood (Carandini, 2006). Finally, once the posterior distribution has been computed, the brain

needs a decision rule (δ) to obtain β. We assumed that the observer selects the tilt angle with highest probability, the *maximum a posteriori* (MAP) estimate. Note that the internal tilt signal β will vary in repeated trials due to sensory noise. Because the prior and likelihood are approximated as Gaussian distributions, the model predicts that the distribution of internal tilt angles β is also a normal distribution centered at a mean value

$$\bar{\beta}(\rho) = \frac{\sigma_p^2}{\sigma_p^2 + \sigma_{tilt}^2} \cdot \rho \qquad \text{Eq. 2.7}$$

and with SD

$$\sigma_\beta = \frac{\sigma_p^2}{\sigma_p^2 + \sigma_{tilt}^2} \cdot \sigma_{tilt} \qquad \text{Eq. 2.8}$$

with σ_p and σ_{tilt}, the SDs of the prior distribution and the sensory tilt signal, respectively. A more detailed derivation of Equations 2.7 and 2.8 can be found in the *Appendix*. Equation 2.7 quantifies how the bias in β (the difference between β and ρ), caused by the prior, depends on prior width and tilt noise. Note that the *ratio* of prior width and tilt noise determines the bias in β. A further effect of the prior is that the noise in the internal tilt estimate σ_β is smaller than the noise introduced by the tilt sensors σ_{tilt}, as shown in Eq. 2.8. Thus the narrower the prior, the larger the bias and the smaller the scatter in the internal tilt representation. Processing of the visual signal $\hat{\varphi}_r$ in the model involves a likelihood function, $P(\hat{\varphi}_r \mid \varphi_r)$, but no prior knowledge (flat prior, not shown). As a consequence, application of the MAP decision rule means that the most likely retinal orientation $\hat{\varphi}_r$ simply equals the peak of the likelihood function.

Predicted tilt dependence of systematic and random errors

The output of the model is the space-centered orientation of the visual stimulus $\hat{\varphi}_s$, which follows from the linear combination of tilt representation β and retinal orientation estimate $\hat{\varphi}_r$ (see Figure 2.3, *right panel*). Since the visual signal is assumed to be unbiased on average, the model predicts that the systematic errors in the output $\bar{\gamma}$ simply reflect the bias in the internal tilt estimate β with respect to actual tilt angle ρ (see Eq. 2.3). If σ_{tilt} has a constant tilt-independent value, the systematic error $\bar{\gamma}$, given by

$$\bar{\gamma}(\rho) = \frac{\sigma_p^2}{\sigma_p^2 + \sigma_{tilt}^2} \cdot \rho \qquad \text{Eq. 2.9}$$

will depend linearly on the actual tilt angle ρ. However, to account for the nonlinear relationship between $\bar{\gamma}$ and tilt angle ρ, observed in the actual results (see Figure 2.5), we allowed σ_{tilt} to increase rectilinearly with tilt angle

$$\sigma_{tilt}(\rho) = a_0 + a_1 \mid \rho \mid \qquad \text{Eq. 2.10}$$

with parameter a_0, the offset, representing the noise (SD) in the tilt signal at 0° head tilt and parameter a_1, the slope (°/°), specifying how σ_{tilt} increases with tilt angle. Note that the tilt dependence in Eq. 2.10 causes a slight skewness in the likelihood function, which was neglected in fitting the experimental data to enable a straightforward analytical fitting procedure. The

model also makes a quantitative prediction of the random errors σ_γ, which depend on the combination of noise in the visual signal σ_v and noise in the internal tilt estimate σ_β, as specified by Eq. 2.5 ($\sigma_\gamma^2 = \sigma_\beta^2 + \sigma_v^2$). Due to the tilt dependence of the noise in the sensory tilt signal (Eq. 2.10), output scatter also increases with tilt angle.

In conclusion, the Bayesian model contains three parameters —a_0, a_1, and σ_p— to determine the mean value and scatter of the internal tilt estimate β; each of these three parameters has an effect on both. Two additional parameters, σ_{vl} and σ_{vm}, which represent the visual noise in the line task and motion task, respectively, are required to fit the scatter in the output error σ_γ, in the two tasks.

Fitting procedures

Both models make predictions about the relationship between the error in the space-centered orientation of the visual stimulus γ and the physical roll-tilt angle ρ. We used the experimental response errors from both the motion- and line-adjustment tasks, to obtain best-fit parameters for the two models (see *Results*). Motion and line data from all subjects were fitted simultaneously. A maximum-likelihood estimation (MLE) procedure was applied for the two models, which has the advantage of fitting both systematic and random errors at the same time.

Mittelstaedt's idiotropic-vector model

We obtained the best-fit values of M, S, C, σ_{vl}, and σ_{vm} by minimizing the negative log-likelihood using the fmincon routine (Matlab 7.0; The MathWorks) and a multistart procedure using different initial parameters.

The log-likelihood function $L(\theta)$ is given by $L(\theta) = \sum_{i=1}^{n} \log[P_\theta(\gamma_i \mid \theta)]$, in which $P_\theta(\gamma_i \mid \theta)$ represents the chance of obtaining error γ_i given a particular parameter set θ. We reduced the degrees of freedom by allowing only parameter M to account for intersubject differences. This approach resulted in a total of 12 free parameters (8 + 4) to fit the line and motion data from all eight subjects. Confidence intervals of the best-fit parameters were determined by 100 bootstraps (Press et al., 1992).

Bayesian model

Best-fit values for a_0, a_1, σ_p, σ_{vl}, and σ_{vm} were found by minimizing the negative log-likelihood, using the same approach as in the fits of the idiotropic-vector model. Confidence intervals of the best-fit parameter values were obtained using bootstrapping techniques. Since leaving all five parameters free in each subject caused overfitting, we reduced the degrees of freedom by allowing only a single parameter to account for intersubject differences. This approach resulted in a total of 12 free parameters (8 + 4) to fit the line and motion data from all eight subjects. We explored three fit versions of the Bayesian model, in which either the offset a_0, the slope a_1, or the prior width σ_p was chosen as the free parameter.

RESULTS

We investigated the ability to compensate for static body tilt, when judging the spatial direction of visual motion, by determining the motion vertical. For comparison, we also tested the sense of line verticality by using the classical luminous-line task. The main body of results was obtained with an adjustment method in which subjects aligned the direction of a moving-dot pattern or the orientation of a luminous line to the perceived direction of gravity. In a further control experiment, we used a psychometric approach to verify that subjects relied on a global motion percept rather than single-dot motion vectors, when judging the earth-centric motion direction of the random-dot pattern.

Compensation for body tilt is incomplete

The adjustment task measured the ability to set the direction of a moving-dot pattern or the orientation of a visual line parallel to the direction of gravity. Both the motion vertical and the line vertical were tested at various body tilt angles, ranging from -120 to 120°. If subjects were to compensate perfectly for their body orientation, compensation angle β (see Figure 2.1) would be equal to body tilt angle ρ. If they did not compensate for tilt, always taking the long body axis as the direction of gravity, compensation angle β would be zero. Figure 2.4 shows the actual degree of compensation in the two tasks for each tested tilt angle. The *top panels*, which illustrate the results from a typical subject, immediately convey the impression

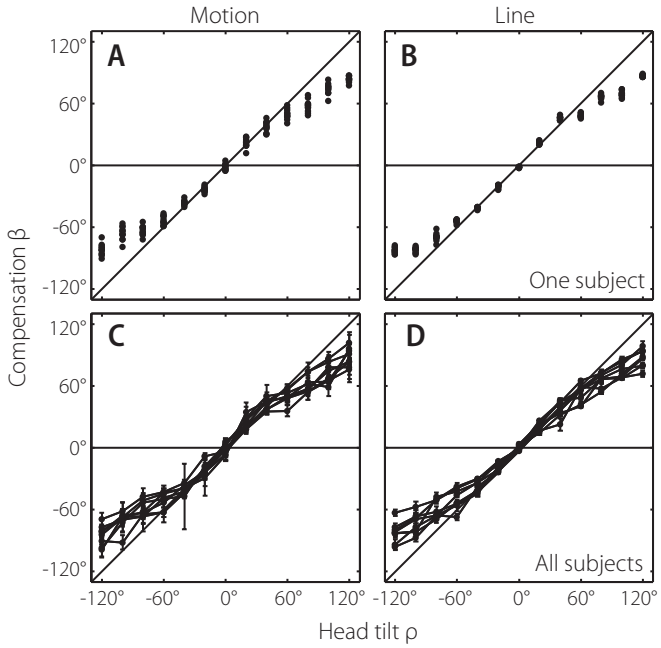

Figure 2.4 Performance in the motion (left) and line (right) adjustment tasks. Compensation angle (β) plotted versus tilt angle ρ. Diagonal line: perfect compensation. Top panels: one subject (SP). Each data point represents one adjustment. Bottom panels: all subjects. Error bars: SD. Compensation patterns in motion and line task are very similar.

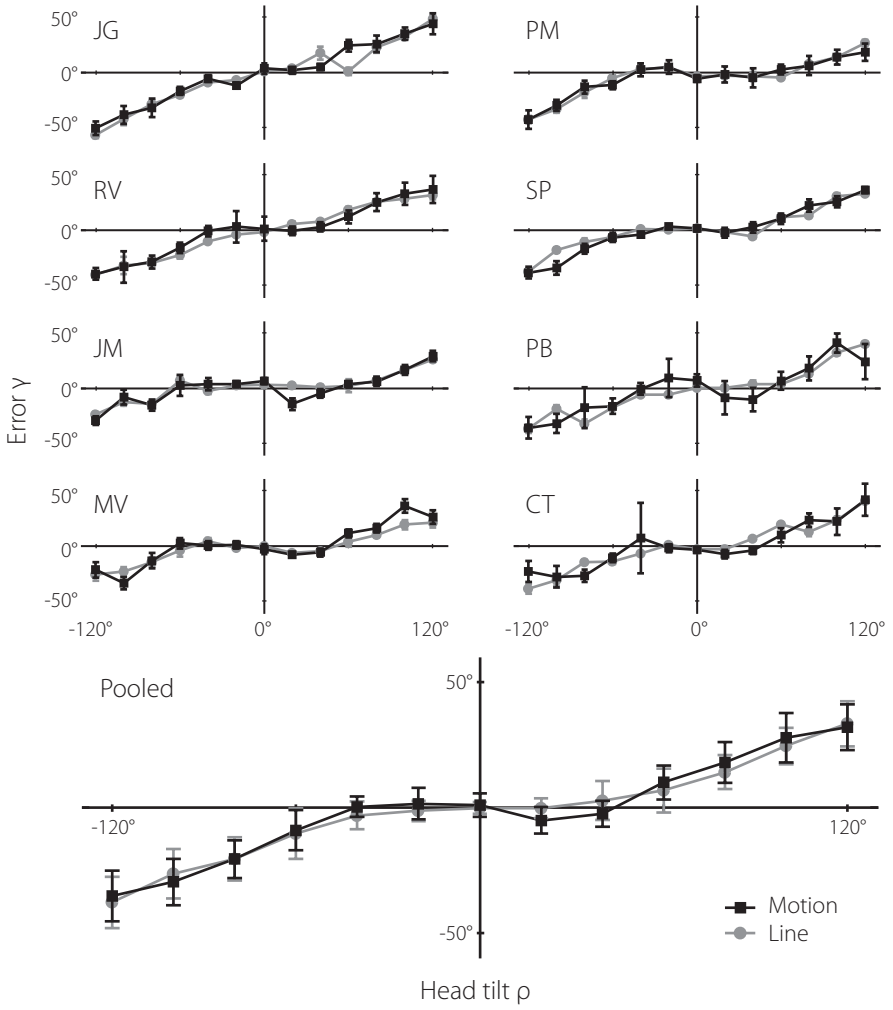

Figure 2.5 Errors γ in the motion and line adjustment tasks, plotted versus head tilt angle ρ for all subjects. Motion task: black squares and line. Line task: gray circles and line. Error bars: SD. Error patterns are qualitatively similar across subjects and tasks, with almost no errors at smaller body tilt angles and sizable errors at the largest body tilt angle. Bottom panel: Mean responses, averaged across all subjects.

of a strikingly similar pattern of compensation in the two tasks. Compensation is nearly flawless for absolute tilts <60°, with misalignments remaining <10°. Furthermore, in both tasks, compensation does fall substantially short for tilt angles >60°, as if the amount of body tilt is underestimated, with errors ranging up to 40° in this subject. The only noticeable difference in task performance is that settings in the motion task are noisier than those in the line task. This phenomenon, however, need not reflect a difference in the actual spatial computation. It probably indicates a visual factor in the sense that detecting the direction of motion was less precise, partly due to our particular task design and partly because this task requires more temporal integration than estimating the orientation of a line.

The other subjects also show a similar compensation pattern in both tasks, as demonstrated in the *bottom panels* of Figure 2.4, although there is some intersubject variability. Thus at first sight, the motion vertical and line vertical are quite comparable, with both tasks showing a pattern of errors that agrees quite well with previous reports about the perception of line verticality (Mittelstaedt, 1983; Van Beuzekom et al., 2001).

To investigate the similarity of performance in the two tasks in more detail, Figure 2.5 makes a direct comparison by showing response error (mean ± SD) as a function of tilt angle for each subject separately. As shown, error profiles for the motion task (black line) and line task (gray line) show strong resemblance within each subject, with only subtle systematic differences. Although only small errors occur at tilt angles <60°, verticality misjudgments become quite substantial at larger body tilts, with clear differences across subjects. For example, subject JG makes errors of about 50° in both tasks when the body is tilted to 120°, whereas the errors of subject JM remain limited to 30°. Although most errors represent an undercompensation for body tilt ($\beta<\rho$), there are occasional signs of overcompensation at smaller tilt angles. For instance, subjects PM and MV produce errors in the direction opposite to body tilt at the smallest body tilt angles (±20 and ±40°). Subject PB overcompensates only in the motion task. The mean pattern of errors across subjects (Figure 2.5, *bottom*) further underlines the similarity of performance in the two tasks. A repeated-measures two-way ANOVA confirmed this by showing no significant main effect of task [$F(1,7) = 1.41$, $P = 0.27$]. Not surprisingly, the effect of tilt angle is highly significant [$F(12,84)=67.9$, $P << 0.001$], consistent with the general increase in systematic errors as a function of tilt angle. The slight overcompensation for small tilt angles (±20 and ±40°) in the motion task is mainly due to subject PB, and to a lesser extent to subjects RV and CT. Across subjects, however, the interaction between task and tilt angle was not significant [$F(12,84)=1.72$, $P = 0.08$].

To further illustrate the comparable performance in the two tasks, Figure 2.6A plots the mean error in the motion task against the mean error in the line task, lumped across all subjects and tilt angles. Data points scatter about the identity line.

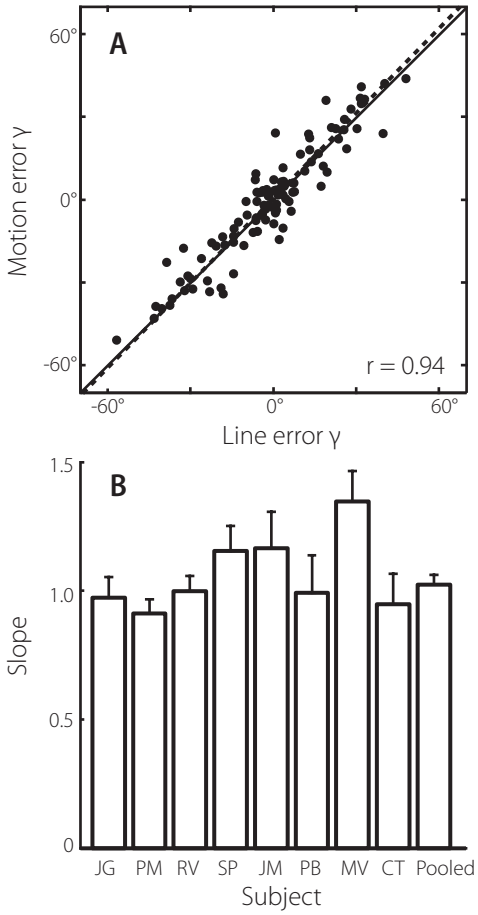

Figure 2.6 Error comparison. A. Motion errors versus line errors pooled across subjects. Regression line: slope = 1.02, r = 0.94. B. Same analysis within subjects, with 0.89 < r < 0.98. Slopes vary between 0.91 and 1.35. Error bars: SD.

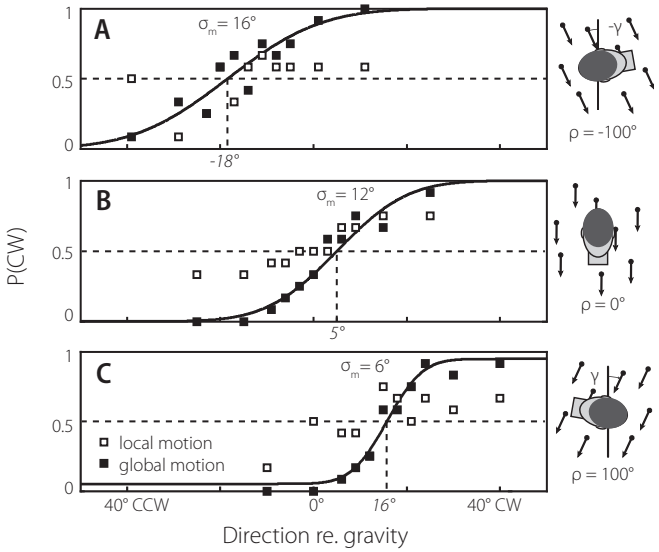

Figure 2.7 Psychometric analysis. Data from one subject (JM) in the local motion and global motion forced-choice tasks at the three tested angles (A: -100°, B: 0° and C: 100° tilt). Clockwise (CW)-response rates, P(CW), of local motion data (□) and global motion data (■) are plotted against stimulus direction (motion task) or orientation (line task) with respect to gravity. Solid line: best-fit cumulative Gaussian through the global motion data. Lapses cause deviations from maximum performance (mean lapse rate: 2.7%). Vertical dashed line: mean μ of the cumulative Gaussian. Local motion data mostly remain close to chance level, P(CW) = 0.5.

Because both variables are subject to measurement errors, a type-II regression (also referred to as a major-axis regression) was used to determine their relationship for each subject. Slope and confidence limits were estimated by the bootstrap method. Correlation coefficients range between 0.89 and 0.98 and slopes vary between 0.91 and 1.35 across subjects (Figure 2.6B). In all subjects but one (MV), a slope of 1 is within the 95%-confidence limits. The average slope (±SD) across subjects is 1.02 ± 0.04, suggesting a one-to-one relationship between the errors in the two tasks. Thus we conclude that systematic errors in the two tasks are virtually identical.

Global versus local motion

Can the quite similar biases in the motion vertical and line vertical be taken as evidence that the alignment with gravity in the two adjustment tasks was facilitated by the same computational strategy? A potential caveat emerges if performance in the motion task was not based on the processing of global motion by spatial integration, as the experimental paradigm intended. Instead, subjects might have derived a percept of visual direction in space by temporally integrating the extrapolated motion paths of individual signal dots. The similarity in results that we found earlier would be trivial if this surrogate line strategy, however unlikely it may seem, had actually been used in the motion task. To exclude this possibility in a further experiment, four subjects were tested in a global and a local motion task, using a forced-choice paradigm (see *Methods*). The local motion forced-choice task enforced a strategy of judging the motion of a single dot, which was subject to the same

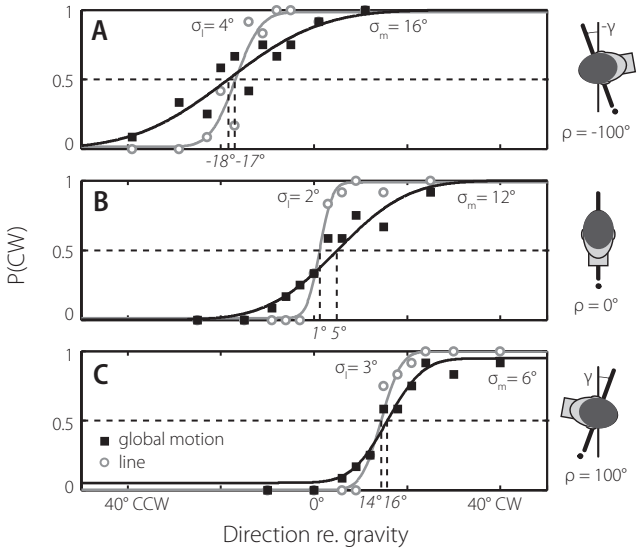

Figure 2.8 Psychometric analysis. Data from one subject (JM) in the global motion and line forced-choice tasks at the three tested angles (A: -100°, B: 0° and C: 100° tilt). CW-response rates, P(CW), of global motion data (■) and line data (O) are plotted against stimulus direction (motion task) or orientation (line task) with respect to gravity. Solid line: best-fit cumulative Gaussian through motion data. Gray line: best-fit cumulative Gaussian through line data. Vertical dashed lines: mean values of curves, representing line and motion vertical. Global motion data and the corresponding best-fit curves were taken from Figure 2.7.

motion statistics as the dots in the global motion task. We may conclude that subjects made use of a global motion percept if their performance in the local motion forced-choice task is significantly worse than that in the global motion forced-choice task.

To compare performance in the two tasks for a typical subject at each of the three tested tilt angles, Figure 2.7 shows the proportion of clockwise responses, P(CW), as a function of motion direction of the stimulus relative to gravity. The results are clear: performance in the local motion task is substantially worse than that in the global motion task. The fraction of CW responses in the global motion task (■) covers the whole range between 0 and 1, indicating that stimulus levels were placed correctly in the relevant tilt range. Data from the local motion task (□) show a very different pattern. Subjects never reach optimal response levels, showing response rates that remain close to the 0.5-chance level for all stimulus directions. In a first step to further quantify these results, we fitted psychometric curves to the global motion data. These curves, shown by the solid lines, provide a good description of the data, with R^2>0.86. This curve is characterized by two parameters: threshold and slope. The threshold, which is the mean of the cumulative Gaussian function, is a measure for the subjective motion vertical. Its value corroborates the results from the motion-adjustment task at these tilt angles. At the large tilt angles, the sense of motion verticality deviates from the actual direction of gravity by an amount ranging from about -18 to -43° at -100° tilt and from 16 to 37° at 100° tilt. At 0° tilt, the motion vertical is quite veridical, with errors <5°. The SD of the fitted Gaussian, which represents the subject's uncertainty about motion verticality, is relatively constant across the three tilt angles. It ranges from 8 to 16° at -100° tilt, from 6 to 12° at 100° tilt, and

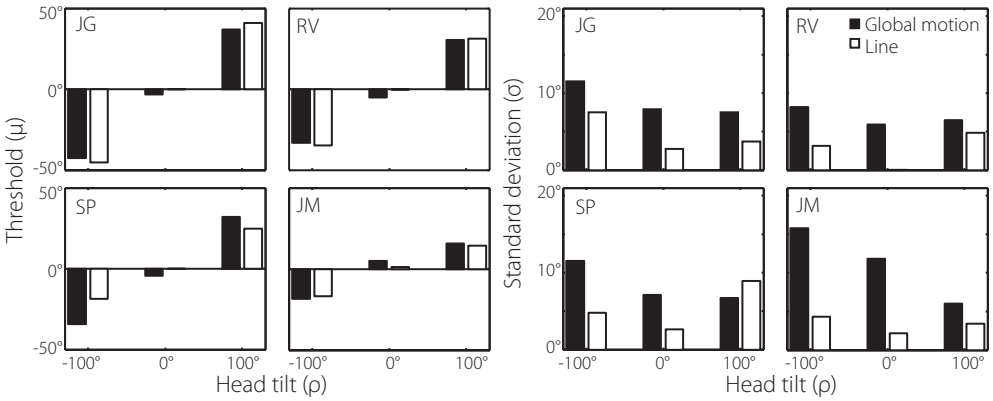

Figure 2.9 Threshold μ and standard deviation σ from psychometric fits to global motion data (white) and line data (black). Left: Individual thresholds for each tested head tilt angle ρ. Right: Corresponding standard deviations

from 6 to 8° at 0° tilt.

Because asymptotic performance in the local motion task remained <100%, fitting a psychometric curve through these data would be questionable. We assessed the difference in performance with the global motion task by examining the deviation of the local motion data points from the psychometric curve fitted through the global motion data. A likelihood ratio test confirmed that the local motion response frequencies, P(CW), were significantly different from the Gaussian probability that was fitted through the global motion data $\chi^2(12,11)>49.4$, $P<<0.01$ for each test performance (4 subjects, 3 tilt angles). Taken together, this analysis firmly rules out that subjects used a single-dot strategy in the global motion task.

Comparison of global motion and line results

To complete analysis of the control experiments, we investigated whether the similarity between motion vertical and line vertical in the adjustment tasks was upheld in the psychometric experiments. Figure 2.8 shows results of the global motion forced-choice and line forced-choice tasks from the same subject as in Figure 2.7. Psychometric curves of the line data (dashed lines) had R^2-values>0.82. Psychometric line and motion thresholds are rather similar at each tilt angle. As indicated by the steeper slopes of the line fits, subjects were less

Table 2.1 Best-fit parameter values of Mittelstaedt's idiotropic model.

Subject	M-vector	S	C (°)	σ_{VL} (°)	σ_{VM} (°)	R^2
JG	0.65 [0.02]	0.64 [0.01]	6.9 [0.5]	0.5 [1.3]	7.6 [0.7]	0.96
PM	0.32 [0.01]					0.83
RV	0.56 [0.02]					0.97
SP	0.39 [0.01]					0.96
JM	0.24 [0.01]					0.87
PB	0.45 [0.01]					0.89
MV	0.30 [0.01]					0.89
CT	0.45 [0.01]					0.92

Bootstrap-based confidence intervals between brackets. Imposed fit limits were, M: 0-10, S: 0-1 C: 0.1°-100°, σ_{vl} and σ_{vm}: 0.2°-20°.

certain about the motion vertical than about the line vertical.

Figure 2.9 depicts the threshold and SD values derived from the psychometric fits in all subjects. Thresholds in the line and global motion tasks are not significantly different (paired t-test, P=0.40). Moreover, thresholds in both tasks are not significantly different from the mean errors found in the adjustment experiment (paired t-test, motion task: P=0.09, line task: P=0.47). Standard deviations are significantly larger in the motion task, for all tilt angles and subjects (paired t-test, P<<0.01). This can be explained, at least partly, by assuming that the visual noise was more pronounced in the global motion task than that in the line task.

Model predictions and fits

In the *Methods*, we described two models to account for the error patterns described earlier, Mittelstaedt's idiotropic vector model (1983) and a new Bayesian model. Since both schemes imply that systematic errors reflect handling of the compensatory tilt signal, rather than processing in the visual pathway, both models predict that error patterns are identical in the line and motion tasks. We fitted the two models to the adjustment data from our eight subjects (see *Methods* for details), the results of which will be described next.

Mittelstaedt's idiotropic-vector model

Figure 2.10 shows fit results of Mittelstaedt's idiotropic-vector model (gray line) to the observed systematic errors in the line vertical and motion vertical. The model fits the data quite accurately, with goodness-of-fit values of R^2>0.82. Note that the model accounts for both underestimation and overestimation errors (see JM and PM). Best-fit parameter values are listed in Table 2.1. Parameter S has a best-fit value of 0.64, which is roughly comparable to the value (S = 0.58) found by Mittelstaedt (1983). As expected, subjects with larger systematic errors also have higher M-values (e.g., M =0.65 for subject JG vs. M =0.24 for JM), in line with the fact that a larger idiotropic vector has a stronger biasing effect. We conclude that the model can account very well for the pattern of systematic errors in both tasks with just a single free parameter for each subject.

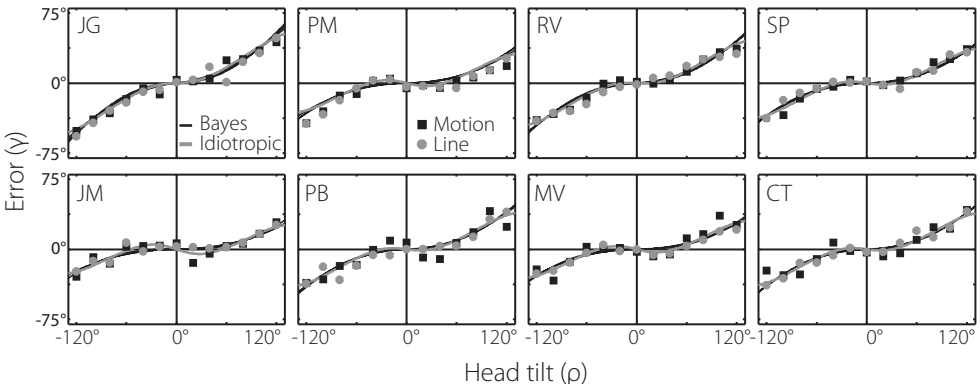

Figure 2.10 Model fits to systematic errors. Individual fits of the three Bayesian fit versions (solid lines) and the idiotropic model (gray line). The three Bayesian fit versions can hardly be distinguished from each other. Fits were performed to motion (■) and line (○) data simultaneously.

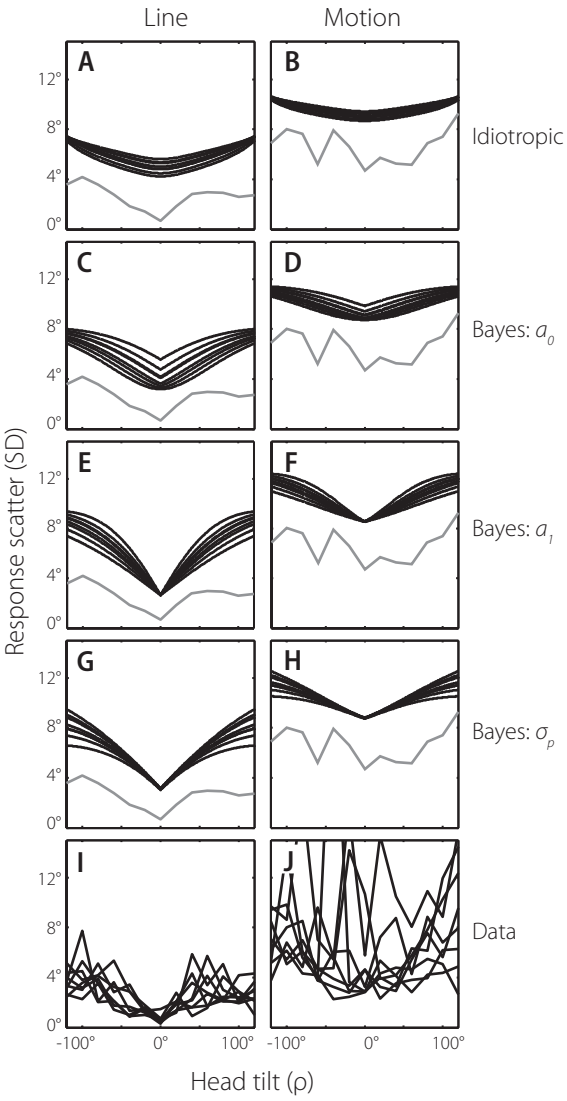

Figure 2.11 Model fits to random errors. Individual response scatter predictions by the two models for the line task (left panels) and motion task (right panels). Top row (A, B): the idiotropic model. Middle three rows (C-H): three Bayesian model fit versions. Plots show the effect of different choices of the free parameter in the Bayesian model. Panels C, D: a_0 (tilt noise at 0° tilt). Panels E, F: a_1 (increase of tilt noise with tilt angle). Panels G, H: σ_p (width of prior distribution). Bottom row (I, J): individual scatter data for the two tasks. Gray lines: mean from the data.

Can the model account equally well for the random errors in the data? Figure 2.11 (*top panels*) shows the model fits for the line task (Figure 2.11A) and the motion task (Figure 2.11B) together with the mean scatter curve across subjects (gray line). As can be seen, Mittelstaedt's model accounts for the increase in response scatter with tilt angle, seen in the data. However, the shape of the scatter–tilt relation is not well captured by the model, which also falls short in fitting the stereotyped scatter level in upright. The most glaring discrepancy between the data and the fit—the fact that the predicted scatter exceeds the actual scatter roughly twofold—calls for an explanation. Why did the MLE fit procedure not simply adopt a smaller *C* value (see Eq. 2.4) to prevent this problem in the first place? To understand why this would not improve model performance, it should be recalled that the scatter level in the MLE fit reflects two factors: not just the actual data scatter at each tilt angle, but also the subtle discrepancies between the fit line and the local data average. Since the former is shown in the panels, but the latter is not, the discrepancy between predicted and actual scatter levels should not immediately be taken as a weak spot in the model. Since it is much more difficult to determine the precision characteristics of the system than its degree of accuracy, the issue cannot be resolved quickly. Only future testing of response scatter on a more massive scale (multiple trials, separate runs) can reveal whether the gap between predicted and actual scatter level is apparent or real.

Table 2.2 Best-fit parameter values of the three fit versions of the Bayesian model.

Common parameter	Fit version 1		Fit version 2		Fit version 3	
a_0 (°)	free		2.5 [0.3]		3.2 [0.2]	
a_1 (°/°)	0.06 [0.00]		free		0.07 [0.00]	
σ_p (°)	14.8 [0.8]		18.7 [0.9]		free	
σ_{VL} (°)	3.2 [0.3]		1.1 [0.7]		0.2 [0.3]	
σ_{VM} (°)	8.7 [0.5]		8.2 [0.6]		8.2 [0.3]	
Subject	a_0 (°)	R^2	a_1 (°/°)	R^2	σ_p (°)	R^2
JG	5.1 [0.3]	0.96	0.12 [0.01]	0.95	13.2 [0.5]	0.96
PM	1.2 [0.2]	0.83	0.07 [0.01]	0.81	20.4 [0.9]	0.81
RV	3.7 [0.2]	0.95	0.10 [0.01]	0.93	15.3 [0.5]	0.94
SP	1.7 [0.2]	0.95	0.08 [0.00]	0.95	18.1 [0.7]	0.95
JM	0.0 [0.0]	0.85	0.05 [0.00]	0.81	24.0 [1.1]	0.82
PB	2.8 [0.2]	0.87	0.09 [0.01]	0.87	17.0 [0.6]	0.87
MV	0.7 [0.2]	0.84	0.06 [0.00]	0.84	21.5 [0.9]	0.83
CT	2.6 [0.2]	0.91	0.09 [0.01]	0.91	17.0 [0.5]	0.91

Bootstrap-based confidence intervals between brackets. Imposed fit limits were, a_0: 0°-10°, a_1: 0-3°/°, σ_p: 2°-50°, σ_{vl} and σ_{vm}: 0.2°-20°. Fit limits were only reached in subject JM in fit version 1, in which tilt-noise parameter a_1 reached its lower limit and in fit version 3, in which visual-noise parameter σ_{vl} reached its minimum value.

Bayesian model

For reasons outlined earlier in *Methods*, we tested three fit versions of the model, each imposing a different set of constraints on the fit. Version 1 allowed tilt noise parameter a_0 (see Eq. 2.10) to vary among subjects, whereas the remaining four parameters were determined as a best-fit value across subjects. The approach in the other fit versions was similar, except that now only tilt noise parameter a_1 (version 2) or the prior width σ_p (version 3) was free to vary among subjects, whereas the remaining parameters were fit as a single value across subjects. The fit was applied simultaneously to both systematic and random errors from the line and motion tasks, using MLE (see *Methods*).

Figure 2.10 presents the results of this analysis for the systematic errors, showing the fits of all three versions superimposed on the data. The fitted curves are practically indistinguishable. All three versions had goodness-of-fit values R^2>0.80 (see Table 2.2). In contrast to Mittelstaedt's model, the Bayesian model cannot account for errors of overestimation, as seen in subjects PM and JM. Table 2.2 lists the best-fit parameter values for the three Bayesian model fit versions. Clearly, it would be pointless to prefer any of these fit versions based on their account of the systematic errors. In other words, according to the model, the pattern of errors may equally well be caused by a higher tilt noise offset, a_0 (version 1); a steeper increase of tilt noise with tilt angle, a_1 (version 2); or a narrower prior, σ_p (version 3). That being said, there is an interesting observation to make across the three fit versions: the best-fit value of parameter a_1 is invariably positive (see Table 2.2). The important implication of this result is that tilt noise must increase with tilt angle if our Bayesian model is to account for the present data. Not surprisingly, all three fit versions indicate that visual noise in the motion task σ_{vm}, which ranged from 8 to 9°, is larger than that in the line task σ_{vl}, where it reached values ≤3.2°.

Following the demonstration that the three fit versions account about equally well for the systematic errors in the data, Figure 2.11, C–H compares their ability to predict the random errors. In general, all three versions predict scatter levels above those in the data (gray line), for similar reasons as mentioned previously for Mittelstaedt's model. Interestingly, all fit versions predict scatter levels to increase with tilt angle, which is consistent with the positive values for a_1, seen in Table 2.2. However, only versions 2 and 3 seem to match the finding that individual scatter levels at 0° tilt are practically identical (see Figure 2.11, I and J).

In conclusion, both models account very well for the virtually identical pattern of systematic errors in the motion vertical and line vertical, which they interpret as the result of central processing of the compensatory tilt signal. Neither model fully matches the random errors in the data, although it appears that the Bayesian model accounts slightly better for the tilt dependence of the variable errors in the data. In this respect, the Bayesian model, which sheds a new light on the origin of biased verticality percepts, has emerged as a viable alternative that deserves further exploration.

DISCUSSION

Recapitulation of main findings

We investigated the brain's ability to account for head tilt when estimating the direction of visual motion in space. We found that incomplete compensation for head tilt at larger tilt angles caused systematic errors in the motion vertical that were virtually identical to those in the line vertical. A trivial explanation of this similarity, implying that the motion vertical might have been based on extrapolated motion paths of single dots, was firmly ruled out by psychometric control experiments. Taken together, our results suggest reliance on a common reference frame for spatial motion and pattern vision during lateral body tilt. Fit results of two spatial orientation models suggest that the pattern of systematic errors in the two tasks may be the downside of a strategy for dealing with imperfections in the sensory tilt signal, which is implemented at a stage preceding the conversion of visual signals from retinal to spatial coordinates. In the following, we explore the merits of these two different modeling perspectives from a wider perspective and in more depth.

Modeling aspects

Both Mittelstaedt's idiotropic-vector model and the Bayesian observer model proposed here link errors in the motion vertical and line vertical at large tilts to a strategy for dealing with imperfections in the sensory tilt signal (MacNeilage et al., 2007). The two models propose that the resulting biased tilt representation is used to convert the retinal signals into an earth-centric reference frame, which explains the strong resemblance of the systematic errors in both visual subsystems.

Rationale behind the biasing mechanisms in the two models differs

Both schemes assume that the raw sensory tilt signal is subject to imperfections, but their ideas about what is imperfect are rather different. Mittelstaedt's model assumes that combining the

signals from the two otolith organs, utricle and saccule, which contain different numbers of hair cells, is a nontrivial problem leading to systematic errors. The Bayesian scheme makes no assumptions about the precise contributions of the otolith organs and allows for the possibility that other sensors may contribute to the raw tilt signal. According to this scheme, the problem with the sensory tilt signal is that it is noisy. Reduction of this noise by using prior knowledge causes systematic errors at large tilt angles. To account for the pattern of systematic errors, it was necessary to extend the standard Bayesian model by the additional parameter a_1, which describes an increase of the noise in the sensory tilt signal with increasing tilt angle.

Are the supposed imperfections of the raw tilt signal realistic?

Although Mittelstaedt's scheme has found wide acceptance in the literature since it can nicely account for the pattern of systematic errors in the subjective vertical, some questions about its basic assumptions can be raised. First of all, the notion that the brain would have problems coping with unequal numbers of utricle and saccule afferents is not immediately convincing. Similar challenges occur in other sensory systems, like vision and the somatosensory system, which show little sign of major distortion in their representation of spatial relationships at the perceptual level. Differences in the number of sensory afferents have well-established perceptual correlates, although these concern primarily differences in discrimination thresholds (e.g., foveal vs. peripheral vision). Second, if the otolith signal is distorted, one would expect this to show up in body tilt estimates as well. Mittelstaedt (1995, 1999) was the first to discover that this was not the case. He showed that subjects, rotated sideways, make distinct errors in the classic line-verticality task, but show virtually no bias in their estimate of body orientation. Other studies have reported similar observations (Mast and Jarchow, 1996; Kaptein and Van Gisbergen, 2004; Bortolami et al., 2006). This clear dissociation between body tilt percept and the visual upright poses an intriguing and nontrivial paradox: Why would errors in the subjective vertical occur when the visual and tilt signals, from which this percept must be derived, are virtually unbiased? Mittelstaedt argued that the idiotropic vector plays a role only in the perception of the subjective vertical but not in the perception of body tilt, which is supported by other sensory cues, such as graviceptors in the trunk.

According to the Bayesian model, the sensory tilt signal is accurate but contaminated by noise, which increases with tilt angle. The suggested dependence of tilt noise on tilt angle may appear controversial since single-unit studies by Fernandez and Goldberg (1976) provide no direct evidence that this is the case. However, at a slightly higher level, the fact that utricle and saccule have unequal numbers of hair cells (Rosenhall, 1972, 1974) may be a relevant factor. As was first shown by Eggert (1998), this arrangement may yield tilt-dependent noise since the utricle, which is most sensitive to head tilts around 0° (upright), would provide a more precise signal than the saccule, which is most sensitive at 90° roll tilt. Further evidence for the dependence of tilt noise on tilt angle comes from perceptual studies showing that the effect of optokinetic stimulation on the subjective vertical (Dichgans et al., 1974) and the sense of body tilt (Young et al., 1975) is stronger at larger tilt angles.

In principle, the Bayesian model can solve the above-mentioned paradox that a rather accurate tilt signal appears not to be used as such in visual verticality judgments. The crucial point is that the visual signal is very precise (Orban and Vogels, 1998; Westheimer, 2003) in

comparison with the sensory tilt signal (Bisdorff et al., 1996; Mast and Jarchow, 1996; Day and Fitzpatrick, 2005). From a Bayesian perspective, it may not be the most optimal strategy to add the noisy tilt signal and the precise retinal signal to facilitate verticality perception. Indeed, Mast and Jarchow (1996) have provided evidence against the notion of simple noise propagation, by showing that scatter in line-verticality judgments was *less* than the noise in the body tilt judgments. The addition of a prior, centered on 0° tilt, suppresses noise in verticality perception at the expense of a systematic bias at larger tilt angles. In this sense, the Bayesian strategy amounts to a precision–accuracy trade-off. Viewed from this perspective, the trade-off appears to have a different outcome in the perception of body tilt where different optimality criteria may apply. The fact that body-tilt percepts show better accuracy but poorer precision compared with the line vertical (see earlier text) suggests that the involvement of prior information is minimal when estimating the orientation of body in space.

In a balanced assessment, it should be noted that Bayesian inference depends heavily on the assumption that the brain is adapted to the noise properties of the sensory tilt signal, which is essential to compute the corresponding likelihood function. It is not a trivial matter to validate this assumption, which can be seen as a weakness of all Bayesian models.

Performance of the two tested models

Both models performed very well in explaining the systematic errors in the adjustment experiments, although Mittelstaedt's model did slightly better, due to its provision to also account for errors of overcompensation (E-effects), seen in some subjects. As an explanation for such errors, Mittelstaedt's model allowed the idiotropic vector to fall short in the full compensation of the inaccuracies in the raw tilt signal. A further factor—that errors of overcompensation may reflect uncompensated eye torsion (Curthoys, 1996)—was ignored in both models.

With respect to the random errors, both models predict an increase of scatter with tilt angle. Recall that, in Mittelstaedt's model, a special parameter (C) was dedicated to this aspect of the data, whereas in the Bayesian model there is a tight coupling between random and systematic errors. The Bayesian model generally allowed for a better qualitative match to the observed scatter data than did the Mittelstaedt model, even though both models systematically overestimate the scatter levels. In this respect, the exact combination of systematic and variable errors cannot be accounted for by either model, which may be partly explained by the fact that differences between the local data average and the model fit must also be accounted for by the models' scatter prediction. We cannot exclude that the scatter in the data was underestimated due to our approach of collecting all responses in a single run, which may have caused some dependence between trials. In terms of systematic errors, the Bayesian model suggests a dependence of the accuracy on the precision of the subjective vertical. If the computation of the a posteriori probability of the gravity direction is adapted to the width of the individual likelihood of the vestibular signal, then subjects with high precision are also expected to show better accuracy (see Equations 2.9 and 2.10). One way to proceed would be to measure psychometric curves of perceived self-tilt at 0 and 90° tilts, to test whether subjects with large systematic errors in the motion vertical and line vertical at 90° also have a less-precise tilt percept at this tilt angle.

Neural aspects

It remains speculative as to where these Bayesian computations may be encoded in the brain, but a brief discussion about the neurophysiological implications of our results seems pertinent. At the peripheral level, the otoliths detect the gravito-inertial force (GIF), meaning that they cannot distinguish head translation from head tilt relative to gravity. Although errors may occur in the disambiguation of the GIF signal under dynamic conditions (Vingerhoets et al., 2007), we tacitly assumed that the brain can accurately disambiguate the GIF signal under static conditions. Support for this assumption comes from several modeling studies (Merfeld et al., 1999; Laurens and Droulez, 2007; MacNeilage et al., 2007). As a correlate of disambiguation, a recent neurophysiological study found that Purkinje cell activity in the cerebellar vermis reflects the transformation of afferent canal and otolith information into earth-referenced self-motion and spatial-orientation signals (Yakusheva et al., 2007). These findings suggest that the brain cares about isolating a head-in-space signal.

Our results raise interesting questions about the neural locus where such a signal may interact with visual signals to solve the spatial constancy problem during lateral tilt. In the early stages of visual processing, up to area V1, information appears to be coded in a retinal frame. A first attempt to look for signs of orientation constancy in the visual cortex has been made by Sauvan and Peterhans (1999). As far as we know, a comparable investigation has not yet been performed in middle temporal (MT) and middle superior temporal (MST) areas, which are key players in the analysis of visual motion. MSTd neurons, which are involved in the coding of self-motion, are sensitive to both visual and vestibular motion cues (Gu et al., 2006), but these signals are not coded in a common spatial frame of reference (Fetsch et al., 2007).

Another area, most closely associated with the dorsal stream, the parietoinsular vestibular cortex (PIVC), has received attention in the context of vestibular processing. PIVC is a multisensory region, responding to vestibular, somatosensory, and visual motion stimuli (Grüsser et al., 1990). It has been reported that patients with lesions in the human homologue of area PIVC show abnormalities in the perceived visual line vertical (Brandt et al., 1994; Brandt and Dieterich, 1999). Regarding our results, it would be interesting to investigate whether these patients have similar abnormalities in their visual motion vertical as well. Paradoxically, patients with such lesions have no affected percept of body posture and subsequent loss of lateral balance. In view of these findings, it seems that area PIVC may play an important role in the implementation of the computational mechanisms that subserve spatial perception.

Conclusion

We have shown that the conversion of motion direction and line orientation from a retinal to a world-centered frame of reference during lateral tilt is subject to the same pattern of errors. This result suggests that this bias probably arises at the level of the compensatory tilt signal used in the reference frame transformation. Modeling efforts, showing that both Mittelstaedt's idiotropic-vector model and a new Bayesian observer model can account for the pattern of systematic errors, suggest that these errors are the downside of a strategy to compensate for imperfections in the sensory tilt signal.

APPENDIX

Mathematical derivation of Bayesian model (Eqs. 2.7 and 2.8)

In the case of a single trial, Bayes' rule implies that the optimal estimate of tilt angle β, given sensory signal $\hat{\rho}$ and prior information, is specified by

$$\beta = \frac{\sigma_p^2}{\sigma_p^2 + \sigma_{tilt}^2} \cdot \hat{\rho} \qquad \text{Eq. 2.A1}$$

which is obtained by calculating the maximum value of the posterior distribution using its derivative. For the case of many repeated trials, the mean value of β is given by

$$\mathbb{E}(\beta) = \bar{\beta}(\rho) = \frac{\sigma_p^2}{\sigma_p^2 + \sigma_{tilt}^2} \cdot \mathbb{E}(\hat{\rho}) = \frac{\sigma_p^2}{\sigma_p^2 + \sigma_{tilt}^2} \cdot \rho \qquad \text{Eq. 2.A2}$$

which equals Eq. 2.7 (see *Methods*). The variance of β depends on the variance of $\hat{\rho}$ according to

$$\mathbb{V}\mathrm{ar}(\beta) = \left(\frac{\partial \beta}{\partial \hat{\rho}}\right)^2 \cdot \mathbb{V}\mathrm{ar}(\hat{\rho}) = \left(\frac{\sigma_p^2}{\sigma_p^2 + \sigma_{tilt}^2}\right)^2 \cdot \sigma_{tilt}^2 \qquad \text{Eq. 2.A3}$$

which is equivalent to Eq. 2.8.

ACKNOWLEDGMENTS

We thank H. Kleijnen, G. van Lingen, S. Martens, and G. Windau for technical support; F. Verstraten for helpful suggestions on the visual stimuli; T. Dijkstra, T. Heskes, and O. Zoeter for valuable advice on Bayesian methods; and T. Eggert for useful discussions about spatial-perception models.

This work was supported by Nijmegen Institute for Cognition and Information and Faculteit der Natuurwetenschappen, Wiskunde en Informatica of Radboud University Nijmegen and by grants from the Netherlands Organization for Scientific Research and the Human Frontier Science Program to W.P. Medendorp.

Chapter 3

Accuracy-precision trade-off in visual orientation constancy

De Vrijer M, Medendorp WP, Van Gisbergen JAM (2009) *Journal of Vision* 9: 1-15.

Spatial awareness involves knowledge about body position in space and the ability to maintain a stable mental representation of space despite changes in body position. One way to assess spatial constancy is to test which line orientation is perceived as earth-vertical when the subject is roll-tilted in the absence of panoramic cues (subjective visual vertical, SVV). Numerous studies have shown that this task is subject to systematic errors (see Figure 3.1): Near upright, SVV errors are typically small (Figure 3.1A) but responses at intermediate tilts may show a shift away from head tilt (Figure 3.1B, E-effect; Müller, 1916) which has been linked to incomplete compensation for eye torsion (de Graaf et al., 1992; Curthoys, 1996). Furthermore, it has been shown that the SVV becomes quite inaccurate at roll tilts beyond 60°, where it is biased toward head tilt (Aubert, 1861; Schöne, 1964; Udo de Haes, 1970; Mittelstaedt, 1983; Van Beuzekom and Van Gisbergen, 2000; Dyde et al., 2006). These errors, also known as the Aubert- or A-effect (see Figure 3.1C), can be very substantial, sometimes reaching values up to 50° at head tilts near 120° (De Vrijer et al., 2008). In this study, our objective is to test whether the accuracy and precision characteristics[1] of the SVV are compatible with optimal observer theory.

Which computations must the brain perform in order to maintain visual orientation constancy? As shown in Figure 3.2, to estimate the visual vertical with respect to earth coordinates, the observer must combine information about line orientation on the retina with central signals compensating for the effects of head tilt and eye torsion. If these compensations are only partial, this will give rise to A- and E-effects, respectively. Accordingly, a simple explanation of the A-effect to be considered first is the possibility that the head tilt sensors systematically underestimate head tilt at large deviations from upright. However, several studies cast doubt on this explanation by showing that the perception of body tilt lacks the large inaccuracies of the SVV. Hence, this finding implies that the brain has access to a relatively accurate tilt signal (Mittelstaedt, 1983; Mast and Jarchow, 1996; Van Beuzekom et al., 2001; Kaptein and

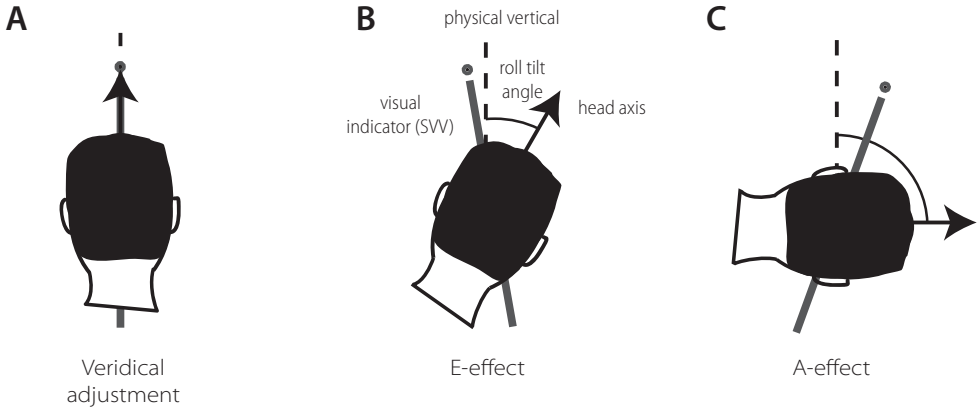

Figure 3.1 Schematic representation of bias patterns in SVV task. A. veridical adjustment at zero tilt. B. E-effect (tilt overcompensation) may occur at intermediate tilt angles. C. A-effect (tilt undercompensation) at larger tilt. Note that over- and undercompensation errors in the SVV are merely a description of the direction of the errors and need not imply that observers in fact over- or underestimated their tilt angle.

1 *The term accuracy refers to constant errors (bias) in the response. Precision is linked to variable errors, which reflect noise in the system (Howard, 1982).*

Van Gisbergen, 2004) but does not use this signal as such in the computations underlying visual orientation constancy. Here we present the hypothesis that A- and E-effects reflect the results of a computational strategy, based on Bayesian observer theory, which aims to increase the precision of the compensatory signals near upright at the expense of reduced accuracy at larger tilt angles (Eggert, 1998; MacNeilage et al., 2007; De Vrijer et al., 2008). The general idea behind this theory is that the observer combines noisy sensory information about actual head tilt in space and eye rotation in the head, with prior knowledge about which tilt angle is most likely on an *a priori* basis.

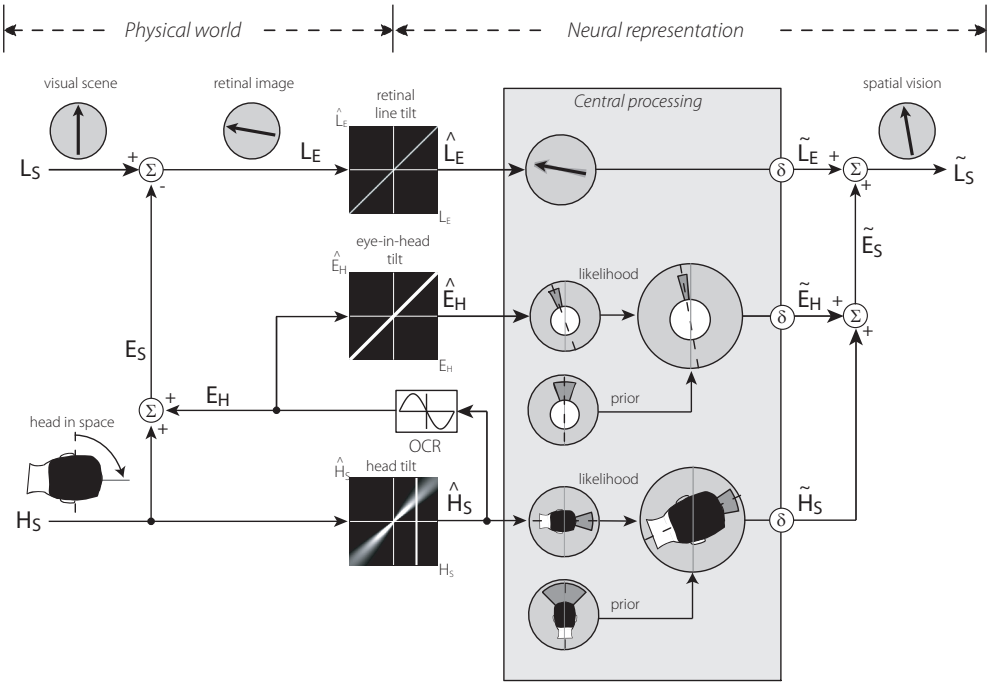

Figure 3.2 Neural compensation for head tilt and eye torsion to maintain visual orientation constancy. The purpose of the scheme is to elucidate the relations between physical variables and internal signals engaged in visual spatial perception. A world-vertical line (line-in-space, $L_S = 0°$) appears in front of a tilted observer (head-in-space, H_S=90°). Head rotation and ocular counterroll (OCR, eye-in-head E_H) result in net retinal image tilt (line-on-eye, L_E) according to: $L_E = L_S - (H_S + E_H)$. Signal $\hat{H}_S$, coding head orientation in space, is assumed to be accurate but contaminated by Gaussian noise with an amplitude that increases linearly with tilt angle (bottom square panel; gray levels encode probability). Likewise, signal $\hat{E}_H$, encoding eye orientation in the head, is accurate but contaminated by independent Gaussian noise. Ideal observer uses Bayesian strategy to obtain an optimal estimate of head in space ($\tilde{H}_S$) and eye in head ($\tilde{E}_H$) to reconstruct eye orientation in space ($\tilde{E}_S$). The latter signal is then combined with retinal signal ($\tilde{L}_E$) to obtain an internal estimate of the orientation of the line with respect to gravity ($\tilde{L}_S$). Dark gray sectors in the Bayesian scheme symbolize the widths of the sensory and prior distributions. Decision rule (δ) picks angle with maximum a posteriori probability (MAP). Note that biased estimates of $\tilde{E}_H$ and $\tilde{H}_S$ have opposite biasing effects on the perceived line orientation in space and that $\tilde{L}_S$ in the illustrated example is not veridical so that a world-vertical line does not appear upright to the tilted observer. If the observer, in this particular example, was to adjust the line to the subjective vertical (SVV), it would be rotated in clockwise direction, which amounts to an A-effect as illustrated in Figure 3.1. If the error in $\tilde{E}_H$ were larger than in $\tilde{H}_S$, this would result in an opposite effect, with the perceived line oriented clockwise of vertical (E-effect).

As shown in Figure 3.2, optimal compensation, necessary to preserve orientation constancy despite head tilt, requires that the retinal line orientation ($\tilde{L}_E$) be compensated by a neural signal ($\tilde{E}_S$) that equals the actual eye orientation in space (E_S). Thus, to obtain a proper compensatory signal, the observer must take account of both the orientation of the head in space (H_S) and the orientation of the eye within the head (E_H). If the corresponding central estimates ($\tilde{E}_H$ and $\tilde{H}_S$) were veridical and precise, the observer would obtain an unbiased and stable percept of line orientation in space ($\tilde{L}_S$). However, if $\tilde{H}_S$ underestimates H_S, this would result in underestimation of eye-in-space angle E_S, thus causing an A-effect. By contrast, underestimation of ocular torsion would give rise to overestimating E_S, which would cause an E-effect. We now proceed to explain how such biases in $\tilde{H}_S$ and $\tilde{E}_H$ may be the downside of a noise-coping strategy in handling the raw neural signals from which they are derived ($\hat{H}_S$ and $\hat{E}_S$), even though the latter are assumed to be accurate, on average.

As proposed in Figure 3.2, the observer interprets the noisy eye-torsion and head-tilt signals by relying on a statistical approach. Their uncertainty is reflected in the width of corresponding likelihood functions that represent the range of potential underlying physical signals (indicated by orange sectors). Additionally, the Bayesian framework uses *a priori* knowledge about head tilt and ocular torsion, expressed in the prior probability distributions, which represent the fact that head tilt and eye torsion are mostly small. To combine the likelihood function and prior distribution optimally, the observer relies on their product, called the posterior distribution. When the subject is tilted, the posterior peaks in-between the peaks of the prior and the likelihood, thus giving rise to systematic errors: both head tilt and ocular torsion are systematically underestimated. However, the posterior distributions are less affected by sensory noise than the likelihood functions, thus yielding a precision that exceeds the precision of the sensory signals (see width of orange sectors). Hence, using prior knowledge affects the head-in-space and eye-in-head tilt estimates in two ways: it biases estimates towards smaller angles (reduced accuracy) but brings down uncertainty caused by sensory noise (increased precision). This strategy, an accuracy-precision trade-off, is particularly useful for small tilt angles, which are most common in daily life. For a full mathematical treatment of the scheme in Figure 3.2, see Methods section *Modeling*.

In *Chapter 2* (De Vrijer et al., 2008), we found that this computational strategy could account for the nonlinear increase of SVV errors with head tilt, if we made the assumption that the precision of the sensory head tilt signal decreases with tilt angle, as indicated by the noise increase in Figure 3.2 (*bottom square panel*). The purpose of the present study was to collect an extensive data set that would allow a thorough test of the Bayesian model. By testing eight subjects in a psychometric SVV experiment, we obtained estimates of SVV accuracy and precision at a range of tilt angles. Our results are consistent with the predictions of the Bayesian observer model, indicating that subjects use an optimal strategy to maintain visual orientation constancy.

METHODS

Subjects

We tested eight subjects (5 male, 3 female), including the three authors who where familiar with the purposes of the experiment. Subjects, aged between 22 and 64 years (mean ± SD: 31 ± 14 yrs.), provided written informed consent to participate in the experiments. Participants were free of known vestibular or other neurological disorders and had normal or corrected-to-normal visual acuity.

Setup

Subjects were seated in a computer-controlled vestibular chair with nested gimbals, which was configured to allow subject rotation in roll. The subject's trunk was tightly fixed using adjustable shoulder and hip supports and a five-point seat belt. The legs and feet were restrained with Velcro straps and the head was firmly fixed in a natural upright position for looking straight ahead, using a padded helmet. For each subject, seat adjustments ensured that the roll-axis of the chair coincided with the naso-occipital axis midway between the eyes. Tilt position was measured using a digital position encoder with an angular resolution of 0.04°. A luminous line, consisting of a roughened glass fiber, lit by a white LED, was mounted in front of the subject at a distance of ~90 cm, so it had an angular subtense of 20°. The rotation axis of the line coincided with the chair rotation axis and its orientation was computer-controlled with an angular resolution of 0.5°. A bright dot at one end served for polarization (see Figure 3.1). Subjects were free to move their eyes in any direction and vision was always binocular. Except for the luminous line, experiments were performed in complete darkness.

Experimental paradigm

The experiment was designed to obtain psychometric curves about subjective visual verticality at 9 roll tilt angles, ranging from -120 to 120° in 30°-intervals, which were tested in random order. Each experimental run started with the subject in upright position. Then, the lights were turned off and subjects were rotated to a tilt angle H_S in total darkness, with right-ear-down angles coded as positive. Rotation was performed at a constant angular velocity of 30°/s, which was reached within 1 s using a peak acceleration of 50°/s^2. After a 30-s waiting period that allowed canal effects to subside, subjects viewed the polarized luminous line with the appearance of an inverted exclamation mark (see Figure 3.1) for a brief period of 20 ms and indicated whether its orientation in space was clockwise (CW) or counterclockwise (CCW) from their perceived direction of gravity, using a toggle switch. Subsequently, a new trial followed with a different line orientation, picked randomly from a set of 11 line orientations (details follow below). This sequence was repeated until all line orientations had been tested, after which subjects were rotated back to upright and lights were turned on, during a 30-s resting period. Positive and negative body tilt angles were alternated regularly. For the 0°-tilt condition, we added an equal number of catch trials, in which subjects were tilted to an angle that was picked randomly from the range of ±5°, using a sub-threshold rotation speed of 2°/s, so that they could not perform the task in body coordinates.

To collect psychometric data we used the method of constant stimuli (Ehrenstein and Ehrenstein, 1999). The set of 11 line orientations was centered on a coarse estimate of the SVV threshold at each tilt angle, which was determined with the method of adjustment in a preceding session. For all tilt angles except for upright (H_S=0°), test orientations were presented at 0, ±3, ±6, ±9, ±12 and ±15° relative to this value. For upright, where performance was typically more precise, we used a narrower test range at 0, ±2, ±4, ±6, ±8, ±10°. Each set of line orientations was presented in 12 experimental runs in random order, yielding a total of 132 responses for each psychometric curve. For each subject, data were collected in a total of 5 sessions of approximately 45 min each. Catch trial responses were excluded from further analysis.

Data analysis

We quantified behavioral performance by measuring the proportion of CW responses as a function of line orientation. Psychometric data were quantified by fitting with a cumulative Gaussian function:

$$P(x) = \lambda + (1 - 2\lambda)\frac{1}{\sigma\sqrt{2\pi}}\int_{-\infty}^{x} e^{-(y-\mu)^2/2\sigma^2}dy \qquad \text{Eq. 3.1}$$

in which x represents line orientation. The mean of the Gaussian, μ, represents the subjective vertical in the SVV task. The width of the curve, σ, serves as a measure for the subject's uncertainty in the SVV and is inversely related to precision. Parameter λ, representing the lapse rate, accounts for stimulus-independent errors caused by subject lapses or mistakes, and was restricted to small values ($\lambda < 0.06$). Fits were performed using Matlab 7.0 software (The MathWorks) with the routine *psignifit* (Wichmann and Hill, 2001b).

Modeling

We first provide a short step-by-step description of the Bayesian observer model, which extends the version from *Chapter 2* (De Vrijer et al., 2008) by including an optimal-observer interpretation of the E-effect. The model, schematically illustrated in Figure 3.2, uses the following conventions: physical variables are denoted by a capital with a subscript denoting the reference frame. For example, E_H represents the (physical) roll orientation of the eye (E) with respect to the head (H). Sensory signals are denoted by a *hat* symbol (^), as in $\hat{E}_H$, reflecting the orientation of the eye in the head as measured by the sensors. The outcome of a Bayesian computation is denoted by a *tilde* symbol (~), as in $\tilde{E}_H$, which represents the optimal estimate of eye-in-head orientation according to sensory information and prior knowledge.

Head-in-space estimation

In the model, we assume that the sensory head tilt signal ($\hat{H}_S$), measured by a variety of tilt sensors, is a noisy but unbiased representation of the physical head tilt angle (H_S). Thus, the sensory tilt signal varies in repeated trials at the same physical tilt angle but the expected value of $\hat{H}_S$ is a veridical representation of the actual head tilt. Conversely, this means that the brain cannot be sure about the physical angle, based on the sensory signal, and needs a statistical approach to determine the best estimate of head tilt angle. The Bayesian model

assumes that the brain is adapted to the noise properties of its sensors, which allows it to deduce the probability of each tilt angle based on the sensory evidence, known as the likelihood function $P(\hat{H}_S|H_S)$. When sensory noise increases, the likelihood function, which is modeled by a Gaussian centered on $\hat{H}_S$ and with standard deviation $\sigma_{\hat{H}_S}$, becomes less peaked and broader. To account for the typical nonlinear increase of the A-effect with tilt, the model allows for the possibility that the precision of the tilt sensors decreases with tilt angle, like in De Vrijer et al. (2008). This is formulated by stating that noise in the sensory head-tilt signal ($\sigma_{\hat{H}_S}$) increases rectilinearly with tilt angle according to:

$$\sigma_{\hat{H}_S} = a_0 + a_1 |H_S| \qquad \text{Eq. 3.2}$$

in which a_0 reflects the noise at H_S=0° and a_1 represents the proportional increase of noise with tilt angle (see *square bottom panel* in Figure 3.2). Note, however, that by setting the lower limit of parameter a_1 to zero, the model did not force tilt-sensor precision to be dependent on head tilt.

To obtain an optimal estimate of the physical tilt position, the brain further takes into account that some tilt angles are more likely on an *a priori* basis. In the model, this is expressed by the prior distribution $P(H_S)$, which is modeled by a Gaussian with standard deviation σ_{Hs}, centered on zero head tilt (H_S=0°), reflecting the knowledge that small head tilts are more likely than large tilts. Multiplication of the likelihood and prior distributions yields the posterior probability distribution $P(H_S|\hat{H}_S)$ according to Bayes' rule:
$P(H_S \mid \hat{H}_S) = k \cdot P(\hat{H}_S \mid H_S) \cdot P(H_S)$, in which *k* serves a normalization purpose. The peak of the posterior probability function is in-between the peaks of the likelihood and prior distributions, depending on their relative widths (Knill and Pouget, 2004; Carandini, 2006; MacNeilage et al., 2007). In the model, the peak of the posterior ($\tilde{H}_S$) is used as the optimal estimate of head tilt angle.

Eye-in-head estimation

Since the eyes typically counterroll in their orbits during roll tilt (de Graaf et al., 1992; Markham and Diamond, 2002; Palla et al., 2006), an ideal observer also needs an estimate ($\tilde{E}_H$) of the actual torsional orientation of the eyes with respect to the head, E_H (see Figure 3.2). Following Palla et al. (2006) we approximated eye-torsion by: $E_H = -A \sin(\hat{H}_S)$, in which *A* represents the maximum torsion amplitude and $\hat{H}_S$ reflects the sensory head-tilt signal. The negative sign reflects the fact that the eyes counterrotate relative to the head. Information about torsional eye-in-head orientation ($\hat{E}_H$), whether based on an efference copy signal, or on proprioception, or both, is treated as a sensory signal, assumed to be accurate but contaminated by noise ($\sigma_{\hat{E}_H}$). It is important to note that this noise is introduced by the systems monitoring the torsion signal and has nothing to do with noisy variations in the torsion signal itself, hence is assumed to be independent of $\sigma_{\hat{H}_S}$. We assumed that the observer again uses a Bayesian strategy to obtain an optimal estimate of eye-in-head orientation ($\tilde{E}_H$), by taking into account which orientations are most likely on an *a priori* basis. Here, prior knowledge entails that the eyes are mostly closely aligned with the head (i.e. E_H~0°). Sensory information about torsional eye position is represented by the likelihood function $P(\hat{E}_H|E_H)$ and prior knowledge is represented by a

Gaussian centered on 0° with standard deviation σ_{E_H}. The peak of the posterior distribution is used as the optimal estimate of eye-in-head angle ($\tilde{E}_H$).

Accuracy and precision predictions of complete model

The estimates of eye-in-head ($\tilde{E}_H$) and head-in-space ($\tilde{H}_S$) are combined to obtain an optimal estimate of the orientation of the eye in space ($\tilde{E}_S$), which is then used as the compensating signal in the SVV task. The expected value of $\tilde{E}_S$ in many repeated trials (μ_{E_S}) follows from the corresponding expected values of $\tilde{H}_S$ and $\tilde{E}_H$. As shown in the *Appendix*, this results in the following relation:

$$\mu_{\tilde{E}_S} = \mu_{\tilde{H}_S} + \mu_{\tilde{E}_H} = \frac{\sigma^2_{H_S}}{\sigma^2_{H_S} + \sigma^2_{\tilde{H}_S}} \cdot H_S + \frac{\sigma^2_{\tilde{E}_H}}{\sigma^2_{E_H} + \sigma^2_{\tilde{E}_H}} \cdot E_H \qquad \text{Eq. 3.3}$$

This relation specifies how prior knowledge and sensory uncertainty bias the eye-in-space estimate. Note that noise in the sensory signals causes an underestimation of head-in-space and eye-in-head. Furthermore, the tilt dependency of $\sigma_{\tilde{H}_S}$ (Eq. 3.2) causes a slight skewness in the head-tilt likelihood function, which was neglected to enable a straightforward fitting procedure.

The variance in the maxima of the posteriors (MAP) in repeated trials is smaller than the variance of the posteriors themselves (see *Appendix*). As a result, the variance in $\tilde{E}_S$ in repeated trials ($\sigma^2_{\tilde{E}_S}$) is given by:

$$\sigma^2_{\tilde{E}_S} = \sigma^2_{\tilde{H}_S} + \sigma^2_{\tilde{E}_H} = \left(\frac{\sigma^2_{H_S}}{\sigma^2_{H_S} + \sigma^2_{\tilde{H}_S}} \cdot \sigma_{\tilde{H}_S} \right)^2 + \left(\frac{\sigma^2_{E_H}}{\sigma^2_{E_H} + \sigma^2_{\tilde{E}_H}} \cdot \sigma_{\tilde{E}_H} \right)^2 \qquad \text{Eq. 3.4}$$

which shows that prior knowledge reduces uncertainty caused by sensory noise. Equations 3.3 and 3.4 provide insight into the structure of the model from a forward perspective. However, attempting to fit all its parameters would confront us with an underdetermined inverse problem. This problem can only be solved by making a few simplifying assumptions which will be detailed in the next subsection where we summarize the fit parameters that were actually determined.

Fit parameters of simplified model

SVV accuracy: To obtain an estimate of the world-centered orientation of the line ($\tilde{L}_S$), required in the SVV task, the central estimate of eye position in space $\tilde{E}_S$ is added to the estimated retinal line orientation $\tilde{L}_E$, which is assumed to be unbiased ($\tilde{L}_S = \tilde{L}_E + \tilde{E}_S$). Thus, according to the model, the systematic errors in the SVV (μ_{SVV}) are caused exclusively by bias in the eye-in-space estimate, as shown in the following relation:

$$\mu_{SVV} = E_S - \mu_{\tilde{E}_S} = (H_S - \mu_{\tilde{H}_S}) + (E_H - \mu_{\tilde{E}_H}) = \frac{\sigma^2_{\tilde{H}_S}}{\sigma^2_{H_S} + \sigma^2_{\tilde{H}_S}} \cdot H_S - \frac{\sigma^2_{\tilde{E}_H}}{\sigma^2_{E_H} + \sigma^2_{\tilde{E}_H}} \cdot A\sin(H_S) \qquad \text{Eq. 3.5}$$

Here, the first term on the right-hand side represents the error in the head-in-space estimate, which contributes to the A-effect, whereas the second term reflects the error in the eye-in-head estimate and contributes to the E-effect. Note that fitting the first term actually involves three parameters: the tilt noise parameters a_0 and a_1 (see Eq. 3.2) and the head prior, σ_{H_S}. Complete

fitting of the second term would also involve three parameters (A, σ_{E_H} and $\sigma_{\hat{E}_H}$). To prevent problems of overfitting, we simplified the second term to a single parameter (ΔE_H), representing the uncompensated magnitude of eye torsion based on the following consideration: If we assume that both the noise in the central estimate of eye torsion ($\sigma_{\hat{E}_H}$) and the width of the torsion prior (σ_{E_H}) are constant (i.e. independent of H_S), the second term on the right-hand side of equation 2 reduces to a scaled version of the actual eye torsion E_H. In other words, uncompensated torsion is a scaled version of the actual torsion, with the same sinusoidal tilt relation:

$$\frac{\sigma^2_{\hat{E}_H}}{\sigma^2_{E_H} + \sigma^2_{\hat{E}_H}} \cdot A \sin(H_S) = \frac{1}{r^2 + 1} A \sin(H_S) = \Delta E_H \sin(H_S), \text{ with } 0 \leq \Delta E_H \leq A \qquad \text{Eq. 3.6}$$

Here ΔE_H represents the uncompensated part of the eye-in-head amplitude (A) and r^2 reflects the ratio of the variances of the eye-torsion prior and sensory eye-in-head signal ($\sigma_{E_H}/\sigma_{\hat{E}_H}$). Thus, the narrower the prior relative to the torsion noise distribution, the larger the uncompensated torsion ΔE_H.

SVV precision: SVV scatter (σ_{SVV}) is determined by a combination of head-in-space noise ($\sigma_{\hat{H}_S}$), which is assumed to be tilt dependent (see Eq. 3.2) and two tilt-independent terms, viz. eye-in-head noise ($\sigma_{\hat{E}_H}$) and retinal noise ($\sigma_{\hat{L}_E}$). However, to prevent problems of overfitting, the contributions of the latter two terms were not fitted separately. This means that both tilt-independent noise terms were attributed to the first term in Equation 3.4. Effectively, the simplified model fitted SVV variability with 3 parameters (a_0, a_1 and σ_{H_S}), using:

$$\sigma^2_{SVV} \approx \sigma^2_{\hat{E}_S} \approx \sigma^2_{\hat{H}_S} = \left(\frac{\sigma^2_{H_S}}{\sigma^2_{H_S} + \sigma^2_{\hat{H}_S}} \cdot \sigma_{\hat{H}_S} \right)^2 \qquad \text{Eq. 3.7}$$

Because of this simplification, both $\sigma_{\hat{H}_S}$ and σ_{H_S} were somewhat overestimated, but, as we discuss later (see section *Effect of simplifying assumptions* in *Discussion*) the effect is probably minor and does not affect our overall conclusion. Note that the impact of eye-in-head noise on the accuracy of the eye-in-space estimate (Eq. 3.3) was taken into account.

In summary, the simplified model has four fit parameters, (a_0, a_1, σ_{H_S}, and ΔE_H) that determine the accuracy and the precision of the SVV at each head tilt angle (see Table 3.1).

Model fits

The Bayesian model makes simultaneous predictions of systematic SVV errors (μ_{SVV}) and SVV variability (σ_{SVV}) as a function of head tilt angle H_S. We used a maximum-likelihood estimation (MLE) procedure to fit the model to the psychophysical responses. We obtained the best-fit

Table 3.1 *Summary of fit parameters*

Parameter	Definition	Equation
a_0 [°]	Noise in sensory head-tilt signal ($\sigma_{\hat{H}_S}$) at 0° head tilt	3.2
a_1 [°/°]	Increase of noise in sensory head-tilt signal ($\sigma_{\hat{H}_S}$) with tilt angle	3.2
σ_{H_S} [°]	Width of head-tilt prior distribution	3.3 and 3.4
ΔE_H [°]	Maximum amplitude of uncompensated ocular counterroll	3.6

values of the four parameters for each subject by minimizing the negative log-likelihood using the *fmincon* routine (Matlab 7.0; The MathWorks). The log-likelihood function L(θ) is defined as $L(\theta) = \sum_{i=1}^{n} \log(P_\theta[N_i(CW)|\ \theta])$, in which $P_\theta[N_i(CW)|\ \theta]$ represents the chance of obtaining $N_i(CW)$, the number of *CW*-responses at a particular combination of head tilt and line orientation, for a given parameter set θ. $P_\theta[N_i(CW)|\ \theta]$ was computed by first calculating μ_{SVV} and σ_{SVV} at each tilt angle for a given parameter set, using Eq. 3.5 and 3.7. The chance of obtaining a *CW*-response (P[CW]) at a certain combination of tilt angle and line orientation was calculated using the normal cumulative distribution function. Moreover, since subjects may have made stimulus-independent lapses, we included a lapse rate λ into the distribution function. For simplicity, the lapse rate in these model fits was set at a fixed value of 0.06 (Wichmann and Hill, 2001a). Subsequently, the chance of obtaining N_i *CW*-responses (given 12 repetitions) was specified by the binomial distribution, B(12, P[CW]).

Standard deviations of the best-fit parameters (see Table 3.2) were obtained by performing 100 bootstraps.

RESULTS

To test the predictions of the extended Bayesian observer model, we investigated the sense of visual verticality (SVV) in roll-tilted subjects, using a psychometric approach. We start this section with a description of the data, followed by the model fit results.

Psychometric SVV results

To obtain a quantitative assessment of the accuracy and precision of the SVV, subjects performed a psychophysical task (forced-choice), in which they judged the orientations of a set of luminous lines with respect to gravity. Figure 3.3 illustrates how roll tilt (H_S) affected the SVV of a typical subject (RV). Each panel shows how the proportion of *CW*-responses, P(CW), changed as line orientation in space was varied around perceived vertical. At each tilt angle, response rates range from 0 to 1, indicating that the stimulus sets were positioned correctly. In an ideal observer, all psychometric functions would resemble a step centered at zero. In fact, as body tilt increases, psychometric curves shift away from zero and become less steep as a sign that there is decay in both accuracy and precision. For example, an earth-vertical line (0°) is always perceived as '*CW from earth vertical*' at -60° head tilt, whereas it is always perceived as *'CCW from vertical'* at 60° head tilt. For each tilt angle, we fitted the data with a cumulative Gaussian function (see Eq. 3.1), which is characterized by three parameters: mean μ, standard deviation σ, and lapse rate λ. We took μ as a measure for accuracy and used σ as a measure for the precision of the verticality percept. When precision improves, σ becomes smaller and hence the psychometric curve becomes steeper.

In the upright body position (H_S=0°), the percept of visual verticality is virtually unbiased and relatively precise compared to the other tested tilt angles. In the top panel (H_S=-120°), the mean of the psychometric curve is at μ=-38.2°, which means that the line must be tilted away from true vertical by this angle to be perceived as vertical in space, an expression

of the A-effect (Aubert, 1861). In the bottom panel (H_S=+120°), the curve is centered at μ = +28.7°, which again reflects an A-effect. To appreciate the deterioration in precision, notice that the curve is steepest at 0° roll tilt (σ=2.3°) and that σ increases at larger tilt angles, reaching maximum values of 5.8° and 5.1° at H_S=+90° and H_S=-90°, respectively.

Figure 3.4 shows best-fit μ-values from all subjects to illustrate how the accuracy of the verticality percept changes as a function of tilt angle. Model fits through the data will be discussed below (see section *Model fit results*). With one notable exception (DB), all subjects show variations of the response pattern known from the literature (Udo de Haes, 1970; Mittelstaedt, 1983; Van Beuzekom and Van Gisbergen, 2000; Van Beuzekom et al., 2001; De Vrijer et al., 2008), with less consistent systematic errors at small tilts and gradually decreasing accuracy, in the form of increasing A-effects, at larger tilt angles. Furthermore, several subjects show E-effects at the intermediate tilt angles, ranging up to -13.2° at 60° roll tilt for subject FW.

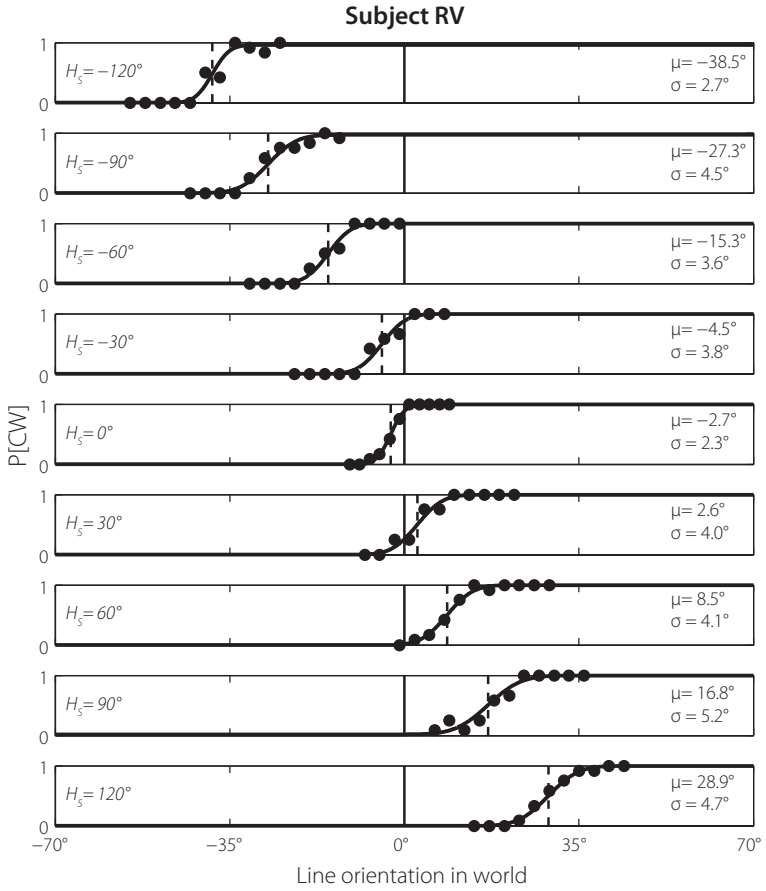

Figure 3.3 Psychometric SVV data, with each panel representing a different head tilt angle H_S. Proportion of CW-responses is plotted against line orientation with respect to gravity. Solid line: best-fit cumulative Gaussian, characterized by μ and σ. Vertical dashed lines denote μ, a measure for SVV accuracy. Verticality perception is less accurate (curves are shifted with respect to 0°) and less precise (curves are less steep) as head tilt increases. Subject: RV.

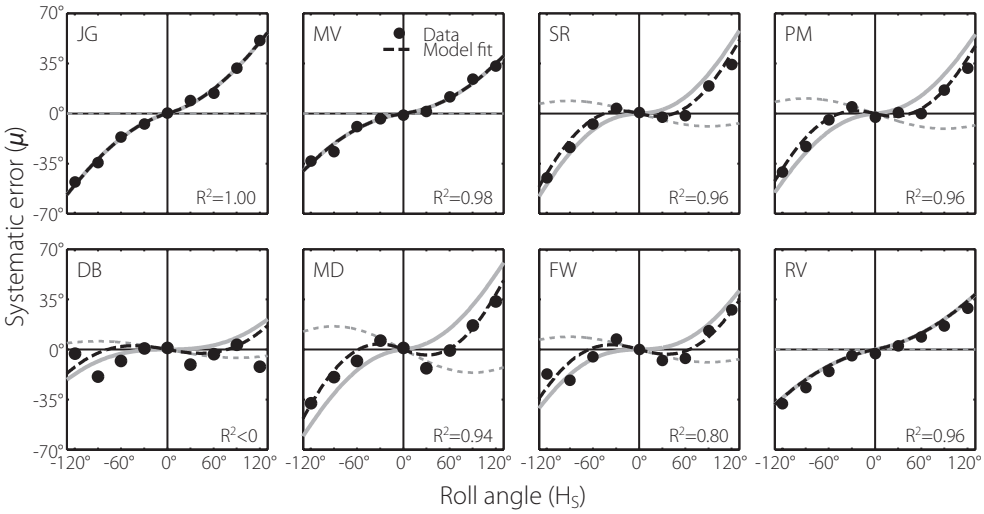

Figure 3.4 Accuracy of the SVV plotted against head tilt angle for all subjects. Filled circles: Systematic errors, based on μ-values from psychometric functions (see Figure 3.3). Dashed black line: Bayesian model fit. Solid gray line: error contribution due to underestimation of head angle. Dashed gray line: error contribution due to underestimation of eye torsion. R^2-values represent goodness-of-fit of model to systematic errors. Maximum A-effects differ significantly among subjects, ranging from 21° for FW, to 50° for JG. Subject DB shows a-typical behavior, with small errors at even the largest tilt angles.

To show how tilt affects SVV precision, Figure 3.5 plots parameter σ of the fitted psychometric curves as a function of tilt angle for all subjects. Again, model fits will be discussed in the section *Model fits results*. Invariably, precision is best at 0° tilt and deteriorates with tilt angle (one-way ANOVA; $F(8,63)=5.3$, $P<0.001$). Values for σ range from ~2° at zero tilt to a maximum of about 7° (PM) at the largest roll tilt angles. These findings are consistent with anecdotal reports from several subjects that judging the visual vertical was more difficult at the largest tilt angles.

The deterioration in SVV accuracy and precision with tilt angle is also manifest in the data pooled across subjects. As Figure 3.6A shows, the population mean has a clear A-effect at the larger tilt angles, as a sign of decreased accuracy. The E-effect, which was observed in several subjects at smaller tilts (≤60°), is negligibly small at the population level. The decay in precision with tilt angle shown by present results is depicted in Figure 3.6B. As shown, σ steeply increases between 0° and ±30° tilt which is then followed by more gradual increments, resulting in the highest σ values at ±120° roll tilt.

Model fit results

To test whether our model could account for the results, we fitted the model to the data from each subject (see *Methods*). Note that systematic errors and σ levels, which are coupled in the Bayesian model, were fitted simultaneously. Figure 3.4 illustrates the fit results of the Bayesian model (dashed black line) in terms of the systematic errors in the SVV. For most

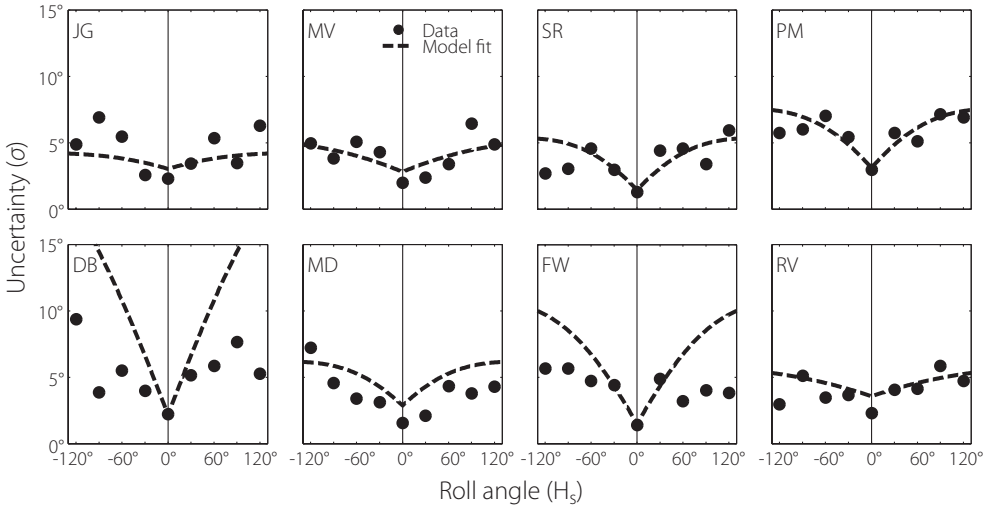

Figure 3.5 Uncertainty levels (σ) in the SVV task plotted vs. head tilt angle for all subjects. Black circles: σ-values from psychometric functions (see Figure 3.3). Dashed lines: model fits. For all subjects, σ increases with tilt angle, indicating a decline of precision. Model fits show a modest trend of overestimating σ in most subjects. In subjects FW and DB, overestimation is considerable at large tilts (see main text for explanation).

subjects, the model fits the systematic error data quite accurately, with R^2-values ≥0.80. Due to the fact that DB has a very unusual error pattern, with only small negative errors at even the largest tilt angles, this fit is considerably worse (R^2<0)[2]. Note that R^2-values are provided merely to show how well the model accounts for the systematic errors, but do not reflect the overall goodness-of-fit, since *σ*-levels are equally important. Since the Bayesian model attributes systematic SVV errors to a combination of errors in the head-in-space estimate (A-effects) and in the eye-in-head estimate (E-effects), see Eq. 3.5, we also depicted these opposite contributions separately (solid and dashed gray lines, respectively). In the three subjects without E-effects (JG, MV and RV), eye-in-head errors are absent (i.e. ΔE_H=0°), as illustrated by the dashed gray lines through the abscissa (0°). For the other subjects, the fits indicate the degree of undercompensation for ocular counterroll, reflected by the sinusoidal function. Additional fits of a reduced model that lacked uncompensated ocular counterroll, showed that model fits of JG, MV and RV did not change. The fits of the five subjects with E-effects worsened significantly (likelihood ratio test, P<<0.01) and parameter a_0 became unrealistically small (0°). Precision fits, shown in Figure 3.5, are equally relevant for a complete evaluation of the model. In most subjects (except DB and FW), model fits and actual data show the same trends. Fits show an increase of σ_{SVV} with tilt angle, which is similar to the actual increase observed in the data. Responses from subject DB were rather atypical, also in repeated testing, and therefore difficult to interpret. The overestimation of σ_{SVV} in subject FW appears related to the fact that the systematic error pattern shows increased accuracy at the most negative tilt angle (H_S=-120°, see Figure 3.4). The model has no solution to account for this observation other than by increasing the value of σ_{SVV}. We confirmed this by performing

2 *R^2 reflects the amount of variance in the data that is explained by the fit and is not really a squared value. Here, an R^2-value < 0 means that a straight line would fit the data better than the Bayesian model fit.*

separate fits at positive and negative tilts for subject FW. This resulted in minor differences with regard to the accuracy fits, but strongly affected precision levels: at negative tilts, σ_{SVV} levels were still overestimated, but at positive tilts, the fit improved greatly. This example illustrates how overestimation of σ_{SVV} may be directly related to small discrepancies in the systematic errors of model and data. Moreover, small asymmetries that are present in each observer (see e.g. the CW-shift of subject FW in Figure 3.3) may also affect the fits, because the present model cannot account for such asymmetry. A possible solution would be to allow a shift of the prior on head-in-space, which could be interpreted as a shift in the internal reference frame of the observer.

Best-fit parameter values and associated SD levels are listed in Table 3.2. The best-fit values of parameter a_1 are positive in all subjects (0.03-0.15 °/°), which means that noise in the tilt sensors must increase with head-tilt angle if the model is to account for the SVV data. Values of a_0 (mean ± SD= 2.8±0.9°), reflecting the sensory head-tilt noise in the upright subject, range from 1.5° for subjects SR and FW, to 4.0° for RV. The width of the head-in-space prior distribution (σ_{Hs}) ranges from 8.5° for subject JG to 21.5° for subject FW (the fit of subject DB reached the arbitrarily chosen limit value). This result indicates that prior knowledge about head tilt has a stronger influence in subject JG than in subject FW. The effect of the width of the head-in-space prior (σ_{Hs}) is best illustrated by comparing subjects JG and MV, where this is the only strikingly different parameter. The prior is narrower in JG than in MV (8.5° vs. 10.5°), which explains why his A-effects are larger. The amplitude of uncompensated eye counterroll (ΔE_H) is significantly larger than zero for the five subjects in which we observed E-effects (SR, PM, DB, MD, and FW). This parameter, which accounts for systematic errors of tilt overcompensation (E-effects), ranges from 8.9° for subject SR to 16.2° for subject MD. In the other three subjects, ΔE_H was zero due to the absence of any E-effects, as shown by Figure 3.4. A further evaluation of parameter variations among all subjects would be contentious,

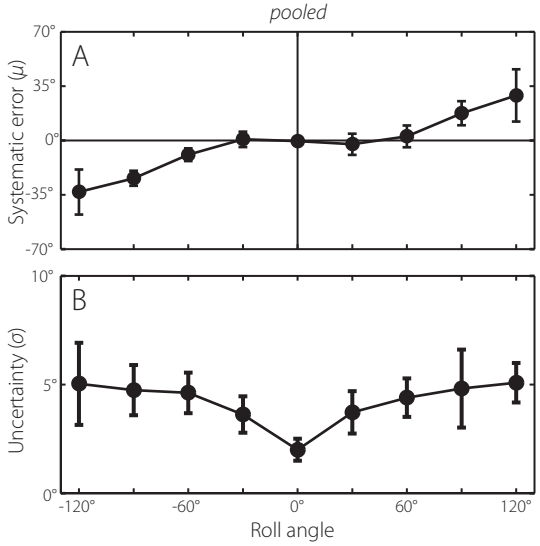

Figure 3.6 Pooled results from SVV task. A. Systematic errors, based on μ values ± SD B. Uncertainty, based on σ values ± SD vs. head tilt angle, averaged across subjects.

Table 3.2 Best-fit parameter values (± SD) of the SVV data fit.

Subject	a_0 [°]	a_1 [°/°]	σ_{Hs} [°]	ΔE_H [°]
JG	3.6 [1.1]	0.03 [0.01]	8.5 [1.0]	0 [n/a*]
MV	3.1 [0.4]	0.03 [0.01]	10.5 [1.0]	0 [n/a*]
SR	1.5 [0.4]	0.06 [0.02]	10.7 [2.4]	8.9 [2.7]
PM	3.3 [1.2]	0.08 [0.02]	15.1 [1.9]	10.6 [2.7]
DB	2.2 [0.9]	0.15 [0.03]	50.0 [1.5]	5.8 [2.8]
MD	3.0 [0.8]	0.07 [0.02]	12.3 [2.6]	16.2 [3.4]
FW	1.5 [0.8]	0.10 [0.03]	21.5 [4.7]	8.9 [2.1]
RV	4.0 [0.7]	0.03 [0.01]	11.7 [1.6]	0 [n/a*]

*Abbreviations: a_0, noise level $\hat{H}_S$ ($\sigma_{\hat{H}s}$) at upright; a_1, increase in $\sigma_{\hat{H}s}$ with tilt angle; σ_{Hs}, width of head prior distribution; ΔE_H, uncompensated eye torsion (see Eq. 3.6). Imposed fit limits, a_0: 0 – 50°, a_1: 0 – 3°/°, σ_{Hs}: 0 – 50°, ΔE_H: 0 – 20°. *No SD-values are available for cases where bootstrapped values formed a skewed distribution.*

since parameters a_0, a_1 and σ_{Hs} have a combined effect on the systematic errors and uncertainty levels and thus cannot be compared in isolation.

DISCUSSION

Main findings

We investigated the accuracy and precision of the subjective visual vertical (SVV) at nine roll tilt angles in eight subjects, using a psychometric approach. In line with previous studies (Mittelstaedt, 1983; Van Beuzekom and Van Gisbergen, 2000; Kaptein and Van Gisbergen, 2004), we found that SVV accuracy was best at small tilt angles, but decreased at large tilts by showing errors of tilt undercompensation (A-effects). In some subjects, we also observed small but systematic errors of overcompensation (E-effects) at intermediate tilts. Likewise, SVV precision was best at upright (0° head tilt) and deteriorated at larger tilt angles. We fitted a Bayesian model to the set of combined accuracy and precision data, to test the hypothesis that the systematic errors of undercompensation at larger tilts reflect the downside of a strategy to improve precision of the central head-tilt signal at small tilt angles. Similarly, E-effects are interpreted as the side-effect of a Bayesian strategy to reduce uncertainty in the estimate of ocular counterroll.

Evaluation of the Bayesian model

Visual signals in the brain are initially encoded in an eye-centered (retinal) frame of reference. To obtain a world-centered percept of visual orientation when the retina's vertical meridian is not aligned with gravity, the brain must convert the original visual signal from retinal to spatial coordinates, using information about eye tilt in space. As early as the 19th century, Aubert already discovered that this transformation is not performed flawlessly (Aubert, 1861). He noticed that subjects who roll-tilted their heads to substantial angles in total darkness, misjudged the world-centered orientation of a visual line, as if they undercompensated for head tilt angle (Aubert or A-effect). Since then, the SVV has been subject of many studies,

which confirmed the A-effect at tilt angles >60° and regularly found opposite errors (E-effect) at smaller tilts (Schöne, 1964; Udo de Haes, 1970; Mittelstaedt, 1983; Van Beuzekom and Van Gisbergen, 2000; Kaptein and Van Gisbergen, 2004; Daddaoua et al., 2008). Mittelstaedt (1983) was the first to interpret systematic errors in the SVV as the downside of a computational strategy. He hypothesized that the raw head-tilt signal is distorted due to an unequal number of hair cells in the two otolith organs, utricle and saccule. In his model, the brain compensates for these errors by adding a head-fixed idiotropic vector to the biased otolith-based gravity vector. As a result, this strategy reduces errors at small tilts but increases errors at large tilts. More specifically, in Mittelstaedt's model, the E-effect is a remnant of the tilt-signal distortion at modest tilt angles whereas the A-effect at larger tilts partly reflects the additional error induced by the idiotropic vector. Later, Eggert (1998) reformulated Mittelstaedt's model in Bayesian terms and showed that the role of the idiotropic vector was mathematically similar to the role of a head prior in the Bayesian framework. Compared with Eggert's model, the present Bayesian scheme makes different assumptions and proposes a generalized strategy to account for both A- and E-effects. The basic assumption is that the sensory signals concerning head tilt and ocular torsion are veridical, on average, but noisy. This assumption is partly based on the fact that head tilt estimates do not show clear signs of distortion (Mast and Jarchow, 1996; Van Beuzekom et al., 2001) but are corrupted by noise which, if used directly, would lead to high SVV variability. By implementing a generalization of previous schemes (Eggert, 1998; MacNeilage et al., 2007; De Vrijer et al., 2008) the present model reduces noise propagation into the spatial vision stage by relying on knowledge about which head tilt and which eye position are most likely on an *a priori* basis, thereby providing a unified explanation of both A- and E-effects.

Explanation of systematic errors

In the present Bayesian model, the SVV is determined by combining retinal information and information about the orientation of the eyes in space. Computing the eye-in-space estimate involves two stages: estimation of head tilt and estimation of eye-in-head orientation, each incorporating the associated prior knowledge. Whereas the head tilt prior has the beneficial effect of increasing precision of the sensory head tilt estimate, it also causes undercompensation for head tilt, which accounts for A-effects. Likewise, prior knowledge on ocular torsion increases precision in the sensory estimate of ocular torsion, but results in an undercompensation for eye-in-head counterroll and thus leads to an E-effect. Hence, the model accounts for the two types of systematic errors in the SVV by invoking two independent computational stages in the reconstruction of the eye-in-space signal that operate independently and cause opposite bias effects (cf. de Graaf et al. 1992). It can be shown that merging the two stages, using only a single prior for eye in space -relying on an *a priori* assumption that the eyes are generally nearly aligned with gravity- would only explain A-effects.

Once the internal eye-in-space signal is obtained, the model simply adds this signal to the retinal signal. If this linear addition assumption is correct, systematic errors in earth-centric vision should only depend on the tilt angle of the observer, independent on the retinal line orientation used for testing. Findings from two studies (Van Beuzekom et al., 2001; Vingerhoets et al., 2008) confirm this prediction. Both studies found that earth-centric

estimates of many different line orientations were all subject to virtually the same bias, the magnitude of which depended only on the body tilt angle. This previous work indicates that, apart from a limited degree of distortion (Betts and Curthoys, 1998; Van Beuzekom and Van Gisbergen, 2000), visual space in a tilted observer is virtually uniformly rotated. These findings support the simple linear addition stage and argue against an important role for complex visual-nonvisual interactions or for purely visual phenomena, like the oblique effect (Luyat et al., 2001; Westheimer, 2003).

Is the proposed link between E-effects and ocular counterroll plausible?

Conclusions from previous studies investigating the relation between visual perception and ocular counterroll (OCR) range roughly between two extremes:

1. OCR is not taken into account in spatial perception
2. The brain compensates perfectly for the effects of OCR

Wade and Curthoys (1997) argued for the first possibility by showing that the difference between the visual and the manually-indicated haptic horizontal (the latter supposedly unaffected by ocular torsion) is closely related to the presence of ocular torsion during visual testing ($r > 0.85$), with slopes varying between 0.57 and 1.51. A further experiment, rotating upright subjects in yaw (Goonetilleke et al., 2008), which induces ocular counterroll but no tilt perception, also revealed a clear correlation between ocular torsion and visual verticality perception (r between 0.4 and 0.8). However, the slope was not unitary, indicating that there was some level of compensation by the visual system. Pavlou et al. (2003) performing a similar experiment, found clear effects on the SVV, suggesting that approximately 76% of the torsional eye position change was uncompensated and thus affected the SVV. A similar observation was made by de Graaf and colleagues (1992) in roll-tilted subjects, but only in subjects with persistent E-effects. However, conclusions by Mast (2000) point in a different direction. In this study, SVV results were found to dissociate from ocular torsional changes induced by centrifugation or barbecue rotation. The Bayesian model provides a rational explanation for the variable results of these previous studies, by suggesting the possibility that OCR may only be *partially* taken into account during visual verticality perception.

Table 3.3 Precision levels of signals involved in spatial vision.

Signal		0° tilt	90° tilt	Evidence	References
Visual, measured	(σ_{L_e})	1°	1°	data	Vandenbussche et al., 1986
SVV, measured	(σ_{SVV})	2.0 ± 0.6°	5.0 ± 1.5°	data	present study
SBT, measured	(σ_{SBT})	4.5 ± 1.0°	10.5 ± 3.4°	data	0° tilt: see chapter 4 90° tilt: Mast & Jarchow, 1996
SBT, predicted	($\sigma_{\hat{H}_S}$)	2.8 ± 0.9°	7.7 ± 1.9°	fit result	present study

Abbreviations: SVV= subjective visual vertical, SBT= subjective body tilt. SBT precision is assumed to reflect the precision of the sensory head-tilt signal ($\sigma_{\hat{H}_S}$). The 0° tilt value (3rd row) is based on psychometric data introduced in Chapter 4. Predicted SBT precision values (4th row) directly result from average best-fit parameter values of a_0 and a_1 (see Table 3.2).

Since the model fits merely specify the amount of uncompensated ocular counterroll, we could not determine whether a subject with ΔE_H =5°, for example, had an OCR amplitude of 10° and 50% compensation, or an amplitude of 5° and 0% compensation. All we can do is to regard ΔE_H as the *minimum* OCR amplitude. This implies that, according to the model, the eyes of subject MD counterrolled by at least 16.5°, whereas JG, MV and RV may not have had any OCR at all (which is rather improbable). Clearly, direct measurements of ocular counterroll in our study would have helped in clarifying this issue, but these were beyond the scope of the study. Another possibility is that the subjects without E-effects had quite normal OCR amplitudes, but compensated perfectly. In the literature, various peak amplitudes of ocular counterroll during static and very slow (quasi-static) tilts have been reported. Population averages roughly vary between 6 and 10° in normal subjects (Diamond et al., 1979; Diamond and Markham, 1983; Kingma et al., 1997; Palla et al., 2006). However, most studies also reported large differences among subjects and Diamond and Markham even found an amplitude range of 2 to 20° during slow (3°/s) dynamic tilts (Diamond and Markham, personal communication, June 11, 2008). Whether the high inter-subject variability in OCR explains the equally variable E-effect, can only be assessed by simultaneous measurement of both variables.

Effect of simplifying assumptions

The question arises to what extent the fit results may have been affected by the fact that visual noise and noise in the eye-torsion estimate were not fitted separately. As a result, in the fits, the parameters representing head-in-space noise and head-tilt prior width (a_0, a_1, σ_{Hs}) also partially reflected the contributions of these additional noise sources (see *Methods*). We performed several simulations with the Bayesian model to test how large these effects may have been in a worst-case scenario. To do so, we created data through forward simulations of the complete Bayesian model (without simplifications) using the best-fit parameter values of a single subject (PM, see Table 3.2) combined with a set of values for visual noise (σ_{Γ_E}), eye-in-head noise ($\sigma_{\dot{E}_H}$) and eye-in-head prior width (σ_{E_H}). The simulated data sets were then fitted with the simplified model, resulting in new parameter values, which were compared with the 'real' values. Even when large values for eye-in-head noise and eye-in-head prior width were used (both 8°) and visual noise was 1°, we found only a slight change in best-fit parameter values. Not surprisingly, parameter a_0, reflecting the offset of tilt noise, was affected most (changing from 3.3 to 6.5°), whereas the other parameters showed only minor changes. We conclude that these simplifying assumptions (see *Methods* section *SVV precision*) were warranted and that conclusions remain unchanged.

Evidence for precision-accuracy trade-off in earth-centric vision

Why would the brain apply a strategy that gives rise to systematic errors if the involved sensory signals are all accurate? The answer to this question may be found in the relative precision levels of the sensory systems that are involved in spatial vision. Table 3.3 gives an overview of the precision levels of the SVV and its underlying signals, as suggested by previous experimental data and the present study.

The visual system is known to be very precise, with just-noticeable-difference (JND) levels for orientation discrimination of maximally 1° for the line length used in our study

(Vandenbussche et al., 1986). Since the SVV task requires additional sensory information about the spatial orientation of the eyes, SVV precision is worse than in a simple orientation discrimination task and deteriorates with head tilt angle, with average SD values of 2.0° at upright and 5.0° at 90° tilt. Can this tilt dependency and the overall decrease of precision be ascribed to the precision characteristics of the compensatory head-tilt and eye-torsion signals? A measure for the precision of the head-tilt signal comes from a study by Mast and Jarchow, (1996), who tested subjective body tilt (SBT) in human subjects and found that the average SD of body tilt settings was 10.5 ± 3.4° at 90° body tilt. Unpublished psychometric SBT data from our laboratory show a somewhat lower average SD level of ~8° at 90° body tilt and an SD of ~4.5° near upright. It is interesting to compare these experimental data with the head-tilt noise fit results derived from the present experiments. As can be seen by comparing rows 3 and 4 in Table 3.3, the model prediction based on the population averaged parameters a_0 and a_1, amounting to an increase from 2.8° at upright to 7.7° at 90° tilt, shows the same trend as the experimentally obtained values in perceived body-tilt experiments. Taken together with the scatter fits in Figure 3.5, these findings strongly support the model assumption (Eq. 3.2) that noise in the head tilt signal increases with tilt angle. Other studies provide indirect support for this notion. For example, the perturbing effect of roll-optokinetic stimulation on the SVV (Dichgans et al., 1974) and on body tilt estimates (Young et al., 1975) becomes more pronounced at larger tilt angles. Similarly, after prolonged roll rotations, the SVV is more strongly affected by residual semicircular canal signals at larger tilt angles (Lorincz and Hess, 2008). Diamond and Markham, (1983) showed that variability in OCR, which is thought to be mediated by the utricles (Suzuki et al., 1969), increases with tilt angle during dynamic tilting. Likewise, Tarnutzer, Bockisch and Straumann (2007) observed that both SVV and OCR variability increased with tilt angle.

Given that the Bayesian strategy that we propose is geared at reducing noise in the SVV, it is sensible to ask how much noise reduction is actually achieved compared with the scenario of straightforward noise propagation in the contributing signals. Table 3.3 lists experimentally determined noise levels of the visual signal and the head tilt signal, but none of the internal estimate of eye torsion, since such data are (understandably) not available. Even if we ignore the contribution of eye-torsion noise in a noise propagation scenario, simple computations show that precision levels in visual spatial perception would be quite poor (4.6° at 0° tilt and 10.5° at 90° tilt) based on these three sensory signals in a straightforward manner. The fact that the actual SVV precision is so much better can now be understood as being the result of a precision-accuracy trade-off based on a Bayesian strategy that aims at high precision, at the cost of reduced accuracy.

APPENDIX

Bayesian model: derivation of Equations 3.3 and 3.4

In case of a single trial, the optimal estimate of head tilt angle ($\tilde{H}_S$), for given sensory signal $\hat{H}_S$ and prior information, is obtained by applying Bayes' rule, and is defined by:

$$\tilde{H}_S = \frac{\sigma^2_{H_S}}{\sigma^2_{H_S} + \sigma^2_{\hat{H}_S}} \cdot \hat{H}_S \qquad \text{Eq. 3.A1}$$

This relation is obtained by taking the maximum value of the posterior distribution. The expected value μ of $\tilde{H}_S$ in many repeated trials is then specified by:

$$\mu_{\tilde{H}_S} = \frac{\sigma^2_{H_S}}{\sigma^2_{H_S} + \sigma^2_{\hat{H}_S}} \cdot \mu_{\hat{H}_S} = \frac{\sigma^2_{H_S}}{\sigma^2_{H_S} + \sigma^2_{\hat{H}_S}} \cdot H_S \qquad \text{Eq. 3.A2}$$

which equals the first term of Eq. 3.3. The variance of $\hat{H}_S$ determines the variance of $\tilde{H}_S$ according to:

$$\mathrm{var}(\tilde{H}_S) = \left(\frac{\partial \tilde{H}_S}{\partial \hat{H}_S}\right)^2 \cdot \mathrm{var}(\hat{H}_S) = \left(\frac{\sigma^2_{H_S}}{\sigma^2_{H_S} + \sigma^2_{\hat{H}_S}}\right)^2 \cdot \sigma^2_{\hat{H}_S} \qquad \text{Eq. 3.A3}$$

which is equivalent to the first term of Eq. 3.4. The same principle applies to the mean value and variance of the eye-in-head estimate ($\tilde{E}_H$):

$$\mu_{\tilde{E}_S} = \frac{\sigma^2_{E_H}}{\sigma^2_{E_H} + \sigma^2_{\hat{E}_H}} \cdot \mu_{\hat{E}_H} = \frac{\sigma^2_{E_H}}{\sigma^2_{E_H} + \sigma^2_{\hat{E}_H}} \cdot A\sin(H_S) \qquad \text{Eq. 3.A4}$$

which equals the second term of Eq. 3.3. Here we use the assumption that the expected value of $\hat{H}_S$ is equal to the real head-in-space angle (H_S). For the variance in the eye-in-head estimate we deduce,

$$\mathrm{var}(\tilde{E}_H) = \left(\frac{\partial \tilde{E}_H}{\partial \hat{E}_H}\right)^2 \cdot \mathrm{var}(\hat{E}_H) = \left(\frac{\sigma^2_{E_H}}{\sigma^2_{E_H} + \sigma^2_{\hat{E}_H}}\right)^2 \cdot \sigma^2_{\hat{E}_H} \qquad \text{Eq. 3.A5}$$

which is equal to the second term of Eq. 3.5.

ACKNOWLEDGMENTS

We thank H. Kleijnen, G. van Lingen, S. Martens, and G. Windau for technical support, and F. van Wamel for experimental assistance. This work was supported by Donders Centre for Cognition and Faculteit der Natuurwetenschappen, Wiskunde en Informatica of Radboud University Nijmegen and by grants from the Netherlands Organization for Scientific Research and the Human Frontier Science Program to W.P. Medendorp.

Chapter 4

Multisensory processing for orientation perception

De Vrijer M, Van Gisbergen JAM, Medendorp WP, *under revision*

One of the challenges for the brain is to take advantage of redundant information from multiple noisy sensors to create a coherent and stable percept of the outside world. Instead of just selecting and processing the best signal, it has been proposed that an even more optimal strategy would be to combine all relevant inputs, by assigning more weight to the most reliable information (van Beers et al., 1999; Ernst and Banks, 2002; Zupan et al., 2002; Niemeier et al., 2003; Ernst and Bülthoff, 2004; Knill and Pouget, 2004; Körding and Wolpert, 2004; Jürgens and Becker, 2006; Stocker and Simoncelli, 2006; Angelaki and Cullen, 2008).

Here, we investigate whether optimal information processing can explain the strikingly different performance in two spatial orientation tasks that require different combinations of the same sensory modalities. In the subjective visual vertical (SVV) task, subjects estimate the orientation of a visual line with respect to gravity, in otherwise total darkness. At large tilts, it has been shown that substantial systematic errors occur as if tilt angle is underestimated (Aubert, 1861; Mittelstaedt, 1983; Van Beuzekom et al., 2001; Kaptein and Van Gisbergen, 2004). Recent studies have explained this systematic SVV bias by the optimal integration of sensory information and prior knowledge relying on the assumption that small head tilts are most likely. Remarkably, when the same subjects are asked to estimate their tilt angle in the subjective body tilt (SBT) task, their responses are more accurate, but also much more variable (Mittelstaedt, 1983; Mast and Jarchow, 1996; Jarchow and Mast, 1999; Van Beuzekom and Van Gisbergen, 2000). Can this difference be explained by the optimal processing of multisensory information for orientation perception?

As we will show, many factors need to be considered for a fair comparison of accuracy and variability in the two tasks. To provide a theoretical framework, we designed a sensory integration model for spatial vision and body tilt perception, based on the optimal processing of all potentially relevant sensory signals. This model, based on Bayesian inference, links accuracy and variability in the two spatial tasks to the properties of the underlying sensors, which are assumed to be unbiased but noisy. In the scheme, shown in Figure 4.1, three sensory systems contribute the information about the subject's spatial orientation that is required in the SBT and SVV task: 1) Body sensors, providing an estimate of the orientation of the trunk in space, include pressure sensors in the skin and somatic 'graviceptors' in the trunk (Mittelstaedt, 1988). 2) Head sensors, supplying information about the orientation of the head with respect to gravity, correspond to the vestibular system, the otoliths in particular. 3) Neck sensors, providing an estimate of the angle between head and body, comprise the neck proprioceptors. For simplicity, the scheme is limited to SBT and SVV signal processing in darkness. We refer to Dyde et al. (2006) and Vingerhoets et al. (2009) for current ideas about the Bayesian evaluation of visual panoramic cues.

The signals needed in the SBT and SVV computations are derived from these three types of sensors through direct and indirect pathways. Thus, the estimate of body orientation in space ($\tilde{B}_S$), needed for the SBT, can be obtained directly from the body sensors, but also through a reference frame transformation of the head-sensor signal ($\hat{H}_S$), by subtracting the neck signal ($\hat{H}_B$). Likewise, in the SVV task, the brain requires an estimate of head-in-space ($\tilde{H}_S$), which can be obtained from the head sensors ($\hat{H}_S$), but also through an indirect pathway, by combining the body-sensor signal ($\hat{B}_S$) with neck information ($\hat{H}_B$). Along with head-in-space estimate $\tilde{H}_S$, the SVV computations also require estimates of eye-in-head ($\tilde{E}_H$)

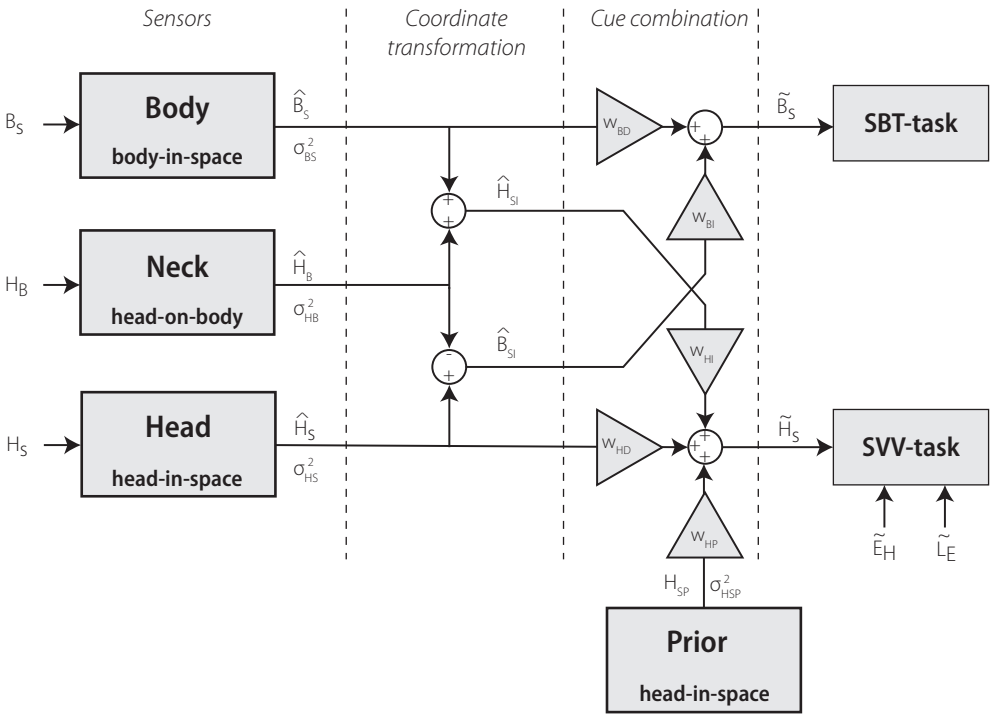

Figure 4.1 Schematic representation of the sensory integration model. Computations in the SBT and SVV task differ in how the same sensory signals are combined and in the application of prior knowledge. Sensory signals, denoted by a hat symbol (^), are assumed to be calibrated accurately, but contaminated by Gaussian noise. Optimal estimates are denoted by a tilde (~). Body sensors, neck sensors and otoliths provide information about orientation of body-in-space (B_S), head-on-body (H_B) and head-in-space (H_S), respectively. Neck signal ($\hat{H}_B$) is used for a reference-frame transformation of otolith information into a body-in-space signal ($\hat{H}_S$-$\hat{H}_B$=$\hat{B}_{SI}$), and for a transformation of body information into a head-in-space signal ($\hat{B}_S$+$\hat{H}_B$=$\hat{H}_{SI}$). For an optimal estimate of body-in-space orientation, $\tilde{B}_S$ (SBT task), the model combines the body-sensor signal ($\hat{B}_S$) with a reference-frame transformed otolith signal ($\hat{B}_{SI}$). Relative contribution of the two pathways (w_{BD} and w_{BI}) depends on their relative precision (see Eq. 4.2). In the SVV task, an optimal estimate of head-in-space ($\tilde{H}_S$) is obtained by integration of otolith information ($\hat{H}_S$), reference-frame transformed information from body sensors ($\hat{H}_{SI}$) and prior information (H_{SP}). Relative weights are denoted by w_{HD}, w_{HI}, and w_{HP}, respectively. Estimate of line-in-space orientation is obtained by combining $\tilde{H}_S$ and estimates of eye-in-head ($\tilde{E}_H$) and line-on-eye ($\tilde{L}_E$) orientation. Noise variance in body sensors (σ^2_{BS}), neck sensors (σ^2_{HB}), otoliths (σ^2_{HS}) and width of prior (σ^2_{HSP}) defines their relative weights (see Methods). Otolith noise may depend on tilt angle (see Eq. 4.6). Note that the process of sensory integration, denoted here by summation of weighted sensory signals, is equivalent to multiplication of the underlying probability distributions (see Eq. 4.2 and 4.4 and Appendix).

and line-on-eye ($\tilde{L}_E$) orientation (De Vrijer et al., 2009).

Following previous model studies (Eggert, 1998; MacNeilage et al., 2007; De Vrijer et al., 2008, 2009), the SVV computation in the scheme also incorporates prior information about head-in-space orientation (H_{SP}). To account for the fact that SBT performance is fairly accurate in most subjects (Mittelstaedt, 1983; Mast and Jarchow, 1996), it is further assumed that the SBT task does not rely on prior information. Thus, *a priori*, all possible body orientations are considered as equally likely. This amounts to a non-informative uniform prior, which is therefore not shown in the scheme.

Why would an observer make use of both direct and indirect pathways? The advantage of such a signal integration strategy is that the variability of the final estimate can be reduced compared to the variability of either pathway in isolation (Ernst and Banks, 2002; Ernst and Bülthoff, 2004). According to optimal signal integration theory, the optimal estimate is obtained as the weighted sum of the available relevant signals, using weights proportional to the relative reliability of each sensor (the normalized reciprocal noise level). Because the SBT and SVV computations require different reference frame transformations, the relative contribution of the sensory signals may differ in the two tasks (see *Methods* section *Sensory integration model*, for further details).

To test the explanatory power of this sensory integration model, we determined the accuracy and variability in the SVV and the SBT of human subjects, using a psychometric approach. We tested the SBT at two well-defined tilt angles: 0° (upright) and 90° (horizontal, right ear down) to ensure that the task instruction was unambiguous. From the same subjects, we obtained SVV data at 9 tilt angles, ranging between -120 and +120°. At 90° tilt, we found that SBT estimates were consistently more accurate but also more variable than the SVV estimates. We further found that the variability in both tasks increased with tilt angle. With only six parameters, our model could account for the complete data set from each subject. These results suggest that performance in the SVV and SBT task is statistically optimal in the sense that all sensory signals are weighted by their relative precision (inverse of variance). In the *Discussion*, we review experimental support for the proposed signal combination in the two tasks.

METHODS

Subjects

Four subjects (3 male, 1 female, one author) provided written informed consent to participate in the experiments. Ages ranged from 23 to 65 yrs. Subjects were free of any known vestibular or other neurological disorder and had normal, or corrected-to-normal visual acuity. All subjects took part in SBT and SVV experiments (see below) without receiving feedback about their performance. Before each experiment started, subjects received careful instructions and performed a few practice runs to get used to the task. Each subject participated in 11 experimental sessions of ≥45 min each.

Setup

Body tilt was controlled by a computer-controlled vestibular chair, which was configured to allow subject rotation in roll. A digital position-encoder measured roll position with an angular resolution of 0.04°. The subject's body was tightly fixated using a five-point seat belt and adjustable shoulder and hip supports. Velcro straps restrained both legs and feet and a padded helmet firmly fixated the head in a natural upright position for looking straight ahead. Subject-specific seat adjustments ensured that the naso-occipital axis midway between the eyes coincided with the roll-axis of the chair. Experiments took place in complete darkness.

Experiments

Subjective body tilt (SBT)

The SBT experiment served to obtain a psychometric measure of each subject's accuracy and precision in body tilt perception at two body orientations: upright (0°, SBT_0 task) and horizontal (90° right ear down, SBT_{90} task). We applied the method of constant stimuli, using a set of 10 equidistant body-tilt angles, centered on tentative estimates of the subject's 0° (SBT_0) and 90° (SBT_{90}) body tilt percept. The latter were determined in a few pilot trials that also served to familiarize the subject with the task. We used test angle intervals of 3° and 4° in the SBT_0 and SBT_{90} task, respectively. Body-tilt angles were tested 14 times in random order, yielding 140 responses for each psychometric curve.

To perform the psychophysical SBT experiments, two methodological problems had to be solved. The first relates to the number of experimental sessions that we could reasonably ask subjects to perform. We realized that returning the subject to upright for reorientation after each trial would require a too large number of experimental sessions. Our overriding concern was that starting each trial from upright would introduce a confound in the SBT_0 task in the sense that subjects could then simply notice the change in chair position. To prevent this, we always inserted a detour rotation before moving the subject to the test angle in a given trial. The detour, always to a tilt position clearly outside the psychometric test range, served to reset the subject's memory of the previous tilt position. These *detour angles* were chosen randomly from a range at 30° - 40° CW and CCW from the presumed threshold (see Figure 4.2, *detour range*). Detour angles preceding each test angle were equally often taken from the CW and the CCW detour range.

Each experimental run started in upright position with the room lights on. After the lights were turned off, subjects were first rotated to a random detour angle, outside of the test angle range at a constant angular velocity of 30°/s, where they remained for 3 s. The chair then moved to a randomly chosen position within the test range with a very slow and noisy profile, defined by the sum of a ramp of 0.4 - 2°/s and Gaussian white noise (bandwidth 0-0.7 Hz, RMS amplitude 3.4 deg). Ramp speed was chosen such that the trajectory between detour angle and test angle was reached in 30 s (see Figure 4.2). These precautions were taken to enforce independent absolute tilt judgments and to deter reliance on sensed changes in tilt position that occurred since the previous trial. Three seconds after arrival at the test angle, a beep signal prompted the subject to indicate whether body orientation was CW or CCW from the reference orientation (0° in the SBT_0 task or 90° in the SBT_{90} task), using a toggle switch. The subject was then rotated at a constant velocity to a new randomly drawn detour angle and the above procedure was repeated. Each run, comprising 7 test angles, lasted about 5 min, after which the subject was rotated back to upright and room lights were turned on. Between runs, there was a 60-s interval allowing the subject to rest before the next run started. The SBT_0 and SBT_{90} task were tested in three separate sessions of approximately 45 min each, thus amounting to a total of 6 sessions per subject.

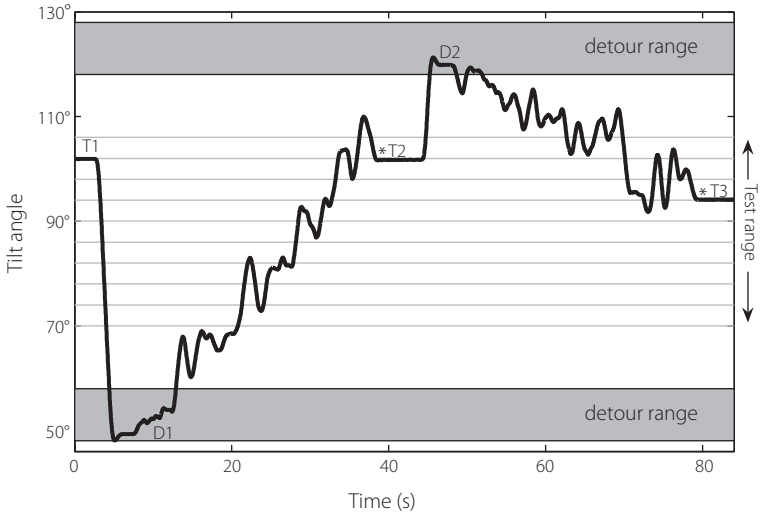

Figure 4.2 Rotational paradigm in SBT_{90} task. T1, T2, T3:, test angles at which the subject was prompted with a beep signal (*) to indicate whether body orientation was CW or CCW from the instructed reference orientation (i.e. 90° in this example). D1, D2: detour angles, randomly drawn from detour range (30-40° CW and CCW from center of test range). Rotations from detour (D) to test (T) angle were performed in a noisy fashion (see text).

Subjective visual vertical (SVV)

The same subjects were also tested in a series of SVV experiments. Their data have been published previously as part of a larger data set on visual verticality perception (De Vrijer et al., 2009). Here we provide a brief summary of the paradigm. SVV was tested at 9 roll tilt angles, ranging from -120 to 120° at 30°-intervals. A luminous line (angular subtense 20°), polarized with a bright dot at one end, was mounted in front of the subject. The line's rotation axis coincided with the chair rotation axis. In each experimental run, the subject was rotated from upright to the chosen test angle at a constant angular velocity of 30°/s. After a 30-s waiting period that allowed canal effects to subside, a luminous line was briefly flashed (20 ms) and the subject indicated whether its orientation in space was clockwise (CW) or counterclockwise (CCW) from their perceived direction of gravity. The line orientation was selected randomly from a set of 11 line orientations. After all line orientations had been tested, the subject was rotated back to upright and room lights were turned on. Positive and negative body tilt angles were alternated regularly. Like in the SBT experiment, we used the method of constant stimuli. The set of 11 line orientations was centered on a coarse estimate of the SVV threshold at each tilt angle. We used orientation intervals of 3°, except for upright, where intervals of 2° were taken. Each set of line orientations was tested in random order in 12 experimental runs, thus yielding a total of 132 responses for each psychometric curve. SVV data were collected in a total of five 45-min sessions per subject.

Data analysis

Clockwise tilt angles of the body and the luminous line were defined positive. We quantified performance by examining the proportion of CW-responses as a function of body orientation

(SBT) and the proportion of CCW-responses as a function of line orientation with respect to the body (SVV). Psychometric data were quantified by fitting a cumulative Gaussian function (see Figure 4.3):

$$P(x) = \lambda + (1 - 2\lambda) \cdot \int_{-\infty}^{x} e^{-(y-\mu)^2/2\sigma^2} dy \qquad \text{Eq. 4.1}$$

in which x represents body orientation in space (SBT experiment) or line orientation with respect to the body (SVV experiment). The mean of the Gaussian μ represents the perceived upright (SBT_0) or horizontal (SBT_{90}) body orientation in the SBT task, or the subjective visual vertical compensation angle (the angle between the apparent visual vertical line and the body axis) in the SVV task. The width of the curve, σ^2, inversely related to precision, serves as a measure of the subject's variability in the SBT or SVV task. Parameter λ, representing the lapse rate, accounts for stimulus-independent errors caused by subject lapses or mistakes, and was restricted to small values ($\lambda < 0.06$). Fits were performed using Matlab 7.0 software (The MathWorks) with the routine *psignifit* (Wichmann and Hill, 2001b).

Sensory integration model

In the scheme (Figure 4.1), we use the following conventions: physical variables are denoted by a capital with a subscript indicating the frame of reference. For example, H_S represents the physical orientation of the head in space. Sensory signals and their reference-frame transformed counterparts are denoted by a hat symbol (^), like in $\hat{H}_S$, which represents the orientation of the head in space as measured by the head-in-space sensors. The optimal estimate of a variable, obtained by integration of all available information, is indicated by a tilde (~), like in , representing the final head-in-space estimate.

It is assumed that all sensory signals are accurately calibrated (i.e. unbiased) but corrupted by independent Gaussian noise with a given variance (σ^2), with subscripts to indicate the sensory modality (e.g. σ^2_{BS} represents noise variance in the body-in-space sensors).

SBT computation

To obtain an estimate of the orientation of the body in space, the brain can use 'direct' sensory information from body sensors ($\hat{B}_S$), such as tactile receptors in the skin or so-called graviceptors in the trunk (see Mittelstaedt, 1997, 1998; Vaitl et al., 2002). Alternatively, an 'indirect' pathway, involving a reference frame transformation, can also provide a body-in-space estimate. For this purpose, sensory head-in-space information, provided by the otoliths, must be combined with information about head-on-body orientation, provided by proprioceptive signals from the neck ($\hat{B}_{SI} = \hat{H}_S - \hat{H}_B$). Since the sensors are contaminated by noise, the direct and indirect signals can be represented as Gaussian probability distributions with mean values of $\hat{B}_{SI}$ and $\hat{H}_S - \hat{H}_B$, and variance levels of σ^2_{BS} and $\sigma^2_{HS} + \sigma^2_{HB}$, respectively. According to optimal observer theory, a statistically optimal estimate of body-in-space orientation ($\tilde{B}_S$) is then given by the peak of the Gaussian distribution that results from the multiplication of these two distributions. It follows that:

$$\tilde{B}_S = w_{BD} \cdot \hat{B}_S + w_{BI} \cdot (\hat{H}_S - \hat{H}_B) \qquad \text{Eq. 4.2}$$

with $w_{BD} = \frac{1/\sigma_{BS}^2}{1/(\sigma_{HS}^2 + \sigma_{HB}^2) + 1/\sigma_{BS}^2}$

and $w_{BI} = \frac{1/(\sigma_{HS}^2 + \sigma_{HB}^2)}{1/(\sigma_{HS}^2 + \sigma_{HB}^2) + 1/\sigma_{BS}^2}$

in which w_{BD} and w_{BI} (see Figure 4.1) represent the respective weights of the direct and indirect pathway, which add up to one (Landy et al., 1995; Jacobs, 1999; Ernst and Banks, 2002; Bays and Wolpert, 2007). Note that the weight of each pathway depends on its reciprocal noise variance (also known as precision), so that precise signals have a stronger influence on the final estimate than noisy signals. Furthermore, since both sensory pathways are supposed to be based on unbiased sensory signals, the mean estimate of body-in-space in multiple trials, $\mu(\tilde{B}_S)$, will also be accurate.

It can further be shown that the variance in $\tilde{B}_S$ in multiple trials, denoted as $\sigma^2(\tilde{B}_S)$ equals:

$$\sigma^2(\tilde{B}_S) = \frac{\sigma_{BS}^2 \cdot (\sigma_{HS}^2 + \sigma_{HB}^2)}{\sigma_{BS}^2 + (\sigma_{HS}^2 + \sigma_{HB}^2)} \qquad \text{Eq. 4.3}$$

which implies that the final estimate has a lower variance than the signal provided by either the direct or the indirect pathway (see Ernst and Banks, 2002; Ernst and Bülthoff, 2004). Because we assume that sensory signals are accurate and that there is no prior information about body-in-space that may bias this percept (see *Introduction*), the model predicts that there are no systematic errors in the SBT, so that $\mu(\tilde{B}_S)=0$. The variance in the SBT task is represented by $\sigma^2(\tilde{B}_S)$.

SVV computation

The scheme applies a similar signal processing strategy to estimate the orientation of head in space, $\tilde{H}_S$, used in the SVV. A direct estimate of head-in-space orientation is provided by the head-in-space sensors ($\hat{H}_S$); an indirect estimate is obtained by a reference frame transformation of the body-in-space signal ($\hat{B}_S$) by adding the head-on-body estimate ($\hat{H}_B$), provided by the neck sensors ($\hat{H}_{SI}= \hat{B}_S + \hat{H}_B$). Again, direct and indirect pathway signals are represented by two Gaussian probability distributions, with mean values of $\hat{H}_S$ and $\hat{B}_S + \hat{H}_B$, respectively, and corresponding variances of σ_{HS}^2 and $\sigma_{BS}^2 + \sigma_{HB}^2$. In the computation of the head-in-space estimate, it is further assumed that the brain uses *prior knowledge* about head-in-space orientation, which entails that small head tilt angles are more probable than large tilts. Mathematically, the prior is represented by a Gaussian distribution that is centered at 0° head tilt ($H_{SP}=0$) with a variance of σ_{HSP}^2. Note that, in our scheme, the head-in-space prior, which contributes to the SVV computations, does not affect the body-in-space estimate. Integration of the direct and indirect sensory pathways and prior knowledge is performed by multiplication of the three Gaussian distributions. The peak of the resulting *posterior* distribution represents the optimal estimate of head-in-space orientation ($\tilde{H}_S$), which is given by:

$$\tilde{H}_S = w_{HD} \cdot \hat{H}_S + w_{HI} \cdot (\hat{B}_S + \hat{H}_B) + w_{HP} \cdot H_{SP} \qquad \text{Eq. 4.4}$$

with $$w_{HD} = \frac{1/\sigma_{HS}^2}{1/(\sigma_{BS}^2 + \sigma_{HB}^2) + 1/\sigma_{HS}^2 + 1/\sigma_{HSP}^2},$$

$$w_{HI} = \frac{1/(\sigma_{BS}^2 + \sigma_{HB}^2)}{1/(\sigma_{BS}^2 + \sigma_{HB}^2) + 1/\sigma_{HS}^2 + 1/\sigma_{HSP}^2}$$

and

$$w_{HP} = \frac{1/\sigma_{HSP}^2}{1/(\sigma_{BS}^2 + \sigma_{HB}^2) + 1/\sigma_{HS}^2 + 1/\sigma_{HSP}^2}$$

In this equation, w_{HD}, w_{HI} and w_{HP} (which add up to one) represent the weights of the direct and indirect pathways and the prior, respectively, which are proportional to the relative precision of the sensory signals and the width of the prior. Equation 4.4 would result in an accurate estimate of , if all three pathways were accurate by themselves. However, since the prior is centered on zero ($\hat{H}_{SP}$ =0°), it introduces more and more bias toward upright, as body tilt increases further. Thus, optimization in terms of variance has a downside by causing underestimation of the actual head tilt. The amount of underestimation depends on the width of the prior and the reliability of the sensory inputs (see also Figure 4.A1 in the *Appendix*).

The variance in the head-in-space estimates, measured across many trials, $\sigma^2(\tilde{H}_S)$, can be derived directly from Eq. 4.4 by applying the rules of error propagation (see *Appendix* for complete derivation). From these calculations it follows that:

$$\sigma^2(\tilde{H}_S) = w_{HD}^2 \cdot \sigma_{HS}^2 + w_{HI}^2 \cdot (\sigma_{HS}^2 + \sigma_{HB}^2) \qquad \text{Eq. 4.5}$$

in which the variance contributions of the direct and indirect pathways are represented by their squared weights. Although it does not appear explicitly in Equation 4.5, it is important to notice that the prior has a noise reducing effect by down-scaling the sensory related weighting terms (w_{HD} and w_{HI}). The narrower the prior, the larger its relative weight (w_{HP}), and the smaller the sensory weights, since $w_{HD}+w_{HI}+w_{HP}=1$. Thus, the effect of the head-in-space prior is twofold: it reduces the variance but, as noticed above, this occurs at the cost of a bias in the final estimate of head-in-space orientation which becomes pronounced at large tilts (see *Appendix* for further details).

Previously, we have shown that in order to account for the typical nonlinear increase of the systematic SVV errors with tilt, the variability of the head tilt signal in the model must increase with tilt angle (*Chapter 2* and *3*, De Vrijer et al., 2008, 2009). This feature was incorporated by allowing the noise in the sensory head-tilt signal, σ_{HS}, to increase rectilinearly with tilt angle:

$$\sigma_{HS} = a_{HS} \cdot |H_S| + b_S \qquad \text{Eq. 4.6}$$

in which a_{HS} reflects the proportional increase of noise with tilt angle and b_{HS} represents the noise at H_S=0°. Note that, in the data fits, parameter a_{HS} was allowed to be zero, so that the present model did not force σ_{HS} to depend on head tilt.

To compute the SVV, the brain not only requires an estimate of head orientation in space ($\tilde{H}_S$), but also needs estimates of eye-in-head orientation ($\tilde{E}_H$) and retinal line orientation ($\tilde{L}_E$). Together, these signals determine the orientation of a visual line in space ($\tilde{L}_S$) according to $\tilde{L}_S = \tilde{H}_S + \tilde{E}_H + \tilde{L}_E$. The error in the SVV experiment (ΔSVV) corresponds to the error in $\tilde{L}_S$ and is thus given by $\Delta SVV=\Delta H_S + \Delta E_H + \Delta L_E$, in which Δ denotes the error in each estimate. For simplicity, we assumed that the visual signal representing retinal line orientation

is accurate, so that ΔL_E=0. As explained in a previous study (*Chapter 3*, De Vrijer et al., 2009), underestimation of eye torsion causes errors in the eye-in-head estimate (ΔE_H), which can be represented by ΔE_H=-A_{OCR}·sin($\hat{H}_S$), where parameter A_{OCR} denotes uncompensated ocular counterroll. Finally, the error in the head-in-space estimate is obtained by subtracting $\tilde{H}_S$ (see Eq. 4.4) from the actual head tilt H_S, which ultimately leads to the following relation for the mean SVV error, μ(ΔSVV), in multiple trials:

$$\mu(\Delta SVV) = (1 - w_{HD} - w_{HI}) \cdot H_S - A_{OCR} \sin(H_S) \qquad \text{Eq. 4.7}$$

In this equation, the influence of the prior works through the weight factors wHD and wHI. Since these weights do not add up to one (see above, $w_{HD}+w_{HI}= 1-w_{HP} <1$), the result is a systematic error in the head-in-space estimate, which becomes more pronounced at large tilt. Because the noise level in the eye-in-head and line-on-eye estimates is probably relatively small compared to the noise in the head-in-space estimate (Vandenbussche et al., 1986), the model assumes that SVV variance is determined mainly by the variance in the latter estimate, so that $\sigma^2(\Delta SVV) \approx \sigma^2(\tilde{H}_S)$.

In summary, the model contains 6 fit parameters (a_{HS}, b_{HS}, σ_{HSP}, σ_{BS}, σ_{HB} and A_{OCR}) that determine performance in the SBT and SVV task at each tilt angle (see Table 4.1). Parameters a_{HS} and b_{HS} represent the increase and offset of sensory noise in the head-in-space estimate (σ_{HS}), respectively. Parameter σ_{HSP} denotes the width of the prior distribution, reflecting *a priori* knowledge about head-in-space. Noise levels in the body and neck sensors are represented by parameters σ_{BS} and σ_{HB}. Finally, the amplitude of uncompensated ocular counterroll is denoted by A_{OCR}.

Model fits

The best-fit parameters of the model were obtained using the experimental responses. Due to its structure, the model cannot account for two aspects of experimental errors: 1) systematic errors in the SBT, if any, and 2) asymmetries in the SVV between CW and CCW tilt angles. Therefore, we applied two preprocessing steps to the data, prior to fitting the model. First, we removed any systematic SBT bias, since otherwise the model would try to account for such bias by an excessive increase in the overall variance. In other words, an actual lack of accuracy would be falsely interpreted as a sign of poor precision. Second, left-right asymmetries in the SVV data were removed by averaging the systematic errors at equal but opposite tilt angles.

Using the preprocessed data, the sensory integration model yields simultaneous fits of the accuracy and variance in the SBT and SVV, given by μ_{SBT} and μ_{SVV}, and σ^2_{SBT} and σ^2_{SVV}, respectively. For each subject, we fitted the model to the preprocessed psychometric responses (2 SBT and 9 SVV curves) by maximizing the likelihood of the data (maximum likelihood estimation, MLE), in relation to the set of 6 model parameters (θ=a_{HS}, b_{HS}, σ_{HSP}, σ_{BS}, σ_{HB} and A_{OCR}). Optimal parameter values were obtained by minimizing the negative likelihood function using the Matlab routine *fmincon*. The log-likelihood function L(θ) is defined by:

$$L(\theta) = L_{SVV}(\theta) + L_{SBT}(\theta)$$

$$= \sum_{i=1}^{N_{SVV}} \log\left(P_{SVV,\theta}\left[N_i(CW_{SVV})\right|\ \theta\right]) + \sum_{j=1}^{N_{SBT}} \log\left(P_{SBT,\theta}\left[N_j(CW_{SBT})\right|\ \theta\right]) \qquad \text{Eq. 4.8}$$

in which $P_{SVV,\theta}[N_i(CW_{SVV})|\theta]$ represents the chance of obtaining N_i CW-responses in the SVV task, for a given combination (i) of tilt angle and line orientation and for parameter set θ. Likewise, $P_{SBT,\theta}[N_j(CW)|\theta]$ represents the likelihood of observing N_j CW-responses in the SBT task, for a specific combination (j) of test angle and task (SBT_0 or SBT_{90}), for parameter set θ. N_{SVV} and N_{SBT} denote the total number of combinations i and j in the SVV and SBT task, which equal 99 (11 line orientations x 9 tilt angles) and 20 (10 test angles x 2 tasks), respectively.

To obtain $P_{SVV,\theta}[N_i(CW_{SVV})|\theta]$ and $P_{SBT,\theta}[N_j(CW)|\theta]$, we first calculated μ_{SVV} and σ_{SVV} (using Equations 4.5 and 4.7) and σ_{SBT} (using Equation 4.3) at each tilt angle, for the given parameter set. Then, we used μ_{SVV} and σ_{SVV} to construct a normal cumulative distribution function, from which we calculated the chance of obtaining a CW-response ($P_{SVV}[CW]$) in the SVV task, at the given combination of tilt angle and line orientation. Subsequently, the chance of obtaining N_i CW-responses, given the 12 repetitions in the SVV task, was specified by the binomial distribution, $B(12,P_{SVV}[CW])$. For the SBT_0 and SBT_{90} task, we constructed normal cumulative distribution functions that were centered on 0 and 90°, respectively, and with σ_{SBT}, which also depended on tilt angle. From these functions we obtained the probability of obtaining a CW-response ($P_{SBT}[CW]$) in the SBT task, at the given test angle. Likewise, the probability of obtaining N_j CW-responses, for the 14 repetitions in the SBT task, was defined by the binomial distribution, $B(14,P_{SBT}[CW])$. Standard deviations of the best-fit parameters were obtained by performing 100 bootstraps.

RESULTS

To test the main assumptions and predictions of a sensory integration model (see Figure 4.1), we investigated the perception of body tilt (SBT) and the subjective visual vertical (SVV) in roll-tilted subjects, using a psychophysical approach. We start with a description of the data, and subsequently present the model fit results.

Psychometric results

The SBT experiment tested the accuracy and precision of subjective body tilt percepts, near upright (SBT_0) and 90° right-ear-down (SBT_{90}). Figure 4.3A shows the fraction of CW-responses as a function of body tilt for the SBT_0 task (open circles) and SBT_{90} task (filled circles) for all four participants. We fitted a psychometric curve through these data (see *Methods*, Eq. 4.1), to obtain estimates for the mean (μ), SD (σ) and lapse rate (λ). Parameter μ is a measure for the accuracy of the subject's body-tilt percept. Perceptual variability, inversely related to precision, is reflected by σ^2, while the lapse rate (λ<0.06) accounts for stimulus-independent errors (Wichmann and Hill, 2001a). In the SBT_0 task, the μ-values, ranging from 0.4° to 4.1°, are on average close to the veridical 0° orientation. In the SBT_{90} task, where μ=90° is veridical, μ-values range from 78.4 to 94.6°, Note that, when μ is below 90° in the SBT_{90} task (SR and JG), the subject in fact *over*estimates body tilt angle, whereas μ-values >90° (MD and FW) indicate tilt *under*estimation. The psychometric fits further show that variability is lower in the SBT_0 task, where σ-values range from 3.3 to 5.7°, than in the SBT_{90} task, where σ ranges between 6.7 and 10.7°.

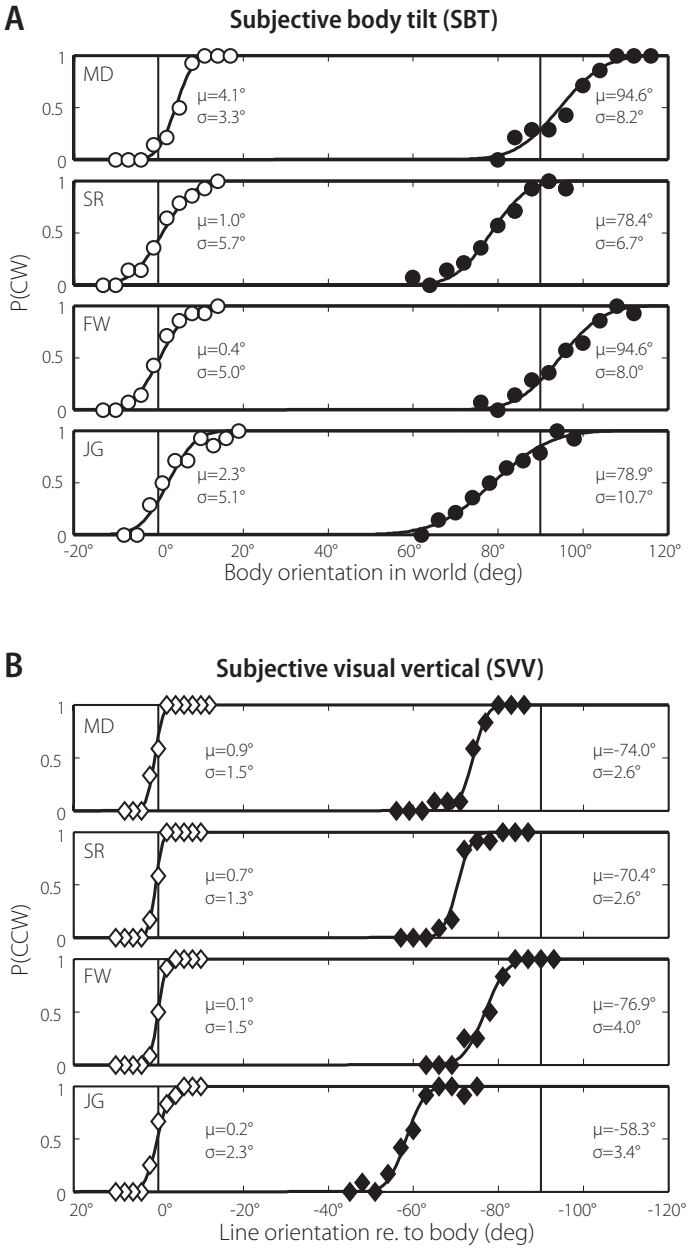

Figure 4.3 SBT and SVV performance for all subjects. A. SBT: Proportion of CW-responses is plotted against body orientation with respect to gravity: SBT_0 task (open circles); SBT_{90} task (filled circles). B. SVV: Proportion of CCW-responses plotted against line orientation with respect to body: SVV_0 (open diamonds); SVV_{90} (filled diamonds). Veridical performance would yield step functions at 0° (SBT_0 and SVV_0) and +90°(SBT_{90}) or -90°(SVV_{90}). Solid lines: best-fit cumulative Gaussians, typified by μ and σ.

Corresponding SVV data are depicted in Figure 4.3B, for 0° (open diamonds) and 90° (filled diamonds) tilt, plotted as a function of the line orientation with respect to the longitudinal body axis. Perfect performance would yield unity step functions at 0° and 90°, respectively. Cumulative Gaussian curves were fitted through the data to obtain estimates of subject's accuracy (μ) and precision (σ). As shown by the left-hand curves, accuracy is close to perfect in the SVV_0-task in all subjects, with mean values ranging between 0.1 and 0.9°. However, in the SVV_{90}-task, where -90° would be perfect, perceptual thresholds are clearly biased to smaller angles, ranging from -58.3 to -76.9°, which corresponds to substantial errors of tilt undercompensation. The variability in the SVV_0 task ranges between σ=1.3° and 2.3°, which is consistently lower than in the SVV_{90}-task, where values range between σ=2.6° and 4.0°. Note that the SVV was not only determined at 0° and 90° tilt, but across a broad tilt range (-120 to 120°) and that all these results were used in the model fits (see next section).

The results presented thus far indicate that SVV and SBT have different accuracy and precision characteristics. However, a proper comparison between these tasks requires a comparison of these characteristics at the same *physical* tilt angles (0 and 90°). Recall that the SBT task determines the tilt angles that are perceived as 0° and 90° tilt, which are not necessary equal to the physical 0 and 90°. To infer the SBT accuracy and variability at 0 and 90° tilt, we linearly extrapolated the μ and σ values from the SBT_0 and SBT_{90} task. In Figure 4.4, we

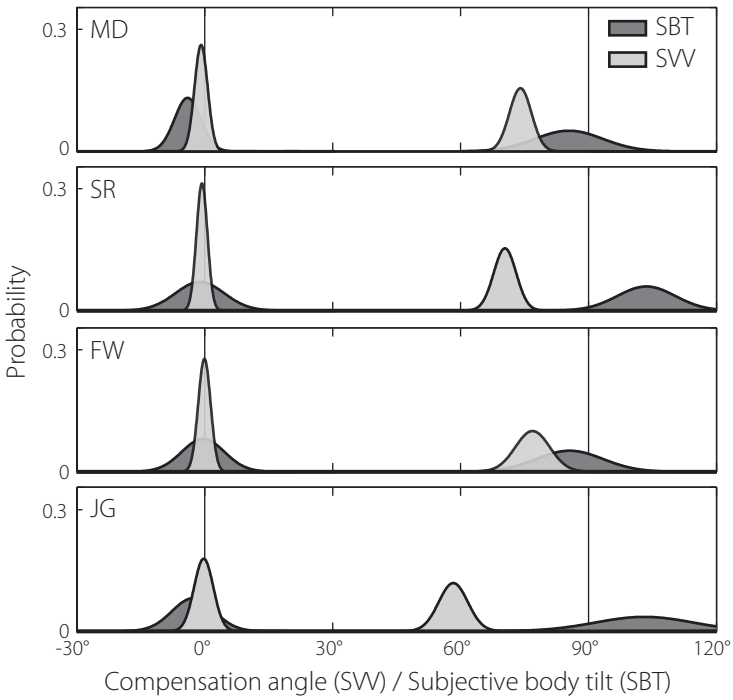

Figure 4.4 Comparison of variability and accuracy in SBT and SVV. Non-cumulative best-fit Gaussian functions (see Figure 4.3). SVV curves at 90° head tilt show consistent undercompensation; SBT curves are closer to accurate performance at 90° tilt. Variability is lower in the SVV task than in the SBT task at both tilt angles.

plotted the (non-cumulative) SVV_0 and SVV_{90} distributions (blue curves) together with the extrapolated SBT distributions at 0 and 90° tilt (orange curves). At 0° roll tilt, subject's accuracy is similar in the two tasks, with both curves positioned close to veridical (0°). However, at 90° roll tilt, the two curves are clearly separated: SVV curves show clear tilt undercompensation (mean: μ_{SVV}=69.9°), whereas SBT curves are closer to veridical performance (mean: μ_{SBT}=94.4°). Thus, subjects perceive their body tilt angle more accurately than the spatial orientation of the visual line. However, when it comes to variability, performance is reversed: SVV curves are narrower than the SBT curves in all subjects, at both tilt angles, meaning that they are consistently less variable in the SVV task than in the SBT task.

Model fit results

Figure 4.5 shows the fit results of the model, fitted simultaneously to both data sets, including SVV data from all nine tested tilt angles. Systematic SBT errors, shown in the first row of Figure 4.5, reveal moderate deviations in either direction from perfect performance. The sensory integration model cannot account for these errors, as shown by the horizontal fit line through μ_{SBT} =0°. SBT precision is depicted in the second row of Figure 4.5. The fits show an increase of noise with tilt angle similar to the actual increase of noise between 0 and 90° tilt, for all subjects. These model fits further suggest that the increase of SBT noise is steepest at small tilt angles, and levels off at larger tilts. As can be seen in Table 4.1, the increase of SBT noise with tilt angle is entirely attributable to the corresponding increase of noise in the head sensors (parameter a_{HS}). The third row in Figure 4.5 depicts the systematic SVV errors across the entire tilt range (circles) together with the model fit (curve). All subjects show SVV errors of undercompensation at tilts >60°, and three of them (MD, SR and FW) also show errors of overcompensation in the smallest tilt range (<60°). With respect to SVV variability, depicted in the fourth row, fits and data show similar trends, suggesting an increase of SVV noise with tilt angle, which levels off at larger tilts.

For each subject, best-fit parameter values and their bootstrap-based SD levels are listed in Table 4.1. Parameter b_{HS}, representing the noise (σ_{HS}) in the otolith signal in the upright subject, ranges between 1.1 and 1.3° for subjects MD, SR and FW, and a value of 4.1° for subject JG, who made substantially larger systematic SVV errors. Best-fit values of parameter a_{HS} are significantly positive (P<0.05) for all subjects, ranging from 0.07 (JG) to 0.18°/° (MD). This implies that the noise in the otoliths increases with tilt angle. The width of the head-in-space

Table 4.1 Best-fit parameter values and bootstrap-based SD values (between square brackets).

Model parameters	MD	SR	FW	JG	Average
a_{HS} [°/°]	0.18 [0.01]	0.11 [0.01]	0.17 [0.02]	0.07 [0.02]	0.13
b_{HS} [°]	1.1 [0.4]	1.3 [0.3]	1.1 [0.5]	4.1 [2.2]	1.9
σ_{HSP} [°]	10.4 [0.9]	9.0 [0.7]	13.8 [1.3]	11.6 [0.9]	11.2
σ_{BS} [°]	10.9 [1.1]	7.5 [0.5]	9.1 [0.6]	15.9 [2.4]	10.8
σ_{HB} [°]	3.3 [1.9]	7.1 [1.8]	5.9 [1.7]	4.6 [n/a*]	5.2
A_{OCR} [°]	25.3 [1.7]	17.3 [1.8]	16.5 [1.9]	0.0 [n/a*]	14.8

** SD-values are not shown when bootstrapped values formed a skewed distribution. Abbreviations: a_{HS}, tilt-related increase in otolith noise; b_{HS}, otolith noise in upright position; σ_{HSP}, width of head-tilt prior; σ_{BS}, noise in body-in-space sensors; σ_{HB}, noise in neck sensors; A_{OCR}, uncompensated ocular counterroll.*

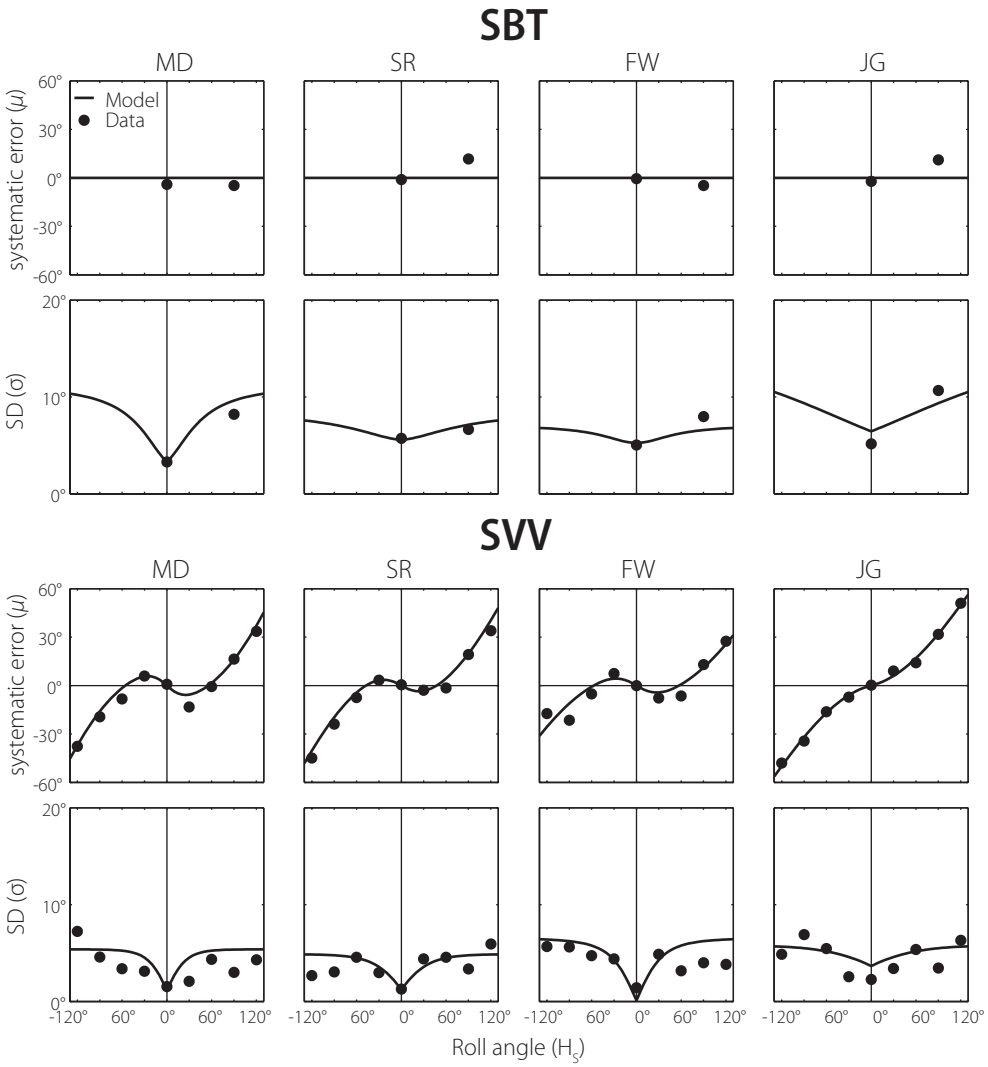

Figure 4.5 Model fits superimposed on SBT and SVV data. Accuracy and variability characteristics as a function of tilt angle; data (circles) and fits (line) from all subjects. Systematic error and SD of data are based on μ- and σ-values from psychometric curve functions (see Figure 4.3).

prior (σ_{HSP}) ranges from 9.0° to 13.8°, consistent with previous literature (De Vrijer et al., 2009). Best-fit values of parameter σ_{BS}, reflecting the noise in the sensory body-in-space signal, range between 7.5 and 15.9° (mean±SD= 10.8±3.7°), which is about twice as large as the best-fit values of parameter σ_{HB}, reflecting noise in the head-on-body signal, ranging from 3.3 to 7.1°, (mean±SD=5.2±1.6). Thus, the parameter fits imply that the neck sensors are more precise than the body-tilt sensors. As has been discussed extensively in *Chapter 3* (De Vrijer et al., 2009), the amplitude of uncompensated ocular counterroll (A_{OCR}), shows large inter-subject variability, ranging from 0° for subject JG to 25.3° for subject MD.

DISCUSSION

In this study, we have investigated the accuracy and precision characteristics in two spatial orientation tasks: the perception of body tilt (SBT) and the visual vertical (SVV). The main experimental findings were: (i) the SBT is more accurate than the SVV, (ii) the SBT is more variable than the SVV and, (iii) both SBT and SVV variability is larger at 90° than near upright. We will discuss how the sensory integration model can explain these results, based on Bayesian computations in the processing of multisensory information.

Comparison with previous work

A world-vertical visual line appears tilted in space when the head is tilted in a darkened room (Aubert, 1861). Mittelstaedt (1983) was the first to emphasize that this phenomenon cannot be explained by errors in the body tilt percept. He showed that subjects could accurately adjust themselves to a horizontal position, but, once in this position, made substantial systematic errors in the perception of visual verticality. Later, combined tests confirmed the apparent discrepancy between SVV and SBT accuracy (Mast and Jarchow, 1996; Jarchow and Mast, 1999; Van Beuzekom and Van Gisbergen, 2000; Van Beuzekom et al., 2001; Kaptein and Van Gisbergen, 2004; Vingerhoets et al., 2008). The present study is consistent with these findings, showing substantial systematic SVV errors at tilts >60°, and fairly accurate SBT performance.

Compared to the abundant literature on SBT and SVV accuracy, data on the perceptual variability in these tasks are scarce. In contrast to Mittelstaedt's observation (1983), Mast and Jarchow (1996) found that the SBT was much more variable than the SVV. The present study, the first to measure both SVV and SBT precision using an extensive psychometric approach, has clearly established that SBT variability is consistently higher than SVV variability, both in upright and in the horizontal (90°) tilt position.

Furthermore, while various studies have noted that SVV variability increased at larger tilts (Schöne, 1964; Schöne and Udo de Haes, 1968; Udo de Haes, 1970; Van Beuzekom et al., 2001; De Vrijer et al., 2008), little is known about SBT variability as a function of tilt angle. Nelson (1968) showed that subjects were more variable when adjusting themselves to a horizontal position than to a vertical (upright) position. The present findings are consistent with these early observations.

Implications of the model

Previous studies have often suggested that the SVV computations are primarily based on otolith information, whereas body sensors are crucial in the SBT computations (e.g. Mittelstaedt, 1983). The question arises whether this view is in accordance with the results of the present study. Furthermore, according to our model, statistically optimal performance would require the use of information from both direct and indirect pathways (see Figure 4.1) to estimate body and head orientation in space. What can be concluded about the relative contribution of both pathways, based on the fit results?

SBT

To obtain the body-in-space estimate, necessary for the SBT, the model uses both direct information from the body sensors and indirect information from the combination of otolith and neck information. Since, as shown in Table 4.1, the variability of the otolith signal (σ_{HS}) increases with tilt-angle ($a_{HS}>0$), the relative importance of direct and indirect pathways becomes tilt dependent. This can be seen in Figure 4.6 (top row), which shows the relative weights of these signals for each subject, derived from Equation 4.2 and the best-fit parameter values in Table 4.1. All subjects show roughly the same qualitative pattern of results. Instead of an overall dominance of body receptors in the direct pathway, the model implies that it is actually the indirect pathway, carrying the otolith signal, which dominates the behaviorally important range near upright. In three of our subjects (MD, SR and FW) it is only when the otoliths become less reliable, at larger tilts, that the body sensors (direct pathway) get the upper hand ($w_{BD}>0.5$); in subject JG the otoliths are even dominant throughout.

After earlier indications that both the otoliths and body sensors contribute to the SBT (e.g. Clark and Graybiel, 1963, 1964; Nelson, 1968), Mittelstaedt (1997) made a quantitative assessment of their impact, using an ingeniously designed experiment. Subjects lay on their side in a horizontal centrifuge. The crux of the experiment was to vary the distance between rotation axis and the interaural axis in order to equalize the opposite contributions from the otoliths and the body sensors so that the subject felt horizontal. By testing normal, paraplegic and nephrectomized subjects, Mittelstaedt inferred how much each sensory system contributes to body tilt perception. It was shown that, apart from the otoliths, also internal 'graviceptors' in the trunk (like the viscera) participate in the computation of the SBT. Later, some related studies provided evidence that the distribution of blood in the body also affects postural perception (Vaitl et al., 1997; Vaitl et al., 2002). According to Mittelstaedt (1998), the weight of the somatic graviceptors to estimate horizontal body orientation in healthy subjects is about 0.6 on average, with considerable intersubject variability. This estimate compares remarkably

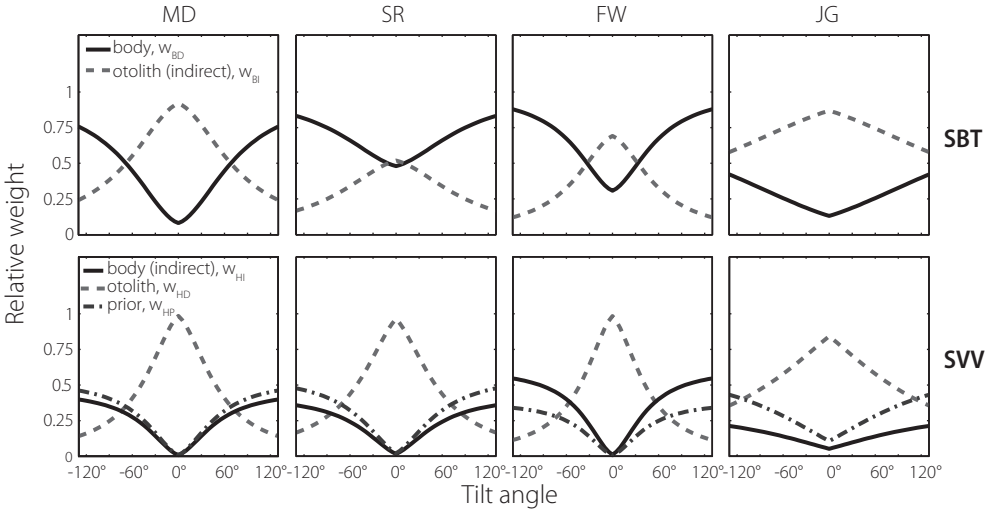

Figure 4.6 Tilt dependence of weight factors in SBT (top row) and SVV (bottom row) for each subject. Trends are similar for all subjects. Head-in-space prior is only involved in SVV computations.

well to our w_{BD} values at 90° tilt, which range between 0.33 (JG) and 0.79 (FW).

Bisdorff et al. (1996) investigated postural sensitivity near upright in healthy subjects and in bilateral labyrinthine-defective patients (see also Bronstein, 1999). They found that the patients performed quite accurately, but were about 40% more variable than normal subjects. From the perspective of our model, the increased SBT variability in the vestibular patients can be attributed to the loss of the otolith contribution through the indirect body-in-space pathway.

SVV

Our model suggests that both information from the otoliths (direct), and the combination of body and neck information (indirect) is used in the computation of the SVV. Figure 4.6 (bottom row) illustrates the relative contributions from these sensors as well as from the prior, based on the model fits (Table 4.1) and Equation 4.4. The SVV pattern looks similar to the SBT pattern (top row): in all subjects, the otoliths are very dominant near upright, with weights close to 1, but their contribution declines when tilt angle increases. As we saw above in the discussion of SBT signal weights, this decline reflects increasing otolith noise levels. In the SVV the decline is steeper than in the SBT, where addition of the neck signal leads to an enhanced noise level with a less pronounced tilt dependence. As the otolith contribution decays, the contributions of the prior and indirect pathway become more manifest. According to our model fits, the weight of the body sensors in the SVV task (w_{HI}) at 90° tilt ranges between 0.18 (JG) and 0.49 (FW).

Previous attempts to identify the separate contributions of the otoliths, neck, and body sensors on the SVV have yielded mixed results. Whereas Mittelstaedt (1998) found no evidence that the SVV was affected by the body sensors in his centrifuge experiment, other studies indicate that neck and trunk tilt aftereffects (Wade, 1968), neck muscle vibration (McKenna et al., 2004) and manipulation of tactile and interoceptive body cues (Trousselard et al., 2004) can affect the SVV. Additional evidence favoring a contribution of an indirect head-in-space signal comes from a study by Bronstein et al. (1996). These authors showed that bilateral labyrinthine-defective patients still compensated for their tilt angle when testing the SVV at 90°, but their systematic errors of undercompensation were about twice as large as in normal subjects. In other words, even in the absence of direct head-in-space information from the otoliths, the brain can still obtain an estimate of head orientation in space through the indirect sensory pathway. These findings suggest that these modalities operate together with the otoliths in the computation of the SVV, consistent with our model. The increased bias in the SVV when the otolith signal is lost is to be expected: as the sensory-derived head tilt estimate becomes more noisy, the effect of the prior becomes more noticeable.

Model evaluation

As shown by Figure 4.5, the sensory integration model accounts remarkably well for the present findings. A major prediction, that the spatial information needed in the SBT and the SVV is based on a weighted combination of gravity-referenced tilt signals in head and trunk, finds independent support in the literature. Accordingly, our results suggest a crucial role for neck receptors in intervening coordinate transformations, reminiscent of earlier findings in yaw

rotation perception (Mergner et al., 1991). Although we feel that the scheme has considerable potential, some uncertainties and limitations need to be discussed.

The architecture of the model, as far as the reference-frame transformations and the sensory integration is concerned, follows entirely from the principles of Bayesian inference. However, to account for the data, we had to make two less straightforward assumptions. First, to explain the increased variability in both tasks at 90° tilt, we allowed for the possibility that the otoliths become more noisy with increases in tilt. Second, we hypothesized that prior knowledge is used in the visual vertical but not in body tilt perception. With these assumptions, the model could well explain our major findings and inter-subject differences. But can these assumptions also be justified on physiological and rational grounds?

One reason to assume that otolith noise depends on tilt angle is based on the fact that the utricle contains considerably more hair cells than the saccule (Rosenhall, 1972, 1974). Since the utricle is most sensitive to tilts around 0°, whereas the saccule is most sensitive around 90° tilt (Jaeger et al., 2008), this may well cause the proposed increase of otolith noise with tilt angle. A tilt-dependent noise level of the otoliths would also help to explain why the perturbing effect of roll-optokinetic stimulation on the SVV (Dichgans et al., 1974; Fernandez and Goldberg, 1976) and on the SBT (Young et al., 1975) is more pronounced at larger tilt angles, and why the SVV is more strongly influenced by residual canal signals at larger tilt angles, after prolonged roll rotations (Lorincz and Hess, 2008). Additional support comes from Diamond and Markham (1983) and Tarnutzer et al. (2007), who reported that variability in ocular counterroll (OCR), which is thought to be mediated by the otoliths, increases with tilt angle.

In the extensive literature on the SVV it is widely assumed that the visual vertical is determined by a weighted combination of a sensory head-tilt signal and a head-fixed reference, denoted as the idiotropic vector (Mittelstaedt, 1983). Recently, this idiotropic vector has been reinterpreted in terms of a Bayesian prior (Eggert, 1998; MacNeilage et al., 2007; De Vrijer et al., 2008), with which it is mathematically equivalent. Interestingly, when tested in gravity-free conditions, subjects still retain a sense of visual vertical, always aligned with their long-body axis, compatible with the idea of head-fixed prior (Mittelstaedt, 1983). Vingerhoets et al. (2008) recently found a similar phenomenon in the SVV during multiple-cycle dynamic roll rotation in normal gravity. They explained this by supposing that the tilt signal becomes more noisy due to a lack of integration time in these dynamic conditions. The resulting noisier tilt signal leads to more weight of the prior, causing the final estimate to be biased more toward the longitudinal head axis. Remarkably, when the same subjects who adopted an almost egocentric reference frame in the SVV were tested in a dynamic SBT experiment, their responses showed very little bias on average, indicating that the prior is used only in the SVV and not for body tilt estimation. To explain how this difference in computational approach might make sense, Vingerhoets et al. (2008) speculated that precision is more important than accuracy for the visual system, for reasons of visual stability Combining the sensory tilt signal with prior knowledge yields a more stable percept of visual space than can be derived from the sensory signal alone. By contrast, for body tilt perception, it is probably less important to be precise and more useful to be accurate and therefore the prior does not take part in this process.

APPENDIX

In this Appendix, we provide further explanation about the Bayesian computations underlying the SVV as expressed in Equations 4.4 and 4.5 in the main text. Figure 4.A1 illustrates graphically that the variance of the posterior distribution in a single trial ($\sigma^2_{\hat{H}s}$) is not simply the same as the variance in its peak location in multiple trials, $\sigma^2(\tilde{H}_S)$. In a single trial (panels A-C), the optimal estimate of head tilt is based on the likelihood (solid black curve, panel B) associated with the combined sensory input from the direct and the indirect pathway (black line, $\hat{H}_S$, panel A) and the prior (dashed curve, panel B), by multiplication of the two probability distributions. The prior distribution is a Gaussian with mean H_{SP} and variance σ^2_{HSP}. The peak of the resulting posterior distribution (gray curve, panel B) is used as the optimal estimate of head tilt ($\tilde{H}_S$), given by:

$$\tilde{H}_S = w_{HS}\hat{H}_S + w_{HP}H_{SP} \qquad \text{Eq. 4.A1}$$

with:

$$w_{HS} = \frac{1/\sigma^2_{HS}}{1/\sigma^2_{HS} + 1/\sigma^2_{HSP}}$$

and

$$w_{HS} = \frac{1/\sigma^2_{HS}}{1/\sigma^2_{HS} + 1/\sigma^2_{HSP}} \qquad \text{Eq. 4.A2}$$

in which σ_{HS} denotes the noise in the sensory signal, known to the observer, and w_{HS} and w_{HP} represent the relative weights of the sensory signal and the prior, respectively. Note that Equation 4.A1 is equivalent to Equation 4.4 in the main text. The variance of the posterior distribution in a single trial is given by:

$$\sigma^2_{\hat{H}S} = w_{HS} \cdot \sigma^2_{\hat{H}s} = \frac{\sigma^2_{HSP}}{\sigma^2_{HS} + \sigma^2_{HSP}} \cdot \sigma^2_{HS} \qquad \text{Eq. 4.A3}$$

and is reflected by the width of the gray curve in panel B. Panels D-F illustrate performance in multiple trials, in which the posterior distributions vary due to sensory noise (σ_{HS}), whereas the prior remains fixed. The variance of each posterior distribution is fixed and is given by Equation 4.A3.

That the variance of the peak locations across multiple trials, $\sigma^2(\tilde{H}_S)$, is smaller can be shown by applying the rules of noise propagation to Equation 4.A1:

$$\sigma^2(\tilde{H}_S) = \left(\frac{\partial\tilde{H}_S}{\partial\hat{H}_S}\right)^2 \cdot \sigma^2(\hat{H}_S) + \left(\frac{\partial\tilde{H}_S}{\partial H_{SP}}\right)^2 \cdot \sigma^2(H_{SP}) = w^2_{HS}\sigma^2_{HS} = \left(\frac{\sigma^2_{HSP}}{\sigma^2_{HS} + \sigma^2_{HSP}}\right)\sigma^2_{HS} \qquad \text{Eq. 4.A4}$$

which is equivalent to Equation 4.5. Corresponding panels G-I illustrate the distribution of the sensory signals for a given tilt angle (filled black curve), the prior distribution (dashed curve), and the optimal estimates (filled gray curve), respectively. Panel I illustrates that the distribution of the optimal estimates across many trials has a lower variance than the posterior distribution in each single trial (panel B), which follows from the comparison of Equations 4.A3 and 4.A4, respectively.

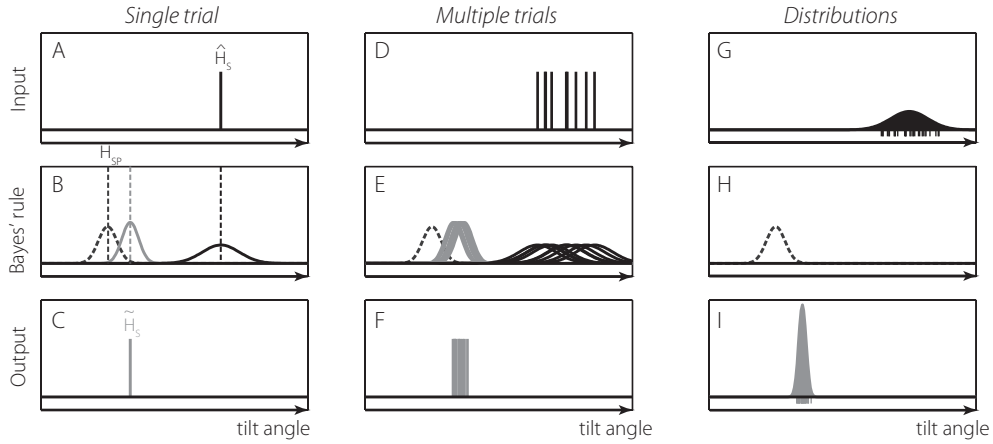

Figure 4.A1 Bayesian computations in single and multiple trials. A-C: single trial, D-F: multiple trials, G-I: resulting distributions.

ACKNOWLEDGMENTS

We thank S. Martens, G. Windau, G. van Lingen, and H. Kleijnen for technical support, and F. van Wamel for experimental assistance. This work was supported by The Donders Centre for Cognition, Faculteit der Natuurwetenschappen, Wiskunde en Informatica (FNWI) of Radboud University Nijmegen, and by grants from the Netherlands Organization for Scientific Research and the Human Frontier Science Program to W.P. Medendorp.

Chapter 5

Roll-optokinetic effects on visual vertical and postural orientation judgments

De Vrijer M, Van Gisbergen JAM, Medendorp WP, *under revision*

INTRODUCTION

A large visual pattern rotating about the line of sight can induce a sensation of continuous body rotation in the opposite direction (Dichgans et al., 1972). Paradoxically, the accompanying change in perceived body tilt remains limited, showing only a slow buildup to a maximum level (Held et al., 1975). This discrepancy between the sense of rotation and the percept of tilt-displacement is thought to arise because the visually induced percept of roll motion conflicts with the veridical graviceptive information provided by otoliths and other gravity sensors.

The strength of the optokinetically induced tilt-displacement can be measured in various ways, such as by testing subjective body tilt (SBT) or with the subjective visual vertical (SVV) task, in which subjects align a luminous line with the perceived direction of gravity. It has been shown that the optokinetic effect increases at larger tilt angles, both for the SBT (Young et al., 1975) and the SVV (Dichgans et al., 1974). These findings suggest that changes in the SVV may simply reflect similar changes in the SBT (Dichgans et al., 1972; Dichgans et al., 1974), but this hypothesis has never been tested in a combined experiment. We refer to this hypothesis as *Hypothesis 1*: ΔSVV=ΔSBT.

For several reasons, however, it is not trivial that a one-to-one relationship will hold. One finding casting doubt on this hypothesis is that the same optokinetic stimulus has been shown to cause asymmetric shifts of the SVV, depending on the direction of the body tilt (Dichgans et al., 1974). Comparable SBT experiments have not shown such a clear-cut asymmetry (Young et al., 1975). Second, it has recently been shown that large roll-optokinetic patterns, along with small-amplitude torsional optokinetic nystagmus, evoke a slowly increasing torsional drift of the eyes, which can amount up to 7.5° in upright subjects (Ibbotson et al., 2005). These optokinetically induced torsional drifts, may bias the SVV (Wade and Curthoys, 1997), but cannot affect the SBT. On this basis, one could also hypothesize that the SVV shift reflects not only the change in perceived body tilt, but also a shift in perceived line orientation, due to a change in eye torsion. The latter factor, to be denoted as *visual shift*,

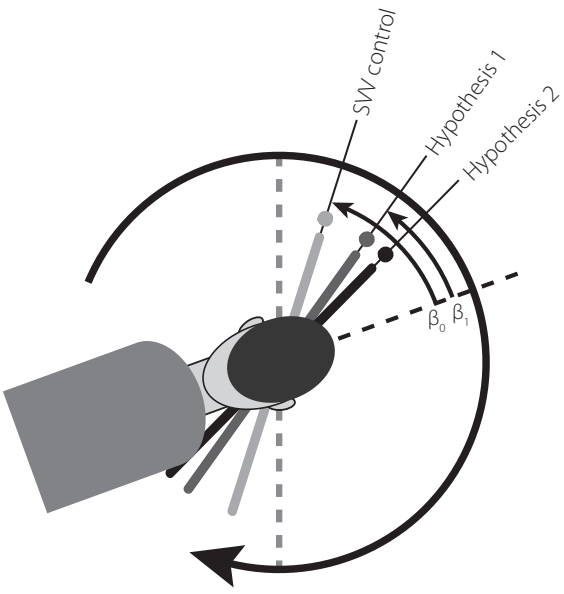

Figure 5.1 Schematic representation of hypotheses. Optokinetic stimulation (large circular arrow) causes shift in perceived body tilt in opposite direction. Hypothesis 1: resulting SVV shift relative to setting in control condition (light gray) reflects change in perceived body tilt (ΔSBT), so that tilt-compensation angle is reduced from β_0 in the SVV control condition to β_1 in optokinetic condition (dark gray line). Hypothesis 2: In addition to ΔSBT, unaccounted ocular torsion (ΔSLB) results in a further shift of the SVV (black line), so that ΔSBT + ΔSLB = ΔSVV represents total optokinetic effect on SVV.

can be assessed by using a subjective line body task (SLB), in which subjects align a luminous line with the perceived direction of the longitudinal body axis. Accordingly, our alternative hypothesis –*Hypothesis 2*– states that ΔSVV=ΔSBT + ΔSLB. In the present study, we tested these two hypotheses by disentangling the putative optokinetic effects on the SVV, SBT and SLB at a range of tilt angles.

Figure 5.1 illustrates schematically how the optokinetic effects on the SVV might be linked to the changes in SBT and SLB. As shown, it is important to note first of all that the SVV line control setting at such a large tilt angle (*light gray line*) already diverges from true vertical, as if tilt angle is underestimated. This phenomenon, known as the Aubert-effect, has been reported before by many studies (Aubert, 1861; Mittelstaedt, 1983; Eggert, 1998; Van Beuzekom and Van Gisbergen, 2000; Van Beuzekom et al., 2001; Kaptein and Van Gisbergen, 2004), and serves as the baseline in our tests. During roll-optokinetic stimulation, observers typically feel their body tilt shifting away from the direction of visual rotation (Young et al., 1975) - a CCW shift in this example. According to Hypothesis 1 (*dark gray line*), this change in perceived body tilt (ΔSBT) is taken into account by adjusting the SVV compensation angle from β_0 to β_1 (ΔSBT= Δβ), which results in a line shift in the direction of the long body axis, in the same direction as the optokinetic flow. According to Hypothesis 2, the optokinetically induced torsional eye movements also affect the SVV. When the observer is unaware of these eye movements, the perceived orientation of a world-fixed visual line is shifted in the direction opposite to the ocular roll-movements. To nullify this apparent line rotation, the observer must rotate the line in the opposite direction, which is in the same direction as the optokinetic rotation (*black line*, Hypothesis 2). We assume that the systematic SLB errors that can be detected during roll-optokinetic stimulation (see also Parker et al., 1983) reflect these unaccounted torsional eye movements, plotted as the 'visual shift' effect in Figure 5.1.

Our experimental results show striking differences between SBT and SVV optokinetic shifts, which clearly argue against the first hypothesis. In line with the second hypothesis, incorporating the visual shift measured in the SLB task provided a better -but still incomplete- account of the SVV data.

METHODS

Subjects

Eight subjects (6 male, 2 female), aged between 20 and 64 yrs, gave written informed consent to participate in the experiments. All participants, five naïve subjects and three authors, had normal or corrected-to-normal visual acuity and were free of any known vestibular or other neurological disorders. Each subject participated in all SVV, SBT and SLB experiments (see below) and never received feedback about performance. At the start of each experiment, subjects were carefully instructed about the task and performed a few practice runs to get used to the task.

Setup

The subject was seated in a computer-controlled vestibular chair that allowed whole-body roll-rotations. Roll position (ρ) was measured with an angular resolution of 0.04°, using a digital position-encoder, with clockwise tilt angles defined positive. Feet and legs were stabilized with Velcro straps and the body was tightly fixed by seat belts and shoulder supports. The head was restrained in a natural upright position using a padded helmet. For each subject, small seat-height adjustments ensured that the midpoint between the eyes was centered at the vestibular rotation axis. In front of the subject, an optokinetic drum was attached to the chair, such that its rotation axis was also aligned with the vestibular rotation axis. The drum consisted of a large hollow sphere that filled 90° of the visual field and contained hundreds of pseudorandomly distributed red light-emitting diodes (LEDs). These LEDs were programmed to switch on and off in a random fashion, with an average life time of 0.5 s, to ensure that the drum contained no orientation clues by itself. A 23°-diameter circular area in the center of the drum was free of LEDs to avoid potential interactions between the luminous line (see below) and the visual flow field. Vision was always binocular and subjects were instructed to stare at the center of the LED-free area to prevent them from tracking individual LEDs. During the experiments, participants looked through a 2.7 log-unit neutral density filter, to eliminate stray-light cues.

In the SVV and SLB experiments (see below), a luminous line (angular subtense 20°), polarized by a bright green dot at one end, was mounted in the center of the drum. The line's rotation axis coincided with the rotation axes of the chair and the drum, and its orientation could be adjusted with an accuracy of 0.5°, using a toggle switch.

Experiments

All participants performed three different tasks in separate experiments. I) The subjective visual vertical (SVV) task, in which they aligned the luminous line with the perceived direction of gravity. II) The subjective body tilt (SBT) task, in which they gave a verbal estimate of their body tilt angle in space on a clock scale (Van Beuzekom and Van Gisbergen, 2000). III) The subjective line-body (SLB) task, in which they aligned the luminous line with their longitudinal body axis. Each task was performed in three optokinetic conditions: the flow field rotated either clockwise (CW) or counterclockwise (CCW) at a constant rotation speed of 35°/s, or it remained stationary (control stimulus).

Starting from upright, subjects were roll-rotated to a randomly drawn tilt angle, while in complete darkness. The chair rotated with a peak acceleration of 50°/s^2 to a constant velocity of 30°/s, which was reached within 1 s. As soon as the vestibular chair had reached its final orientation, the optokinetic drum started rotating in CW or CCW direction, or remained stationary, and the LEDs in the drum were switched on. Before responses were recorded, the subject viewed the optokinetic pattern during a 30 s waiting period so that the optokinetic effect would have reached its saturation level (Held et al., 1975) and canal after-effects would have dissipated. In the SVV and SLB experiments, the luminous line was then switched on and the subject made three line adjustments, each within a period of maximum 30 s. The optokinetic drum kept rotating during these adjustments. Each adjustment started with a random line orientation and ended when the subject verbally indicated task completion.

Subsequently, the line was turned off and its orientation was stored offline. If a line adjustment was not finished within 30 s, the entire trial was repeated at the end of the session.

In the SBT task, the luminous line was absent and the subject provided a verbal estimation of body orientation in space, using a clock scale as if the body were the minute hand (Van Beuzekom and Van Gisbergen, 2000). Verbal responses were recorded on a voice recorder and written down by the experimenter. After the verbal tilt estimate (SBT) or the line adjustments (SBT or SLB) had been completed, the LEDs were switched off and the optokinetic drum stopped rotating. The subject was then roll-tilted back to upright for a 30-s rest period with the room lights on.

In the SVV and SLB experiments, subjects were tested at 9 tilt angles between -120 and 120° at regular 30°-intervals, whereas the SBT task included 19 tilt angles, ranging between -135 and 135° at 15°-intervals, to increase subject's uncertainty about the tilt angle. The order of the tilt angles was pseudorandom, with a regular alternation between CW and CCW tilts. The SVV and the SLB experiments each comprised 27 runs, which were divided across three sessions of ~45 minutes each. SVV and SLB experiments were tested separately to avoid confusion about the task. The SBT experiment included 57 separate runs, which were tested in two experimental sessions.

Data analysis

Data analyses on responses within the tilt range -120° to 120° were performed offline using Matlab software (Matlab 7.7, The MathWorks). The estimated body tilt angle in the SBT experiment, denoted by β_{SBT}, was defined positive for CW tilt angles (see Figure 5.2). To allow a direct comparison with the SBT, the compensation angle in the SVV task, β_{SVV}, was defined as the angle between the luminous line and the long body axis, so that perfect performance in both tasks would yield $\beta_{SBT} = \beta_{SVV} = \rho$ (see Figure 5.2). Response errors in SBT (γ_{SBT}) and SVV (γ_{SVV}) were computed as the angular difference between these β-values and the true tilt angle ($\gamma = \rho - \beta$). As a result, positive errors at positive tilts and negative errors at negative tilts

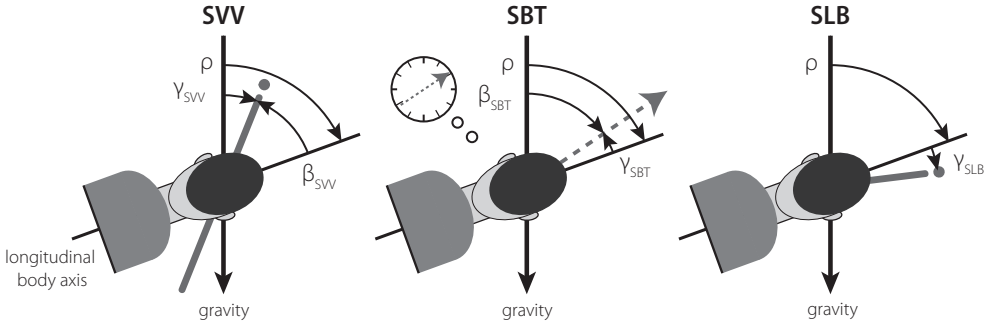

Figure 5.2 Schematic representations of SVV, SBT and SLB tasks. SVV task: subject, shown from behind, aligns the orientation of the luminous line with the perceived direction of gravity. Compensation angle β_{SVV}, angle between line setting and the longitudinal body axis; alignment error γ_{SVV}, difference between roll angle ρ and compensation angle β_{SVV}. SBT task: subject provides a verbal estimate of body tilt (β_{SBT}, indicated by dashed arrow) using a clock scale. Estimation error γ_{SBT}, angular difference between roll angle ρ and estimated body tilt β_{SBT}. SLB task: subject aligns the orientation of the luminous line with the perceived orientation of the longitudinal body axis. Alignment error γ_{SLB}, difference between line orientation and longitudinal body axis.

denote undercompensation (SVV plots) or underestimation (SBT plots) of body tilt. Positive errors at negative tilts and negative errors at positive tilts denote tilt overcompensation (SVV plots) or overestimation (SBT plots). In the SLB task, where errors serve as a measure of the 'visual shift' induced by the rotating pattern, response error (γ_{SLB}) was computed as the angular difference between the luminous line and the longitudinal body axis, with CW tilts defined positive. As a consequence of these definitions, positive optokinetic shifts in the SBT and SLB would lead to positive SVV shifts, as explained in the Introduction (see Figure 5.1). To obtain a measure for the optokinetic effect, the error shift (Δ) was calculated by subtracting the response error in the control condition from the response error during drum rotation, e.g. $\Delta SVV_{CW} = \gamma_{SVV,CW} - \gamma_{SVV,S}$. The labels *CW*, *CCW* and *S* (stationary) were appended as subscripts to indicate the optokinetic condition.

RESULTS

Overview of results in the three tasks

We investigated the effects of roll-optokinetic stimulation on three orientation-judgment tasks in eight roll-tilted human subjects. Figure 5.3 illustrates the population response errors in these tasks as a function of tilt angle for each of the three optokinetic conditions (CW/CCW/stationary). In the three following subsections, devoted to the description of the results of each task, we focus first on the response in the control condition without optokinetic stimulation. We then describe the effect of the optokinetic stimulus (CW and CCW) in relation to the direction and magnitude of body tilt. We also consider to which extent the results in individual subjects, as depicted in Figure 5.4, correspond to the population average.

SVV

In the SVV task (Figure 5.3A), subjects aligned a luminous line with the perceived direction of gravity. In the stationary control condition (circles), response errors at the smallest tilt angles were negligible, but substantial errors, reflecting tilt undercompensation, emerged at larger tilts, consistent with previous SVV literature (Aubert, 1861; Udo de Haes and Schöne, 1970; Mittelstaedt, 1983; De Vrijer et al., 2008, 2009). During CW roll-optokinetic stimula-

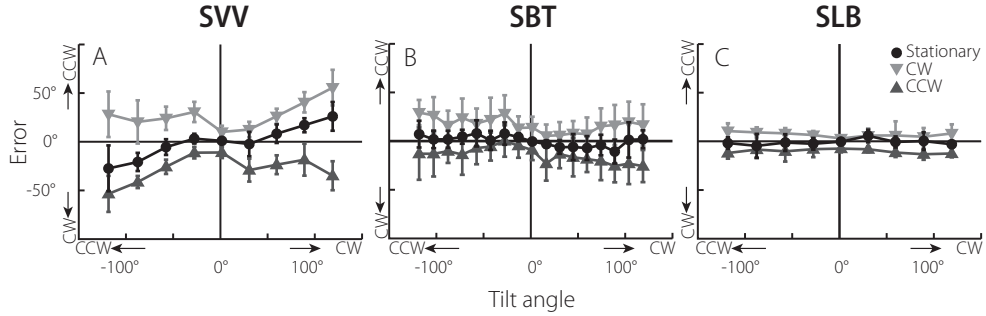

Figure 5.3 Pooled response errors (γ) plotted vs. tilt angle in the SVV, SBT, and SLB tasks. Black circles: stationary (control) condition. Downward-pointing triangles: CW optokinetic stimulation. Upward-pointing triangles: CCW optokinetic stimulation. Error bars denote SD across subjects.

tion (downward-pointing triangles), line settings were shifted in the CW direction, leading to increased errors at positive tilt angles and error reversal at negative tilt angles. Similarly, CCW optokinetic stimulation (upward-pointing triangles) led to CCW shifts in line settings, resulting in larger SVV errors at negative tilt angles and reversal of errors at positive tilt angles. For a schematic explanation of the physiological processes that may underlie these observations we refer to Figure 5.1. A further feature to be noticed is a marked asymmetry in the optokinetic SVV effect: optokinetic stimulation in the direction opposite to the imposed body tilt (CCW rotation at CW tilts, and CW rotation at CCW tilts) induced a larger shift of the line settings than rotation toward the tilted side. This phenomenon, which can be recognized in the data of most subjects (Figure 5.4, left-hand column), will be considered further in the *Results* section *Response asymmetries and tilt-angle dependence*.

SBT

Mean population response errors in the SBT task, in which subjects verbally estimated their body tilt angle, are depicted in Figure 5.3B. Average systematic errors in the stationary control condition were quite small, consistent with previous SBT studies (Van Beuzekom et al., 2001; Kaptein and Van Gisbergen, 2004). During CW optokinetic stimulation, pooled SBT errors show a positive shift with respect to the control condition, whereas CCW optokinetic stimulation evoked a negative shift. This means that subjects felt roll-tilted away from their true position in the direction opposite to optokinetic drum rotation, corroborating earlier reports (see Young et al., 1975). Inspection of the individual SBT results (center column of Figure 5.4) reveals more inter-individual variability than in the SVV. While five subjects (SB, JG, RE, PM, and MV) show a clear optokinetic effect, the shift appears very small or even absent in three subjects (EV, JW, and JV). In a related study, testing the effect of roll-optokinetic stimulation on perceived body tilt with a somatosensory bar, Zupan and Merfeld (2003) found similar inter-individual differences. We will discuss these individual and task-related differences in more detail in section *Sensory conflict* of the *Discussion*.

SLB

Figure 5.3C illustrates the pooled response errors in the SLB task, in which subjects had to align the visual line with their long-body axis, showing that performance in the stationary control condition was quite accurate. Optokinetic effects were very modest, but pooled responses nevertheless show reliable positive shifts for CW drum rotations and negative shifts for CCW drum rotations. This means that the setting of the luminous line shifted in the same direction as optokinetic drum rotation. Individual SLB performance (Figure 5.4, right-hand column) was in line with the pooled results, except for subject PM, who showed larger errors and more pronounced optokinetic SLB effects.

Response asymmetries and tilt-angle dependence

To simplify the description of the response asymmetry in the SVV, we made a distinction between situations in which the optokinetic stimulus caused an increase in perceived body tilt (tilt-increasing condition) and situations in which it caused a reduction in perceived tilt (tilt-reducing condition). As we saw in the description of SBT responses, the shift in perceived

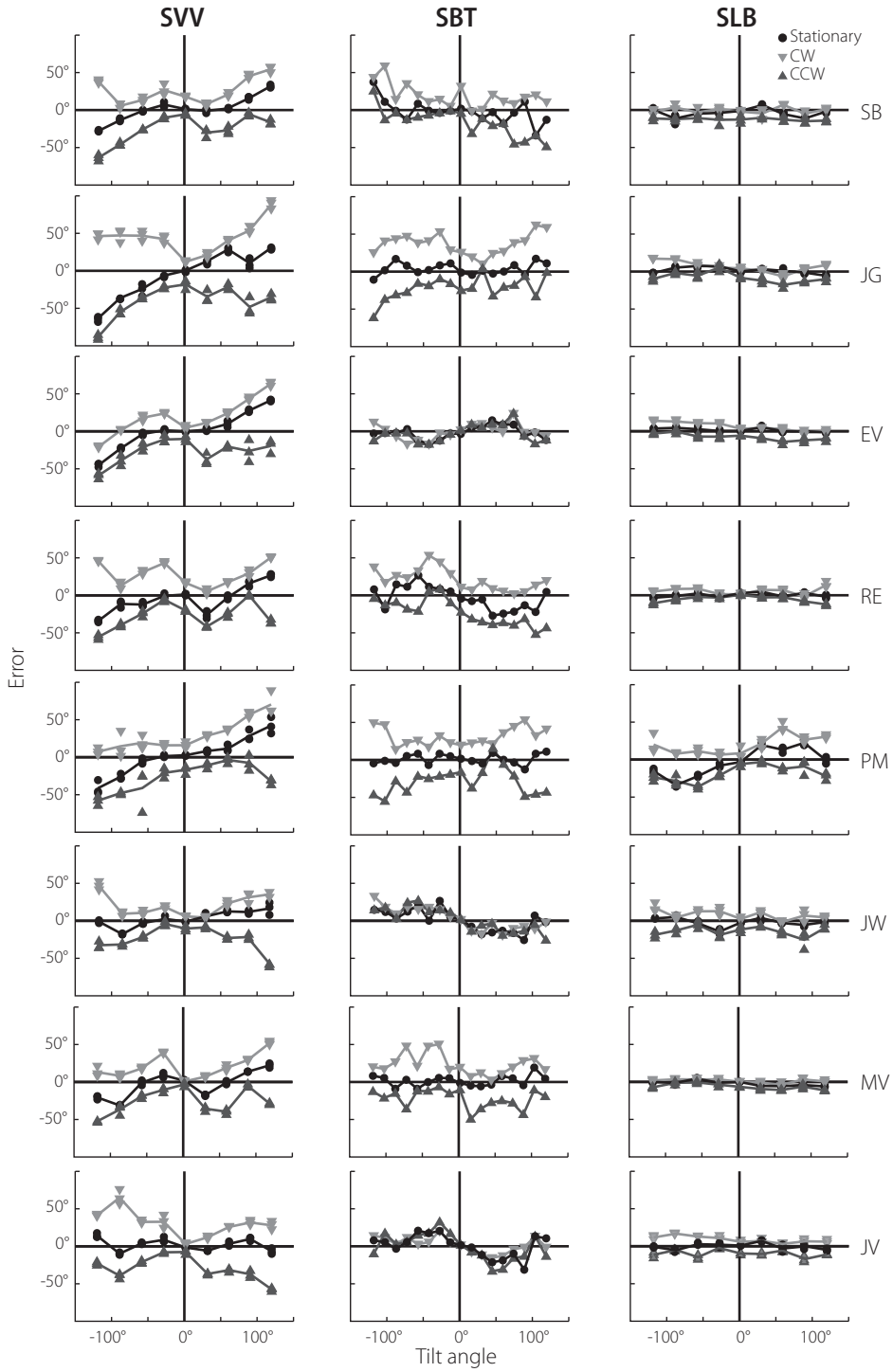

Figure 5.4 *Individual response errors vs. tilt angle in the SVV, SBT and SLB tasks. Symbol coding as in Figure 5.3.*

body tilt is always away from the direction of optokinetic stimulation. Accordingly, CCW stimulation has a tilt-increasing effect in a right-tilted subject and a tilt-reducing effect in a left-tilted subject, and vice versa for CW stimulation. In Figure 5.5A, we therefore relabeled the optokinetic stimulation data from Figure 5.3A, based on whether the stimulation had a tilt-increasing or a tilt-reducing effect (see Lorincz and Hess, 2008 for a similar approach). The asymmetric response behavior can now be described in simpler terms. Under tilt-reducing optokinetic stimulation (*squares*), SVV errors become more pronounced, showing an almost linear tilt dependence. Tilt-increasing optokinetic stimulation (*diamonds*) has an opposite effect, causing a complete reversal to substantial errors of overcompensation across all tilt angles. Since this shift with respect to the control condition is much larger than during tilt-reducing stimulation, the overall pattern shows a distinct asymmetry. A similar graphical reconstruction was made for the SBT and SLB responses, as shown in panels B and C of Figure 5.5.

To distinguish the effects of the optokinetic stimulation, the bottom row of Figure 5.5 (panels D-F) plots the difference (Δ) between the error in the optokinetic and the control condition. In the SVV task (Figure 5.5D), the optokinetic effect is smallest at upright (about 10°) and increases at larger tilt angles, reaching values beyond 50° in the tilt-increasing condition, whereas the magnitude of the tilt-reducing effect does not exceed 30°. In contrast to the SVV, the magnitude of the SBT effect (Figure 5.5E) is about the same for the two optokinetic conditions, ranging between 0 and 30° across the entire tilt range, with only a weak tilt-dependence. The optokinetic effect on the SLB (Figure 5.5F) is rather modest, ranging between 0 and 15°. SLB effects resemble those in the SBT by showing little tilt-dependence, but are similar to the

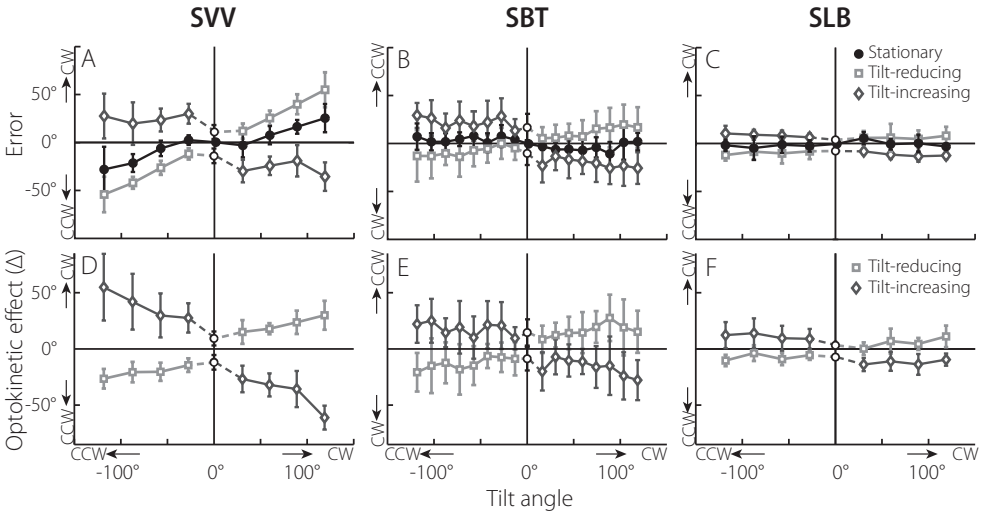

Figure 5.5 Response errors and optokinetic effects plotted vs. tilt angle. Data were relabeled according to optokinetic effect on perceived body tilt (see main text). Squares: tilt-reducing effect. Diamonds: tilt-increasing effect. These groups are not defined at 0° tilt, where the open circles denote errors induced by CW and CCW stimulation. Panels A,B, and C: relabeled response errors (pooled across subjects) in the SVV, SBT and SLB task, respectively. Panels D, E, and F: pooled optokinetic effects (Δ) in the SVV, SBT and SLB task, respectively.

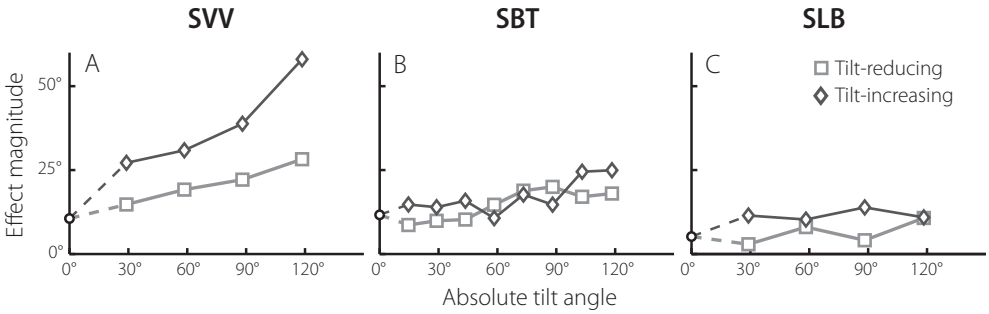

Figure 5.6 Magnitude of optokinetic effect in pooled data as a function of absolute tilt angle. Tilt-increasing optokinetic condition (diamonds) and tilt-reducing condition (squares). Effect amplitude at 0° tilt (circles) reflects average effect size of CW and CCW optokinetic stimulus.

SVV in showing an asymmetry between the tilt-increasing and tilt-reducing conditions.

For a quantitative assessment of the degree of asymmetry and tilt-dependence of the tilt-increasing and tilt-reducing stimulus effects, we first computed their magnitude by pooling across positive and negative tilt angles. Using these values, plotted in Figure 5.6, we quantified the asymmetry between the tilt-increasing and tilt-reducing condition by computing an asymmetry index (AI), following $AI = (\Delta_{tilt\text{-}increasing} - \Delta_{tilt\text{-}reducing}) / (\Delta_{tilt\text{-}increasing} + \Delta_{tilt\text{-}reducing})$. This index ranges between +1 (i.e. only tilt-increasing effects) and -1 (i.e., only tilt-reducing effects). A value of 0 indicates symmetric behavior; the tilt-increasing and tilt-decreasing conditions impose opposing effects of similar magnitude.

In line with Figure 5.6A, we found a significant asymmetry in the SVV (paired t-test, $t(63)=6.6$, $P<<0.001$), as shown by $AI_{SVV}=0.29\pm0.05$. Furthermore, we found a significant increase of the SVV effect with tilt angle for both conditions (slope±SD: tilt-increasing condition, 0.34±0.07, $P<<0.001$, tilt-reducing condition, 0.15±0.03, $P<<0.001$). The major difference with the SVV data is that the SBT results (Figure 5.6B) show no significant asymmetry between the two optokinetic conditions (paired t-test, $t(127)=1.4$, $P=0.18$), as confirmed by $AI_{SBT}=0.00\pm0.19$. In addition, both stimulus conditions revealed a weaker but still significant relation between the size of the optokinetic SBT effect and tilt angle (slope±SD: tilt-increasing condition, 0.10±0.05, $P=0.03$, tilt-reducing condition, 0.11±0.04, $P=0.01$). Finally, the optokinetic effect on the SLB (Figure 5.6C) was significantly larger in the tilt-increasing than in the tilt-reducing condition (paired t-test, $t(63)=3.4$, $P<0.01$). This asymmetry is confirmed by the asymmetry index $AI=0.32\pm0.30$, which seems more in line with the situation in the SVV. On the other hand, SLB effects only showed a significant tilt-dependence for the tilt-reducing stimulus (slope±SD: 0.06±0.03, $P=0.02$).

Test of hypotheses

So far, the optokinetic effects in the SVV, SBT and SLB task have been analyzed separately. We conclude our results section with an assessment of the two hypotheses, outlined in the Introduction. To recall, Hypothesis 1 states that the optokinetic changes in the SVV reflect the changes in the SBT. According to Hypothesis 2, the SVV shift equals the sum of the SBT shift and a visual shift due to an uncompensated change in eye torsion, as measured by the

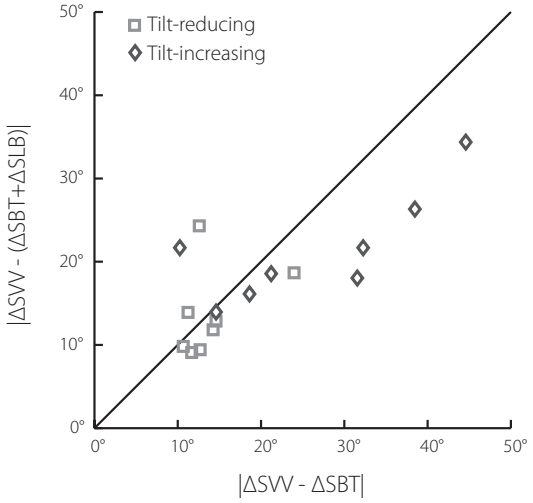

Figure 5.7 Comparison of average residual magnitude in the two hypotheses. Each symbol represents data from a single subject. Open squares: tilt-reducing condition; Black diamonds: tilt-increasing condition. Residuals were calculated as the absolute difference between SVV-effect and SBT-effect (Hypothesis 1) or between SVV-effect and SBT-effect + SLB-effect (Hypothesis 2), averaged across all tilt angles. Most data conform better with Hypothesis 2. The two outliers far above the identity line represent data from a single subject (PM), who had exceptional SLB responses (see Figure 5.4, right-hand column).

SLB. To test the two hypotheses we calculated the difference between (1) the SVV effect and the SBT effect, and (2) the SVV effect and the sum of the SBT and SLB effects. In Figure 5.7, the absolute residuals of all data (tilt-reducing and tilt-increasing conditions) in terms of these hypotheses, averaged across tilt angles, are plotted against each other, separately for each subject. In the majority of subjects, Hypothesis 2 produces a smaller residual than Hypothesis 1 (most data points fall below the identity line), which suggests that the visual shift measured in the SLB contributes to the SVV effect. At the same time it is clear that this can only partially account for marked asymmetry in the SVV data (see Figure 5.5D). Whereas the prediction of Hypothesis 2 is statistically indistinguishable from the tilt-reducing SVV data subset (paired t-test, $t(63)=-0.4$, $P=0.66$), a significant gap (paired t-test, $t(63)=3.6$, $P<0.001$) remains in the explanation of the tilt-increasing SVV data.

DISCUSSION

Approach and main results

In this study, we determined to which extent the effect of roll-optokinetic stimulation on the subjective visual vertical (SVV) can be linked to a changed percept of body tilt (SBT) and a visual shift due to uncompensated eye torsion (SLB). To test this, within the context of two specific hypotheses (Figure 5.1), we designed a comprehensive set of experiments testing SVV, SBT and SLB under three optokinetic conditions at a broad range of tilt angles. To our knowledge, these combined experiments on the same subjects provide the first thorough test

of Hypothesis 1, with very clear results. Since optokinetic changes in the SVV and the SBT show very different behavior (see Figure 5.6A,B), this hypothesis obviously falls short. Its main problem is that the major asymmetry in the SVV shifts, induced by tilt-increasing and tilt-decreasing optokinetic stimulation, is totally absent in the SBT data. The second hypothesis proposes that uncompensated shifts in eye torsion induced by optokinetic stimulation (Ibbotson et al., 2005) may have an additional effect on the SVV (Wade and Curthoys, 1997; Goonetilleke et al., 2008). Our simple line-body alignment task (SLB), provided a measure of a purely visual shift which we attribute to the induced torsional change. Indeed, including the SLB effects reduced the difference between the SVV and SBT effects in the large majority of subjects. Although the SLB effect showed a similar asymmetry as the SVV, its magnitude was too modest to fill the gap.

Relation to previous studies

Our SVV observations confirm and extend the studies by Dichgans et al. (1972; 1974), who tested roll-optokinetic stimulus effects on the SVV in a more limited tilt range and were the first to report an increase of the effect with larger head tilts. They also found an asymmetry between the tilt-increasing and tilt-reducing stimulus conditions, similar to our observations. Dichgans et al. interpreted the fact that optokinetically induced tilt becomes stronger at larger tilts as evidence for the notion that the precision of the otoliths worsens at larger tilt angles. According to this view, otolith information is weighted less strongly as it becomes less reliable, thus permitting a stronger influence of the optokinetic stimulus. A similar conclusion was drawn by Young, Oman and Dichgans (1975), who showed that the influence of roll-optokinetic stimulation on the perception of head tilt was larger at tilts of 90° and 180° than at upright. In line with these observations, Vingerhoets et al. (2009) found that static visual orientation cues (such as panoramic cues) have a stronger influence on the SVV at larger tilt angles, which was also attributed to an increase of otolith noise with tilt angle.

Although many studies have investigated the effects of roll-optokinetic stimuli on spatial orientation, the majority has focused only on a single task, which prohibited a direct comparison between the two. To our knowledge, Dichgans, Held, Young and Brandt (1972) were the first and only investigators who performed optokinetic experiments in which both SVV and SBT were tested in upright subjects. However, due to dissimilarities between the experimental conditions, a direct comparison between the two optokinetic effects was unwarranted. Nevertheless, Dichgans et al. found clear optokinetic effects in both tasks (SVV: 15-40°, SBT: ~9°) and concluded that the roll-optokinetic stimulus affects the internal representation of the gravity vector, thereby suggesting that SBT and SVV may be modified in a similar fashion. Our data show clear discrepancies between the two data sets, not only in the degree of response asymmetries and tilt-angle dependence (see above), but also in the response to the sensory conflict inherent to the experiment, as we will explain next.

Sensory conflict

The roll-optokinetic stimulation provided in our SVV and SBT experiments introduces a sensory conflict between the vestibular and visual system. On the one hand, the vestibular sensors correctly sense that head orientation is stationary in space, whereas, on the other

hand, the visual system suggests that the head is continuously rotating. In such a conflict situation, two different perceptual solutions may emerge (Porrill et al., 1999; van Ee et al., 2003). If the conflict is rather profound, perception may simply be built on one of the two sensory modalities, neglecting the other. For example, if the brain relied solely on (accurate) vestibular information and completely ignored the visual stimulus, optokinetic effects would be absent. Alternatively, the brain could merge the information from the two modalities (sensor fusion), arriving at an intermediate solution (Vingerhoets et al., 2009). This scenario results in an optokinetic effect, as shown by all participants in the SVV task (Figure 5.4, left-hand column). The results were less uniform in the SBT task, in which we observed two response modes among subjects. One group showed clear optokinetic effects (SB, JG, RE, PM, and MV), whereas the other group (EV, JW, and JV) revealed virtually no optokinetic SBT effects. Thus, it appears as if the latter subjects relied exclusively on accurate information from the vestibular system and other graviceptors in the SBT task, while adopting the compromise strategy in the SVV task. This finding indicates that optokinetic information can be weighted differently in the two tasks, but which factors mediate this weighting remains an open question.

Modeling implications

It has been suggested that optokinetic information may be used as a complementary system for the semicircular canals (Dichgans and Brandt, 1978). Particularly, in situations when the canals do not provide reliable information, such as during low-frequency rotations, visual information may be essential to maintain accurate spatial orientation (Angelaki and Cullen, 2008). In the case of yaw rotation, this type of visual-vestibular interaction is supported by neurophysiological studies in various species, showing that neurons in the vestibular nuclei can be modulated by a moving visual surround (Dichgans et al., 1973; Henn et al., 1974). In our experiments, optokinetic cues were not congruent with the information provided by the otoliths. Against this background, it is of interest to discuss a recent study by Lorincz and Hess (2008), who tested the SVV in normal subjects at various tilt angles after a sudden stop following prolonged constant-velocity roll-rotation. Their paradigm evokes a sensory conflict that is similar to the sensory conflict in our optokinetic experiments, in the sense that the otoliths detect a static situation, whereas the semicircular canal signals suggest dynamic rotation in the direction opposite to the preceding rotation. Interestingly, Lorincz and Hess found a similar asymmetry in their SVV results, showing that the dynamic effect was considerably larger when a tilt angle had been approached from upside down compared to when it had been approached from upright. To explain their findings, including the asymmetry, Lorincz and Hess proposed a vector model that is partly based on Mittelstaedt's idiotropic vector model (Mittelstaedt, 1983). In their 'gravity-inertial force' model, it is assumed that the subject's internal estimate of gravity results from the combination of three vectors. The first vector represents the gravity estimate based on information from the otoliths, which is assumed to be slightly distorted as a function of tilt angle (Mittelstaedt, 1983). Information about the speed of change in the direction of gravity ('jerk'), provided by the semicircular canals, is contained in the second vector, which is always perpendicular to the first vector, with its direction depending on the preceding direction of rotation. Finally, the third vector is an

extension of Mittelstaedt's idiotropic vector, originally aligned with the subject's longitudinal body axis (z-axis), but now also containing a y-component representing dynamic information. Lorincz and Hess found that this model was well capable of fitting their data set, including the typical asymmetric results between approaches from upright and from upside down. They noted that the y-component of the idiotropic vector (F_y) was essential for explaining this error asymmetry and interpreted F_y as the correlate of the efference copy of a righting reflex, which was suppressed because of head immobilization. Based on our SBT data, which show no sign of asymmetry, one would have to assume that the processing of this suppressed head-righting reflex has only a negligible effect on the perception of body tilt. Lorincz and Hess also mentioned torsional eye movements as a possible alternative interpretation of F_y. Our SLB data suggest that this may have some relevance, but this factor clearly cannot fully explain the gap between the optokinetic SVV and SBT effects.

Acknowledgments

We thank S. Martens, H. Kleijnen, G. Windau, and G. van Lingen for technical support, and R. Hendrix for experimental assistance. This work was supported by the Faculty of Science (FNWI) of Radboud University Nijmegen, The Donders Centre for Cognition, and by grants from the Netherlands Organization for Scientific Research and the Human Frontier Science Program to W.P. Medendorp.

References

Angelaki DE, Hess BJ (**2005**) Self-motion-induced eye movements: effects on visual acuity and navigation. *Nat Rev Neurosci* 6: 966-976.

Angelaki DE, Cullen KE (**2008**) Vestibular system: the many facets of a multimodal sense. *Annu Rev Neurosci* 31: 125-150.

Angelaki DE, Yakusheva TA (**2009**) How vestibular neurons solve the tilt/translation ambiguity. Comparison of brainstem, cerebellum, and thalamus. *Ann N Y Acad Sci* 1164: 19-28.

Asch SE, Witkin HA (**1948**) Studies in space orientation; perception of the upright with displaced visual fields. *J Exp Psychol* 38: 325-337.

Aubert H (**1861**) Eine scheinbare bedeutende Drehung von Objecten bei Neigung des Kopfes nach rechts oder links. *Virchows Arch* 20: 381-393.

Baloh RW, Honrubia V (**2001**) Clinical neurophysiology of the vestibular system, 3rd Edition: Oxford University Press, USA.

Batschelet E (**1981**) Mathematics in Biology: Circular Statistics in Biology. London: Academic Press.

Bays PM, Wolpert DM (**2007**) Computational principles of sensorimotor control that minimize uncertainty and variability. *J Physiol* 578: 387-396.

Betts GA, Curthoys IS (**1998**) Visually perceived vertical and visually perceived horizontal are not orthogonal. *Vision Res* 38: 1989-1999.

Bisdorff AR, Wolsley CJ, Anastasopoulos D, Bronstein AM, Gresty MA (**1996**) The perception of body verticality (subjective postural vertical) in peripheral and central vestibular disorders. *Brain* 119: 1523-1534.

Bortolami SB, Pierobon A, DiZio P, Lackner JR (**2006**) Localization of the subjective vertical during roll, pitch, and recumbent yaw body tilt. *Exp Brain Res* 173: 364-373.

Brainard DH (**1997**) The Psychophysics Toolbox. *Spat Vis* 10: 433-436.

Brandt T, Dieterich M (**1999**) The vestibular cortex. Its locations, functions, and disorders. *Ann N Y Acad Sci* 871: 293-312.

Brandt T, Dichgans J, Buchle W (**1974**) Motion habituation: inverted self-motion perception and optokinetic after-nystagmus. *Exp Brain Res* 21: 337-352.

Brandt T, Dieterich M, Danek A (**1994**) Vestibular cortex lesions affect the perception of verticality. *Ann Neurol* 35: 403-412.

Brandt T, Bartenstein P, Janek A, Dieterich M (**1998**) Reciprocal inhibitory visual-vestibular interaction. Visual motion stimulation deactivates the parieto-insular vestibular cortex. *Brain* 121: 1749-1758.

Bremmer F, Klam F, Duhamel JR, Ben Hamed S, Graf W (**2002**) Visual-vestibular interactive responses in the macaque ventral intraparietal area (VIP). *Eur J Neurosci* 16: 1569-1586.

Bronstein AM (**1999**) The interaction of otolith and proprioceptive information in the perception of verticality. The effects of labyrinthine and CNS disease. *Ann N Y Acad Sci* 871: 324-333.

Bronstein AM, Yardley L, Moore AP, Cleeves L (**1996**) Visually and posturally mediated tilt illusion in Parkinson's disease and in labyrinthine defective subjects. *Neurology* 47: 651-656.

Carandini M (**2006**) Measuring the brain's assumptions. *Nat Neurosci* 9: 468-470.
Clark B, Graybiel A (**1963**) Perception of the postural vertical in normals and subjects with labyrinthine defects. *J Exp Psychol* 65: 490-494.
Clark B, Graybiel A (**1964**) Perception Of The Postural Vertical Following Prolonged Bodily Tilt In Normals And Subjects With Labyrinthine Defects. *Acta Otolaryngol* 58: 143-148.
Curthoys IS (**1996**) The role of ocular torsion in visual measures of vestibular function. *Brain Res Bull* 40: 399-403.
Daddaoua N, Dicke PW, Thier P (**2008**) The subjective visual vertical in a nonhuman primate. *J Vis* 8: 19 11-18.
Dakin SC, Mareschal I, Bex PJ (**2005**) Local and global limitations on direction integration assessed using equivalent noise analysis. *Vision Res* 45: 3027-3049.
Day BL, Fitzpatrick RC (**2005**) The vestibular system. *Curr Biol* 15: R583-586.
de Graaf B, Bekkering H, Erasmus C, Bles W (**1992**) Influence of visual, vestibular, cervical, and somatosensory tilt information on ocular rotation and perception of the horizontal. *J Vestib Res* 2: 15-30.
De Vrijer M, Medendorp WP, Van Gisbergen JAM (**2008**) Shared computational mechanism for tilt compensation accounts for biased verticality percepts in motion and pattern vision. *J Neurophysiol* 99: 915-930.
De Vrijer M, Medendorp WP, Van Gisbergen JAM (**2009**) Accuracy-precision trade-off in visual orientation constancy. *J Vis* 9: 1-15.
Diamond SG, Markham CH (**1983**) Ocular counterrolling as an indicator of vestibular otolith function. *Neurology* 33: 1460-1469.
Diamond SG, Markham CH, Simpson NE, Curthoys IS (**1979**) Binocular counterrolling in humans during dynamic rotation. *Acta Otolaryngol* 87: 490-498.
Dichgans J, Brandt T (**1972**) Visual-vestibular interaction and motion perception. *Bibl Ophthalmol* 82: 327-338.
Dichgans J, Brandt T (**1978**) Visual-vestibular interaction: Effects on self-motion perception and postural control. In: Handbook of Sensory Physiology, VIII of Perception: 756-804. Springer, Berlin Heidelberg.
Dichgans J, Schmidt CL, Graf W (**1973**) Visual input improves the speedometer function of the vestibular nuclei in the goldfish. *Exp Brain Res* 18: 319-322.
Dichgans J, Diener HC, Brandt T (**1974**) Optokinetic-graviceptive interaction in different head positions. *Acta Otolaryngol* 78: 391-398.
Dichgans J, Held R, Young LR, Brandt T (**1972**) Moving visual scenes influence the apparent direction of gravity. *Science* 178: 1217-1219.
Dyde RT, Jenkin MR, Harris LR (**2006**) The subjective visual vertical and the perceptual upright. *Exp Brain Res* 173: 612-622.
Eggert T (**1998**) Der Einfluss orientierter Texturen auf die subjektive visuelle Vertikale und seine systemtheoretische Analyse (PhD Thesis), Munich, Germany: Munich Technical University.
Ehrenstein WH, Ehrenstein A (**1999**) Psychophysical methods. In: Modern Techniques in Neuroscience Research (Windhorst U, Johansson H, Eds.): 1211–1241. Springer-Verlag,

Berlin.
Ernst MO, Banks MS (**2002**) Humans integrate visual and haptic information in a statistically optimal fashion. *Nature* 415: 429-433.
Ernst MO, Bülthoff HH (**2004**) Merging the senses into a robust percept. *Trends Cogn Sci* 8: 162-169.
Fernandez C, Goldberg JM (**1976**) Physiology of peripheral neurons innervating otolith organs of the squirrel monkey. I. Response to static tilts and to long-duration centrifugal force. *J Neurophysiol* 39: 970-984.
Fetsch CR, Wang S, Gu Y, DeAngelis GC, Angelaki DE (**2007**) Spatial reference frames of visual, vestibular, and multimodal heading signals in the dorsal subdivision of the medial superior temporal area. *J Neurosci* 27: 700-712.
Freeman TC, Banks MS, Crowell JA (**2000**) Extraretinal and retinal amplitude and phase errors during Filehne illusion and path perception. *Percept Psychophys* 62: 900-909.
Goldberg JM (**2000**) Afferent diversity and the organization of central vestibular pathways. *Exp Brain Res* 130: 277-297.
Goonetilleke SC, Mezey LE, Burgess AM, Curthoys IS (**2008**) On the relation between ocular torsion and visual perception of line orientation. *Vision Res* 48: 1488-1496.
Grüsser OJ, Pause M, Schreiter U (**1990**) Localization and responses of neurones in the parieto-insular vestibular cortex of awake monkeys (Macaca fascicularis). *J Physiol* 430: 537-557.
Gu Y, DeAngelis GC, Angelaki DE (**2007**) A functional link between area MSTd and heading perception based on vestibular signals. *Nat Neurosci* 10: 1038-1047.
Gu Y, Watkins PV, Angelaki DE, DeAngelis GC (**2006**) Visual and nonvisual contributions to three-dimensional heading selectivity in the medial superior temporal area. *J Neurosci* 26: 73-85.
Held R, Dichgans J, Bauer J (**1975**) Characteristics of moving visual scenes influencing spatial orientation. *Vision Res* 15: 357-365.
Henn V, Young LR, Finley C (**1974**) Vestibular nucleus units in alert monkeys are also influenced by moving visual fields. *Brain Res* 71: 144-149.
Howard IP (**1982**) Human visual orientation. New York: Wiley.
Ibbotson MR, Price NS, Das VE, Hietanen MA, Mustari MJ (**2005**) Torsional eye movements during psychophysical testing with rotating patterns. *Exp Brain Res* 160: 264-267.
Ilg UJ, Schumann S, Thier P (**2004**) Posterior parietal cortex neurons encode target motion in world-centered coordinates. *Neuron* 43: 145-151.
Inaba N, Shinomoto S, Yamane S, Takemura A, Kawano K (**2007**) MST Neurons Code for Visual Motion in Space Independent of Pursuit Eye Movements. *J Neurophysiol* 97: 3473-3483.
Jacobs RA (**1999**) Optimal integration of texture and motion cues to depth. *Vision Res* 39: 3621-3629.
Jaeger R, Kondrachuk AV, Haslwanter T (**2008**) The distribution of otolith polarization vectors in mammals: comparison between model predictions and single cell recordings. *Hear Res* 239: 12-19.

Jaggi-Schwarz K, Hess BJ (**2003**) Influence of dynamic tilts on the perception of earth-vertical. *Exp Brain Res* 149: 340-350.

Jarchow T, Mast FW (**1999**) The effect of water immersion on postural and visual orientation. *Aviat Space Environ Med* 70: 879-886.

Jürgens R, Becker W (**2006**) Perception of angular displacement without landmarks: evidence for Bayesian fusion of vestibular, optokinetic, podokinesthetic, and cognitive information. *Exp Brain Res* 174: 528-543.

Kaptein RG, Van Gisbergen JA (**2004**) Interpretation of a discontinuity in the sense of verticality at large body tilt. *J Neurophysiol* 91: 2205-2214.

Kaptein RG, Van Gisbergen JA (**2006**) Canal and otolith contributions to visual orientation constancy during sinusoidal roll rotation. *J Neurophysiol* 95: 1936-1948.

Kingma H, Stegeman P, Vogels R (**1997**) Ocular torsion induced by static and dynamic visual stimulation and static whole body roll. *Eur Arch Otorhinolaryngol* 254 Suppl 1: S61-S63.

Klein SA (**2001**) Measuring, estimating, and understanding the psychometric function: a commentary. *Percept Psychophys* 63: 1421-1455.

Knill DC, Pouget A (**2004**) The Bayesian brain: the role of uncertainty in neural coding and computation. *Trends Neurosci* 27: 712-719.

Körding KP, Wolpert DM (**2004**) Bayesian integration in sensorimotor learning. *Nature* 427: 244-247.

Krauzlis RJ (**2004**) Recasting the smooth pursuit eye movement system. *J Neurophysiol* 91: 591-603.

Krukowski AE, Pirog KA, Beutter BR, Brooks KR, Stone LS (**2003**) Human discrimination of visual direction of motion with and without smooth pursuit eye movements. *J Vis* 3: 831-840.

Landy MS, Maloney LT, Johnston EB, Young M (**1995**) Measurement and modeling of depth cue combination: in defense of weak fusion. *Vision Res* 35: 389-412.

Lappe M, Bremmer F, van den Berg AV (**1999**) Perception of self-motion from visual flow. *Trends Cogn Sci* 3: 329-336.

Laurens J, Droulez J (**2007**) Bayesian processing of vestibular information. *Biol Cybern* 96: 389-404.

Lindner A, Haarmeier T, Erb M, Grodd W, Thier P (**2006**) Cerebrocerebellar circuits for the perceptual cancellation of eye-movement-induced retinal image motion. *J Cogn Neurosci* 18: 1899-1912.

Lisberger SG, Morris EJ, Tychsen L (**1987**) Visual motion processing and sensory-motor integration for smooth pursuit eye movements. *Annu Rev Neurosci* 10: 97-129.

Löffler G, Orbach HS (**2001**) Anisotropy in judging the absolute direction of motion. *Vision Res* 41: 3677-3692.

Lorincz EN, Hess BJ (**2008**) Dynamic effects on the subjective visual vertical after roll rotation. *J Neurophysiol* 100: 657-669.

Luyat M, Gentaz E, Corte TR, Guerraz M (**2001**) Reference frames and haptic perception of orientation: body and head tilt effects on the oblique effect. *Percept Psychophys* 63: 541-554.

MacNeilage PR, Banks MS, Berger DR, Bulthoff HH (**2007**) A Bayesian model of the disambiguation of gravitoinertial force by visual cues. *Exp Brain Res* 179: 263-290.

Markham CH, Diamond SG (**2002**) Ocular counterrolling in response to static and dynamic tilting: implications for human otolith function. *J Vestib Res* 12: 127-134.

Mast FW (**2000**) Does the world rock when the eyes roll? Allocentric orientation representation, ocular counterroll, and the subjective vertical. *Swiss J of Psychology* 59: 89-101.

Mast FW, Jarchow T (**1996**) Perceived body position and the visual horizontal. *Brain Res Bull* 40: 393-397.

McKenna GJ, Peng GC, Zee DS (**2004**) Neck muscle vibration alters visually perceived roll in normals. *J Assoc Res Otolaryngol* 5: 25-31.

Merfeld DM (**1995**) Modeling human vestibular responses during eccentric rotation and off vertical axis rotation. *Acta Otolaryngol Suppl* 520: 354-359.

Merfeld DM, Zupan L, Peterka RJ (**1999**) Humans use internal models to estimate gravity and linear acceleration. *Nature* 398: 615-618.

Mergner T, Siebold C, Schweigart G, Becker W (**1991**) Human perception of horizontal trunk and head rotation in space during vestibular and neck stimulation. *Exp Brain Res* 85: 389-404.

Mittelstaedt H (**1983**) A new solution to the problem of the subjective vertical. *Naturwissenschaften* 70: 272-281.

Mittelstaedt H (**1986**) The subjective vertical as a function of visual and extraretinal cues. *Acta Psychol* 63: 63-85.

Mittelstaedt H (**1988**) The Information Processing Structure of the Subjective Vertical. A Cybernetic Bridge between its Psychophysics and its Neurobiology. In: Processing structures for perception and action (Marko H, Hauske G, Struppler A, Eds.): 217-263. VCH Verlagsgesellschaft, Weinheim.

Mittelstaedt H (**1995**) The formation of the visual and postural vertical. In: Multisensory control of posture (Mergner T, Hlavacka F, Eds.): 147-155. Plenum Press, New York.

Mittelstaedt H (**1997**) Interaction of eye-, head-, and trunk-bound information in spatial perception and control. *J Vestib Res* 7: 283-302.

Mittelstaedt H (**1998**) Origin and processing of postural information. *Neurosci Biobehav Rev* 22: 473-478.

Mittelstaedt H (**1999**) The role of the otoliths in perception of the vertical and in path integration. *Ann N Y Acad Sci* 871: 334-344.

Müller GE (**1916**) Über das Aubertsche Phänomen. *Zeitschrift für Sinnesphysiologie* 49: 109-246.

Müller JR, Philiastides MG, Newsome WT (**2005**) Microstimulation of the superior colliculus focuses attention without moving the eyes. *Proc Natl Acad Sci USA* 102: 524-529.

Nelson JG (**1968**) Effect of water immersion and body position upon perception of the gravitational vertical. *Aerosp Med* 39: 806-811.

Newsome WT, Paré EB (**1988**) A selective impairment of motion perception following lesions of the middle temporal visual area (MT). *J Neurosci* 8: 2201-2211.

Newsome WT, Wurtz RH, Komatsu H (**1988**) Relation of cortical areas MT and MST to pursuit eye movements. II. Differentiation of retinal from extraretinal inputs. *J Neurophysiol*

60: 604-620.

Niemeier M, Crawford JD, Tweed DB (**2003**) Optimal transsaccadic integration explains distorted spatial perception. *Nature* 422: 76-80.

Orban GA, Vogels R (**1998**) The neuronal machinery involved in successive orientation discrimination. *Prog Neurobiol* 55: 117-147.

Page WK, Duffy CJ (**2003**) Heading representation in MST: sensory interactions and population encoding. *J Neurophysiol* 89: 1994-2013.

Palla A, Bockisch CJ, Bergamin O, Straumann D (**2006**) Dissociated hysteresis of static ocular counterroll in humans. *J Neurophysiol* 95: 2222-2232.

Parker DE, Poston RL, Gulledge WL (**1983**) Spatial orientation: visual-vestibular-somatic interaction. *Percept Psychophys* 33: 139-146.

Pavlou M, Wijnberg N, Faldon ME, Bronstein AM (**2003**) Effect of semicircular canal stimulation on the perception of the visual vertical. *J Neurophysiol* 90: 622-630.

Pelli DG (**1997**) The VideoToolbox software for visual psychophysics: transforming numbers into movies. *Spat Vis* 10: 437-442.

Porrill J, Frisby JP, Adams WJ, Buckley D (**1999**) Robust and optimal use of information in stereo vision. *Nature* 397: 63-66.

Press WH, Flannery BP, Teukolsky SA, Vetterling WT (**1992**) Numerical Recipes in C, 2nd Edition. Cambridge: Cambridge University Press.

Robinson DA (**1977**) Vestibular and optokinetic symbiosis: an example of explaining by modelling. In: Control of gaze by brain stem neurons. Developments in Neuroscience, (Baker R, Berthoz A, Eds.): 49-58. Amsterdam, Elsevier/North-Holland Biomedical Press.

Rosenhall U (**1972**) Vestibular macular mapping in man. *Ann Otol Rhinol Laryngol* 81: 339-351.

Rosenhall U (**1974**) The vestibular sensory regions in man: a morphological study. *Acta Universitatis Uppsala Suppl* 191: 1-37.

Sauvan XM, Peterhans E (**1999**) Orientation Constancy in Neurons of Monkey Visual Cortex. *Visual Cognition* 6: 43-54.

Schöne H (**1964**) On the role of gravity in human spatial orientation. *Aerosp Med*: 764-772.

Schöne H, Udo de Haes H (**1968**) Perception of Gravity-Vertical as a Function of Head and Trunk Position. *J Comp Physiol A*: Neuroethology, Sensory, Neural, and Behavioral Physiology 60: 440-444.

Souman JL, Hooge IT, Wertheim AH (**2005**) Vertical object motion during horizontal ocular pursuit: compensation for eye movements increases with presentation duration. *Vision Res* 45: 845-853.

Stocker AA, Simoncelli EP (2006) Noise characteristics and prior expectations in human visual speed perception. *Nat Neurosci* 9: 578-585.

Suzuki JI, Tokumasu K, Goto K (**1969**) Eye movements from single utricular nerve stimulation in the cat. *Acta Otolaryngol* 68: 350-362.

Tarnutzer AA, Bockisch CJ, Straumann D (**2007**) Variability of subjective visual vertical and ocular counterroll are correlated, Program No. 861.1. In: Neuroscience Meeting Planner, San Diego CA, Society for Neuroscience, 2007. Online.

Trousselard M, Barraud PA, Nougier V, Raphel C, Cian C (**2004**) Contribution of tactile and interoceptive cues to the perception of the direction of gravity. *Cogn Brain Res* 20: 355-362.

Udo de Haes H (**1970**) Stability of apparent vertical and ocular countertorsion as a function of lateral tilt. *Percept Psychophys* 8: 137-142.

Udo de Haes H, Schöne H (**1970**) Interaction between statolith organs and semicircular canals on apparent vertical and nystagmus. *Acta Otolaryngol* 69: 25-31.

Vaitl D, Mittelstaedt H, Baisch F (**1997**) Shifts in blood volume alter the perception of posture. *Int J Psychophysiol* 27: 99-105.

Vaitl D, Mittelstaedt H, Saborowski R, Stark R, Baisch F (**2002**) Shifts in blood volume alter the perception of posture: further evidence for somatic graviception. *Int J Psychophysiol* 44: 1-11.

van Beers RJ, Sittig AC, Gon JJ (**1999**) Integration of proprioceptive and visual position-information: An experimentally supported model. *J Neurophysiol* 81: 1355-1364.

Van Beuzekom AD, Van Gisbergen JA (**2000**) Properties of the internal representation of gravity inferred from spatial-direction and body-tilt estimates. *J Neurophysiol* 84: 11-27.

Van Beuzekom AD, Medendorp WP, Van Gisbergen JA (**2001**) The subjective vertical and the sense of self orientation during active body tilt. *Vision Res* 41: 3229-3242.

van Ee R, Adams WJ, Mamassian P (**2003**) Bayesian modeling of cue interaction: bistability in stereoscopic slant perception. *J Opt Soc Am A Opt Image Sci Vis* 20: 1398-1406.

Vandenbussche E, Vogels R, Orban GA (**1986**) Human orientation discrimination: changes with eccentricity in normal and amblyopic vision. *Invest Ophthalmol Vis Sci* 27: 237-245.

Vingerhoets RA, Van Gisbergen JA, Medendorp WP (**2007**) Verticality perception during off-vertical axis rotation. *J Neurophysiol* 97: 3256-3268.

Vingerhoets RA, Medendorp WP, Van Gisbergen JA (**2008**) Body-tilt and visual verticality perception during multiple cycles of roll rotation. *J Neurophysiol* 99: 2264-2280.

Vingerhoets RA, De Vrijer M, Van Gisbergen JA, Medendorp WP (**2009**) Fusion of visual and vestibular tilt cues in the perception of visual vertical. *J Neurophysiol* 101: 1321-1333.

Wade NJ (**1968**) Visual orientation during and after lateral head, body, and trunk tilt. *Percept Psychophys* 3: 215-219.

Wade SW, Curthoys IS (**1997**) The effect of ocular torsional position on perception of the roll-tilt of visual stimuli. *Vision Res* 37: 1071-1078.

Wertheim A (**1994**) Motion perception during self-motion. The Direct versus Inferential controversy revisited. Behav Brain Sci 17: 293-355.

Westheimer G (**2003**) Meridional anisotropy in visual processing: implications for the neural site of the oblique effect. *Vision Res* 43: 2281-2289.

Wichmann FA, Hill NJ (**2001a**) The psychometric function: I. Fitting, sampling, and goodness of fit. *Percept Psychophys* 63: 1293-1313.

Wichmann FA, Hill NJ (**2001b**) The psychometric function: II. Bootstrap-based confidence intervals and sampling. *Percept Psychophys* 63: 1314-1329.

Yakusheva TA, Shaikh AG, Green AM, Blazquez PM, Dickman JD, Angelaki DE (**2007**) Purkinje cells in posterior cerebellar vermis encode motion in an inertial reference frame. *Neuron* 54: 973-985.

Young LR, Oman CM, Dichgans JM (**1975**) Influence of head orientation on visually induced pitch and roll sensation. *Aviat Space Environ Med* 46: 264-268.

Zupan LH, Merfeld DM (**2003**) Neural processing of gravito-inertial cues in humans. IV. Influence of visual rotational cues during roll optokinetic stimuli. *J Neurophysiol* 89: 390-400.

Zupan LH, Merfeld DM, Darlot C (**2002**) Using sensory weighting to model the influence of canal, otolith and visual cues on spatial orientation and eye movements. *Biol Cybern* 86: 209-230.

Summary

To know one's body orientation in space and to be aware of the spatial orientation of surrounding objects is essential for many of our movements and actions. This ability, referred to as spatial orientation, has been a major theme in neuroscience for many years and is the key topic of this research project. The main objective was to elucidate the computational strategies that underlie human spatial orientation and to uncover the contribution of the involved sense organs. We focused on two perceptual tasks, probing the subject's perception of visual verticality (SVV) and of body tilt (SBT) at a broad range of tilt angles. While these tasks rely mainly on the same sensory inputs, they show some intriguing differences. In chapters two and three, we introduced a theoretical framework, based on optimal Bayesian observer theory, that could account for the accuracy and precision characteristics of the SVV. In chapter four, we proposed an extended model, including both the SVV and SBT tasks, which could explain the discrepancies between the two tasks. In chapter five, we investigated the influence of roll-optokinetic cues on the SVV and SBT, and showed that these effects differed considerably. In the next sections, we provide a detailed summary of Chapters 2, 3, 4 and 5.

Chapter 2: Shared computational mechanism for tilt compensation accounts for biased verticality percepts in motion and pattern vision

To determine the direction of object motion in external space, the brain must combine retinal motion signals and information about the orientation of the eyes in space. In Chapter 2, we assessed the accuracy of this process in eight laterally-tilted subjects who aligned the motion direction of a random-dot-pattern (30% coherence, moving at 6°/s) with their perceived direction of gravity (motion vertical) in otherwise complete darkness. For comparison, we also tested the ability to align an adjustable visual line (12° diameter) to the direction of gravity (line vertical). For small head tilts (below 40°), systematic errors in either task were almost negligible. In contrast, tilts beyond 60° revealed a pattern of large systematic errors (often beyond 30°) that was virtually identical in both tasks. Regression analysis confirmed that mean errors in the two tasks were closely related, with slopes close to 1.0 and correlations beyond 0.89. Control experiments ruled out that motion settings were based on processing of individual single-dot paths. We conclude that the conversion of both motion direction and line orientation on the retina into a spatial frame of reference involves a shared computational strategy. Simulations with two spatial-orientation models suggest that the pattern of systematic errors may be the downside of an optimal strategy for dealing with imperfections in the tilt signal which is implemented before the reference-frame transformation.

Chapter 3: Accuracy-precision trade-off in visual orientation constancy

Using the subjective visual vertical task (SVV), previous investigations on the maintenance of visual orientation constancy during lateral tilt have found two opposite bias effects in different tilt ranges. The SVV typically shows accurate performance near upright but severe undercompensation at tilts beyond 60 deg (A-effect), frequently with slight overcompensation

responses (E-effect) in between. In Chapter 3 we investigate whether a Bayesian spatial-perception model can account for this error pattern. The model interprets A- and E-effects as the drawback of a computational strategy, geared at maintaining visual stability with optimal precision at small tilt angles. In this study, we test whether these systematic errors can be seen as the consequence of a precision-accuracy trade-off when combining a veridical but noisy signal about eye orientation in space with the visual signal.
To do so, we used a psychometric approach to assess both precision and accuracy of the SVV in eight subjects laterally tilted at 9 different tilt angles (-120° to 120°). Results show that SVV accuracy and precision worsened with tilt angle, according to a pattern that could be fitted quite adequately by the Bayesian model. We conclude that spatial vision essentially follows the rules of Bayes' optimal observer theory.

Chapter 4: Multisensory processing for orientation perception

It has been proposed that the brain uses Bayesian inference to convert and integrate information from various sensory pathways to achieve robust perception. To explore this theory further, we tested whether it can explain how different coordinate transformations on the same sensory signals affect perceptual accuracy and variability. In Chapter 4, we examined this question in two spatial orientation tasks: the subjective visual vertical (SVV) task where subjects judge the spatial orientation of a line, and the subjective body tilt (SBT) task where subjects judge their body orientation in space. To allow a quantitative analysis, we formulated a sensory integration model with access to three noisy but unbiased sensory signals: vestibular signals about head-in-space orientation, neck proprioception signaling head-on-body orientation, and somatosensory inputs coding body-in-space orientation. Using a psychometric approach, the SBT was tested at 0° and 90°; the SVV was measured from -120 to 120° tilts in steps of 30°. In all subjects, the SBT was more accurate than the SVV, which showed substantial errors for tilts beyond 60°. In both tasks, variability increased with tilt angle, but was consistently lower in the SVV. Since our sensory integration model can nicely account for these findings, we conclude that Bayesian computations are crucially involved in processing multisensory information for orientation perception.

Chapter 5: Roll-optokinetic effects on visual vertical and postural orientation judgments

Roll rotation of a large optic flow pattern causes response shifts in two spatial orientation tasks: one testing subjective body tilt (SBT), the other assessing the subjective visual vertical (SVV). Since these effects have never been compared directly, it remains unclear whether the latter shift simply reflects the former. In Chapter 5, we tested two hypotheses: (1) the shift in the SVV reflects the change in the SBT, (2) the SVV shift equals the sum of the SBT shift and a visual shift due to an uncompensated change in eye torsion. The visual shift, which would affect the SVV but not the SBT, was measured in a so-called subjective line-body (SLB) task. Eight human subjects were tested in three tasks (SVV, SBT, SLB), at body-tilt angles between

-120° and +120°, in three optokinetic conditions (CW/CCW/stationary). Optokinetic SVV shifts increased markedly with body tilt and were highly asymmetric, being larger/smaller when optokinetic stimulation increased/reduced perceived body tilt, respectively. In the SBT task, optokinetic effects also increased with tilt angle, but without any sign of asymmetry. Optokinetic SLB effects, which were relatively small, showed a similar asymmetry as the SVV effects, but a less robust tilt-angle dependence. Since our second hypothesis, although not perfect, provided the better match to the data, we conclude that the visual-vertical shift is not simply due to the shift in perceived body tilt and that unaccounted eye torsion is probably a further contributing factor.

Samenvatting

We beschouwen het als vanzelfsprekend dat we de oriëntatie van ons lichaam in de ruimte en van de objecten om ons heen kennen. Dit vermogen, aangeduid met de term ruimtelijke oriëntatie, lijkt inderdaad vrijwel automatisch tot stand te komen. In werkelijkheid is hiervoor echter een gecoördineerde verwerking van vele signalen in het centrale zenuwstelsel vereist. Om te bepalen hoe een object is georiënteerd in de wereld (ten opzichte van de zwaartekracht), moet het brein de visuele signalen die binnenkomen op het netvlies combineren met informatie over de oriëntatie van het oog in de ruimte. Om deze oriëntatie-informatie te verkrijgen kan het centraal zenuwstelsel gebruik maken van vele sensorische systemen, zoals het evenwichtsorgaan, het visueel systeem en drukreceptoren in de huid.

Dit proefschrift gaat in op de vraag welke zintuigen betrokken zijn bij ruimtelijke oriëntatie, wat hun bijdrage precies is en welke berekeningen het brein maakt bij de verwerking van deze informatie. In het experimentele onderzoek is gebruik gemaakt van twee perceptuele taken: de subjectieve visuele verticaal-taak (SVV) en de subjectieve lichaamstand-taak (body tilt taak, SBT). Bij de SVV-taak wordt gemeten hoe goed een zijdelings gekantelde proefpersoon in het donker een visuele lijn kan uitlijnen met de richting van de zwaartekracht. Tijdens de SBT-taak vragen we een gekantelde proefpersoon om een inschatting van de lichaamsoriëntatie in de ruimte. Hoewel de proefpersoon bij de twee taken gebruik kan maken van dezelfde bronnen van sensorische informatie, vertonen de resultaten toch opmerkelijke verschillen. Een gezonde persoon blijkt, onafhankelijk van de kantelhoek, een behoorlijk goede schatting te kunnen geven van zijn of haar lichaamsoriëntatie. Als dezelfde persoon echter de oriëntatie van een visuele lijn ten opzichte van de gravitatie moet rapporteren, maakt hij of zij grote systematische fouten bij kantelhoeken boven de 60°, alsof de eigen kantelhoek wordt onderschat.

In *hoofdstuk 2* laten we zien dat deze fouten ook optreden bij de inschatting van de bewegingsrichting van een visueel patroon. Dit suggereert dat er, op verschillende niveaus van visuele corticale verwerking, sprake is van een identieke berekeningsstrategie. *Hoofdstukken 2 en 3* gaan vervolgens in op de computationele processen die mogelijk ten grondslag liggen aan deze systematische SVV fouten. Hiertoe introduceren we een theoretisch kader dat is gebaseerd op optimale Bayesiaanse waarnemingstheorie. Deze theorie stelt ons niet alleen in staat om het systematische foutenpatroon te verklaren maar ook om een verklaring te bieden voor de ruiskarakteristieken van de SVV. In *hoofdstuk 4* breiden we dit optimale perceptiemodel uit voor een verklaring van de SBT-resultaten. Hierbij wordt met name aandacht besteed aan de optimale combinatie van informatie van verschillende sensorische bronnen en de coördinaattransformaties die hiervoor essentieel zijn. Tenslotte onderzoeken we in *hoofdstuk 5* welke invloed een groot optokinetisch patroon heeft op de uitvoering van de twee taken. De resultaten laten zien dat het effect van deze verstorende visuele stimulus sterk verschilt tussen de SVV en SBT taak. De nu volgende tekst bevat een meer gedetailleerde samenvatting van de resultaten en conclusies van deze hoofdstukken

Hoofdstuk 2: Een gemeenschappelijk computationeel mechanisme voor kantelcompensatie verklaart de systematische fouten in het verticaliteitspercept van visuele bewegingen en stationaire patronen.

Om te bepalen in welke richting een object beweegt, moet het brein bewegingssignalen van de retina (het netvlies) combineren met informatie over de oriëntatie van de ogen in de

ruimte. In dit hoofdstuk hebben we onderzocht hoe accuraat het brein dit proces uitvoert door acht proefpersonen zijdelings te kantelen terwijl zij, in het donker, de bewegingsrichting van een random stippenpatroon dienden op te lijnen met de richting van de zwaartekracht (de bewegingsverticaal). Ter vergelijking voerden de proefpersonen ook de SVV taak uit waarbij ze een visuele lijn uitlijnden met de richting van de zwaartekracht (de lijnverticaal). Bij kleine kantelhoeken (<40°), waren de systematische fouten in de twee taken nagenoeg verwaarloosbaar. Bij kantelhoeken >60° ontstond er echter een patroon van substantiële systematische fouten (vaak meer dan 30°) dat praktisch identiek was voor beide taken. Regressie-analyse bevestigde dat de fouten in de twee taken sterk gerelateerd waren, met een helling van ongeveer 1 en correlaties boven de 0.89. Een controle-experiment sloot de mogelijkheid uit dat de proefpersonen de bewegingstaak hadden uitgevoerd op basis van gepercipieerde bewegingspaden van afzonderlijke punten. We concluderen dat de transformatie van retinale bewegingsrichting en lijnoriëntatie naar een ruimtelijk coördinaatstelsel plaatsvindt op centraal niveau, op basis van een gedeelde computationele strategie. Simulaties met twee spatiele-oriëntatiemodellen suggereren dat het patroon van systematische fouten een afspiegeling kan zijn van de negatieve bijwerkingen van een strategie om de imperfecties in het kantelsignaal te beperken.

Hoofdstuk 3: Een afweging tussen ruis en systematische fouten bij spatiele orientatie

Eerdere studies in literatuur hebben aangetoond dat zijdelings gekantelde proefpersonen systematische fouten maken bij het instellen van de subjectieve visuele verticaal (SVV), waarbij de richting en grootte van deze fouten sterk afhangt van de kantelhoek van de proefpersoon. Het foutenpatroon heeft de volgende kernmerken: een rechtopzittende proefpersoon maakt nagenoeg geen fouten, bij kantelingen tot zo'n 30° worden dikwijls kleine overcompensatiefouten gemaakt (het *E-effect*), terwijl er bij kantelhoeken boven de 60° substantiële ondercompensatie (het *A-effect*) optreedt. In dit hoofdstuk onderzoeken we of een Bayesiaans waarnemingsmodel dit foutenpatroon kan verklaren. In het model worden de A- en E-effecten geïnterpreteerd als de bijwerkingen van een computationele strategie die tot doel heeft om visuele stabiliteit te bewaren en de sensorische ruis optimaal te beperken. Om dit model te toetsen, maakten we gebruik van psychometrische methoden waarmee zowel de ruiskarakteristiek als de systematische fouten in de SVV kon worden gemeten. Acht proefpersonen werden getest op hoeken tussen de -120 en 120°. De resultaten laten zien dat zowel de systematische fouten als de ruis in de SVV toenamen met kantelhoek volgens een patroon dat heel redelijk kan worden verklaard door het Bayesiaanse model. We concluderen dat het menselijk ruimtelijk oriëntatievermogen de regels van Bayes' optimale waarnemerstheorie volgt.

Hoofdstuk 4: Multisensorische signaalverwerking bij de perceptie van ruimtelijke oriëntaties

Om een robuust en stabiel beeld van de omgeving te verkrijgen, moet het brein informatie van verschillende sensorische bronnen combineren en integreren. Hierbij vormt de ruizigheid van de sensorische signalen een complicerende factor bij de benodigde berekeningen. In recente jaren is gepostuleerd dat perceptuele berekeningen bij de mens statistisch optimaal zijn. Inderdaad, blijken Bayesiaanse modellen goed in staat te zijn om de prestaties van menselijke proefpersonen in verschillende perceptuele taken te verklaren. In hoofdstuk 4 hebben we

onderzocht of deze Bayesiaanse theorie ook kan verklaren hoe perceptuele ruis en systematische fouten in de SVV en SBT worden beïnvloed door verschillende coördinaattransformaties op dezelfde sensorische signalen. Voor beide taken werd een psychometrische methode gebruikt. We testten de SBT-taak bij twee hoeken (0 en 90°) en de SVV-taak bij negen hoeken in het bereik van -120 tot 120° (in stappen van 30°). Alle proefpersonen maakten systematische SVV fouten bij kantelhoeken >60°. Daarentegen werden bij de SBT taak vrijwel geen systematische fouten gemaakt bij de twee geteste kantelhoeken. Verder nam bij beide taken de perceptuele variabiliteit (onzekerheid) toe met kantelhoek. De variabiliteit in de SBT-taak was beduidend hoger dan die in de SVV-taak. Om deze bevindingen te verklaren formuleerden we een sensorisch-integratiemodel gebaseerd op drie ruizige maar accurate sensorische signalen: 1) vestibulaire informatie over de oriëntatie van het hoofd in de ruimte, 2) proprioceptische informatie over de oriëntatie van het hoofd op de romp, en 3) somatosensorische informatie over lichaamsoriëntatie in de ruimte. In het model worden deze signalen op optimale wijze gecombineerd door middel van coördinaattransformaties die verschillen voor de twee taken. Het model bleek in staat om zowel de systematische fouten als de ruiseigenschappen van de twee experimentele taken te verklaren. Dit duidt erop dat Bayesiaanse inferentiestrategieën cruciaal zijn bij de verwerking van multisensorische informatie voor oriëntatieperceptie.

Hoofdstuk 5: De effecten van een roterend optokinetisch patroon op de perceptie van visuele verticaliteit en lichaamsoriëntatie

Een groot visueel patroon dat ronddraait om de visuele as (een zgn. optokinetisch patroon) verstoort de ruimtelijke oriëntatie van een proefpersoon aanzienlijk. Deze verstoring uit zich zowel in een veranderde perceptie van lichaamsoriëntatie (SBT) als in een verschuiving van de subjectieve visuele verticaal (SVV). Of de SVV-verschuiving eenvoudigweg gelijk is aan de verandering van de SBT, zoals in de literatuur is geopperd, is onbekend omdat deze effecten nog nooit eerder direct met elkaar zijn vergeleken. In hoofdstuk 5 hebben we dit onderzocht aan de hand van twee hypotheses. Onze eerste hypothese was dat de verschuiving van SVV en SBT gelijk zijn; onze tweede Hypothese 2 stelde dat de SVV-verschuiving gelijk is aan de SBT verandering plus een zogenaamde visuele verschuiving door een niet verrekende verandering van oogtorsie. Deze visuele verschuiving, die wél de SVV maar níet de SBT zou beïnvloeden, werd gemeten met een zogenaamde subjectieve lijn-lichaam taak (line-body, SLB). Acht proefpersonen werden aan de drie taken onderworpen (SVV, SBT, SLB) bij verschillende kantelhoeken tussen de -120 en 120° en in drie optokinetische condities (met de klok meedraaiend, tegen de klok indraaiend, en stilstaand). Optokinetische SVV verschuivingen namen aanzienlijk toe met kantelhoek en waren sterk asymmetrisch: Als de optokinetische stimulus het kantelpercept versterkte was het effect veel groter dan wanneer de stimulus het kantelpercept verzwakte. In de SBT taak namen de optokinetische effecten ook toe met kantelhoek maar zonder een duidelijk teken van asymmetrie. Optokinetische SLB effecten, die relatief klein waren, vertoonden een soortgelijke asymmetrie als de SVV-effecten, maar waren minder sterk afhankelijk van de kantelhoek. Onze tweede hypothese verklaarde de resultaten duidelijk beter dan de eerste. De SVV-verschuiving wordt dus niet slechts veroorzaakt door een verschuiving van de waargenomen lichaamskanteling (SBT), maar een effect van niet-verdisconteerde oogtorsie speelt hierbij ook een rol.

Publications

JOURNAL PUBLICATIONS

De Vrijer M, Medendorp WP, Van Gisbergen JAM (2008) Shared computational mechanism for tilt compensation accounts for biased verticality percepts in motion and pattern vision. *J Neurophysiol* 99: 915-930.

De Vrijer M, Medendorp WP, Van Gisbergen JAM (2009) Accuracy-precision trade-off in visual orientation constancy. *J Vis* 9: 1-15.

De Vrijer M, Van Gisbergen JAM, Medendorp WP, Multisensory processing for orientation perception. *Under revision.*

De Vrijer M, Van Gisbergen JAM, Medendorp WP, Roll-optokinetic effects on visual vertical and postural orientation judgments. *Under revision.*

Vingerhoets RAA, De Vrijer M, Van Gisbergen JA, Medendorp WP (2009) Fusion of visual and vestibular tilt cues in the perception of visual vertical. *J Neurophysiol* 101: 1321-1333.

CONFERENCES

De Vrijer M, Medendorp WP, Van Gisbergen JAM (April 2009) Multisensory integration in two spatial orientation tasks. *International Symposium on the Neural Basis of Decision Making*, Groesbeek, The Netherlands [poster]

De Vrijer M, Medendorp WP, Van Gisbergen JAM (November 2008) Optokinetic effects on the subjective visual vertical and body tilt perception. *Society for Neuroscience Annual Meeting*, Washington DC, USA. [slides]

Medendorp WP, Vingerhoets RAA, De Vrijer M, Van Gisbergen JAM (April 2008) The role of visual and vestibular tilt cues in human verticality perception. *Barany meeting*, Kyoto, Japan [slides]

De Vrijer M, Hendrix R, Medendorp WP, Van Gisbergen JAM (June 2008) Optokinetic influences on the subjective visual vertical and body tilt perception. *Dag van de Perceptie*, TNO, Soesterberg, The Netherlands. [poster]

De Vrijer M, Medendorp WP, Van Gisbergen JAM (November 2007) Dependence of the subjective visual horizontal on pitch and roll tilt. *Society for Neuroscience Annual Meeting*, San Diego CA, USA [poster]

De Vrijer M, Medendorp WP, Van Gisbergen JAM (October 2006) Spatial computations in the perception of vertical visual motion and line verticality during whole-body tilt. *Society for Neuroscience Annual Meeting,* Atlanta GA, USA. [poster]

De Vrijer M, Medendorp WP, Van Gisbergen JAM (May 2006) Spatial motion perception during body tilt. *Bi-annual RU-KUL Meeting*, Nijmegen, The Netherlands. [slides]

De Vrijer M, Medendorp WP, Van Gisbergen JAM (October 2005) Perception of visual motion direction during body tilt. *ESF-EMBO Symposium on 3-D Sensory and Motor Space, Probabilistic Mechanisms of Learning and Development in Sensorimotor Systems*, Sant Feliu de Guixols, Spain. [poster]

CURRICULUM VITAE

Maaike de Vrijer werd op woensdag 18 juli 1979 geboren in Wageningen. In deze stad doorliep zij ook haar middelbare schooltijd aan de regionale scholengemeenschap het Pantarijn, waar zij in 1997 haar VWO-diploma behaalde. Hierna verhuisde ze naar Enschede om daar de opleiding Werktuigbouwkunde te volgen aan de Universiteit Twente. Na drie jaar koos ze voor de specialisatierichting Biomedische Werktuigbouwkunde, waarvoor ze ondermeer een stage liep aan de Universiteit van Auckland in Nieuw-Zeeland. Onder leiding van Uwe Kersting deed ze hier bij de faculteit 'Sport and Exercise Science', onderzoek naar een multi-segment voetmodel voor het verbeteren van loopanalyse-technieken. Vervolgens studeerde ze af op een onderzoek naar balansstrategieën bij de mens, waarbij ze werd begeleid door Herman van der Kooij, Edwin van Asseldonk en Frans van der Helm.

Na het afronden van haar studie, vertrok ze in maart 2005 naar Nijmegen, om daar te starten met een promotieonderzoek bij de afdeling Medische fysica en Biofysica van de Radboud Universiteit Nijmegen, onder leiding van Jan van Gisbergen en Pieter Medendorp. Het proefschrift dat nu voor u ligt, is het resultaat van dat onderzoek.

Dankwoord

Bijna klaar! De top bereikt! Mij rest nu nog een belangrijke taak, één van de laatste passages voor het bereiken van die felbegeerde finish, en dat is het schrijven van dit dankwoord. Ongetwijfeld het bestgelezen onderdeel van een proefschrift, dus ik zal mijn best doen niemand te vergeten!

Er zijn heel veel mensen die een plekje verdienen in dit dankwoord, maar het mag duidelijk zijn met wie ik zal beginnen: Jan en Pieter, mijn dagelijkse begeleiders in de afgelopen jaren. Jan, het is een eer en ook wel een beetje vreemd om jouw laatste aio te zijn. Met mij komt er dan echt een einde aan de indrukwekkende reeks promovendi die jij onder je hoede hebt gehad. Ik ken weinig aio's die de luxe kenden die ik had: de betrokkenheid die jij toonde voor mijn onderzoek kende bijna geen grenzen. Je stond altijd klaar, was het niet als zeer gemotiveerde proefpersoon, dan wel als degene die altijd in indrukwekkend korte tijd naar mijn schrijfsels keek en er een stortvloed aan zeer bruikbaar commentaar op leverde. Jij hebt me doen inzien hoe belangrijk het is om elke vraag, hoe schijnbaar simpel of niet-relevant deze ook lijkt, gewoon te stellen. Onze discussies over de te volgen weg in mijn onderzoek leverden vaak een berg nieuwe ideeën op en je indrukwekkende kennis van de literatuur bleef me verbazen; als iemand het predikaat 'wandelende bibliotheek' verdient, dan ben jij het wel, en dat is bedoeld als compliment!

Pieter, al zaten we niet in hetzelfde gebouw waardoor we elkaar niet dagelijks spraken, je was niet minder betrokken bij mijn doen en laten. Je gedrevenheid en enthousiasme voor het onderzoek zijn aanstekelijk en als ik eens vastliep, wist jij vaak me vaak het benodigde duwtje in de goede richting te geven. Ook jij wist mijn stukken binnen *no time* van een goede dosis bruikbaar commentaar te voorzien, al heb ik geregeld met Rens zitten puzzelen op je handschrift om te ontcijferen wat je nu weer had opgeschreven! Daarnaast denk ik met veel plezier terug aan onze gezamenlijke overleggen, die altijd langer duurden dan gepland en waarbij je vaak wel tien keer herhaalde dat je weg moest, om vervolgens toch nog een half uur te laat te vertrekken. Tenslotte waardeer ik het dat je altijd erg je best doet om de betrokkenheid met en tussen je aio's te vergroten door onder andere het organiseren van een Journal Club en de gezamenlijke etentjes bij de SFN-congressen in Amerika.

Ik heb een paar hele leuke jaren gehad bij Biofysica, en dat is toe te schrijven aan een heleboel mensen. Mijn directe kamergenoten wil ik als eerste bedanken. Rens, je bent alweer even weg, maar ik denk nog met veel plezier terug aan de tijd dat we een kamer deelden. We zaten min of meer in hetzelfde schuitje, met hetzelfde begeleidingsduo en onze experimenten met de vestibulaire stoel. Omdat je iets meer dan 2 jaar 'voorliep' op mij, heb je me geregeld kunnen helpen met allerlei zaken, zoals het reilen en zeilen van de stoel en Matlab-gerelateerde uitdagingen. Natuurlijk hadden we ook menig gesprek over andere belangrijke onderwerpen, zoals vakanties, collega's, hartlopen en klimmen, kortom: het was altijd erg gezellig! Denise, jij was een waardig opvolgster van Rens. Jouw ongeëvenaarde vrolijkheid werkt aanstekelijk. Ik ken bijna niemand die zo enthousiast is als jij en ik vond het heerlijk om mijn werkzaamheden af en toe te kunnen onderbreken voor een melig gesprek over een willekeurig onderwerp. Je bent altijd in voor de gekste ideeën en de uitdrukking 'een dag niet gelachen, is een dag niet geleefd' is je op het lijf geschreven. Julian, je werd ongeveer een jaar geleden onze 'derde man', en raakte al snel ingeburgerd. Ik bewonder de georganiseerdheid waarmee jij altijd je werk

doet, ik ken weinig mensen die zoveel dingen tegelijk doen en toch het overzicht weten te houden. Daarmaast moest ik altijd erg lachen als je weer eens in geuren en kleuren vertelde wat je nu weer in je vrije tijd had meegemaakt.

Natuurlijk zijn er nog veel meer mensen bij Biofysica die ik wil bedanken. Josien, Joke, Artem, David, Tom, Marc, Peter, Joollah, Martijn A, Rob, Gleb, Andrew, Vicenc, Bart, Magteld, Kees, Joris, Sigrid, Joyce, Noël, Martijn K, Ronald, Onno, Bastian en alle andere collega's die ik in de loop der jaren heb meegemaakt, jullie hebben allemaal bijgedragen aan de leuke tijd die ik heb gehad bij de afdeling. Door de gezellige koffiepauzes en lunches, filmavonden, jam sessies, junior lunches, kerstvieringen, borrels, carrélopen, dagjes uit en natuurlijk gewoon de serieuze en minder serieuze gesprekken in de wandelgangen heb ik me altijd op de afdeling thuisgevoeld. Stan, mijn promotor, bedankt voor je inzet als voorzitter van de vakgroep. Dankzij jouw inspanningen is Biofysica een gezonde, actieve groep, waar de zaken goed geregeld zijn, een belangrijke voorwaarde voor het slagen van ieder onderzoek.

Ook de technische staf vormt hierbij absoluut een onmisbaar onderdeel. Günter, Hans, Stijn en Ger, zonder jullie hulp was dit proefschrift er nooit gekomen. Bedankt voor alle hulp bij het ontwerpen, maken en verbeteren van mijn experimentele opstellingen.

Nog een paar mensen wil ik graag bij naam noemen. Judith, je zorgt, samen met Annet, Margriet en Irene, niet alleen voor een perfect georganiseerde afdeling, maar je bent in mijn ogen bovendien een essentieel sfeerverhogend element in de groep. Ik heb altijd erg genoten van je ongezouten mening op tal van onderwerpen en je tomeloze inzet en enthousiasme bij de verschillende vakgroepactiviteiten en -borrels. In dit kader wil ik ook John en Thom nog even noemen, die menig koffiepauze wisten op te luisteren met een oneindige reeks aan anecdotes, meningen, stellingen en monologen.

Jurrian, Stan, Sabine, Verena, Frank en, op het laatst, Luc en Ivar, allen lid of lid geweest van het groeiende 'Medendorp-lab': tot voor kort zag ik de meesten van jullie met name tijdens de journal clubs en de SFN-conferenties in de VS, waarbij ik me altijd erg goed heb vermaakt. Nu, na mijn tijdelijke verhuizing, zie ik velen bijna dagelijks en ook dat bevalt prima!

Tenslotte wil ik mijn stagestudenten Frank, Maurice en Rik bedanken voor al het werk dat ze voor me hebben verricht en de prettige samenwerking. Jullie inspanningen hebben in verschillende mate bijgedragen aan dit proefschrift. Frank, jouw werk is terug te vinden in de hoofdstukken 3 en 4. Rik, jouw bijdrage heeft ondermeer geleid tot hoofdstuk 5. En Maurice, jouw werk is dan geen hoofdstuk geworden, maar het is wel gepresenteerd op het SFN-congres van 2007 in San Diego waar het enthousiast werd ontvangen.

Geen inspanning zonder ontspanning. In mijn geval bestaat de (mentale) ontspanning meestal uit (fysieke) inspanning in de vorm van klimmen, mountainbiken, racefietsen of hardlopen. En dat doe ik over het algemeen het liefst samen met anderen. Het is helaas onmogelijk om iedereen te noemen die me hierin de laatste jaren heeft vergezeld, dus wil ik meer in het algemeen iedereen bedanken waarmee ik de laatste jaren rondjes door het bos heb gefietst, op klim- of fietsvakantie ben geweest, avonden in de klimhal heb doorgebracht, (toer)tochten heb gereden, Batavierenracen heb gelopen, wedstrijdjes heb gedaan of adventure races heb doorstaan. Al deze activiteiten zijn ontzettend leuk en ik haal er veel ontspanning en motivatie uit, maar nog belangrijker is dat ik die momenten van inspanning kan delen

met al die vrienden die er net zo blij van worden als ik. Juist de gezelligheid om de sport heen, maakt dat ik het zo leuk vind en dat ik aan het eind van zo'n avond, weekend of week me soms fysiek compleet gesloopt voel, maar desondanks met een zeer tevreden en uitgerust gevoel thuiskom.

Natuurlijk stond mijn leven de afgelopen jaren niet alleen in het teken van sporten en promoveren. Er zijn meerdere mensen met wie ik geregeld een avondje in de stad doorbracht, geregeld in combinatie met een film bij LUX. Marlies, jou wil ik specifiek noemen. Ik leerde je kennen bij Velocidad, maar inmiddels is onze vriendschap uitgegroeid tot veel meer dan alleen het mountainbiken. Zeker toen ook jij besloot om te gaan promoveren hadden we genoeg te bespreken tijdens onze vele gezellige avondjes in stad of gewoon thuis. Het is heerlijk om het met iemand te kunnen hebben over de problemen waar je zoal tegenaanloopt bij zo'n promotie en te merken dat je niet de enige bent.

Tenslotte wil ik afsluiten met mijn directe familie: Ivo, broertje van me. Al zien we elkaar niet zo geregeld, we kunnen het altijd prima met elkaar vinden zodra we elkaar weer eens ergens tegenkomen. Ik ben benieuwd of je me over een tijd weer achternakomt in Nijmegen, net als hiervoor in Enschede, of dat je dit keer je oog op een andere stad laat vallen! Aukje, zussie, hoe weet je het toch altijd voor elkaar te krijgen om ergens ver weg aan de andere kant van de wereld te zitten op dit soort momenten! Bij mijn afstuderen was het Nieuw-Zeeland, nu is het Australië, waar je bezig bent met je eigen promotieonderzoek. Hoewel het natuurlijk erg jammer is dat je mijn promotie waarschijnlijk moet missen, vind ik het aan de andere kant ontzettend mooi om te zien hoe jij toch altijd voor elkaar krijgt wat je je in je hoofd hebt gehaald. Van jou vastbijt-mentaliteit kan ik nog wat leren!

Pap en mam, ik weet eigenlijk niet goed hoe ik jullie kan bedanken voor alles. Jullie onvoorwaardelijke steun is altijd op de achtergrond aanwezig. Ik kan altijd bij jullie terecht, of het nu is voor een heerlijke maaltijd of voor wijze raad op momenten dat ik die goed kan gebruiken. Omdat ik weet dat jullie waarschijnlijk niet zo zitten te wachten op een heel uitgebreide dankbetuiging wil ik dit dankwoord eindigen met één woord: BEDANKT!

Maaike de Vrijer
November 2009

SERIES DONDERS INSTITUTE FOR BRAIN, COGNITION AND BEHAVIOUR

1. van Aalderen-Smeets, S.I. (2007). Neural dynamics of visual selection. Maastricht University, Maastricht, The Netherlands.
2. Schoffelen, J.M. (2007). Neuronal communication through coherence in the human motor system. Radboud University Nijmegen, Nijmegen, The Netherlands.
3. de Lange, F.P. (2008). Neural mechanisms of motor imagery. Radboud University Nijmegen, Nijmegen, The Netherlands.
4. Grol, M.J. (2008). Parieto-frontal circuitry in visuomotor control. University Utrecht, Utrecht, The Netherlands.
5. Bauer, M. (2008). Functional roles of rhythmic neuronal activity in the human visual and somatosensory system. Radboud University Nijmegen, Nijmegen, The Netherlands.
6. Mazaheri, A. (2008). The Influence of Ongoing Oscillatory Brain Activity on Evoked Responses and Behaviour. Radboud University Nijmegen, Nijmegen, The Netherlands.
7. Hooijmans, C.R. (2008). Impact of nutritional lipids and vascular factors in Alzheimer's Disease. Radboud University Nijmegen, Nijmegen, The Netherlands.
8. Gaszner, B. (2008). Plastic responses to stress by the rodent urocortinergic Edinger-Westphal nucleus. Radboud University Nijmegen, Nijmegen, The Netherlands.
9. Willems, R.M. (2009). Neural reflections of meaning in gesture, language and action. Radboud University Nijmegen, Nijmegen, The Netherlands.
10. Van Pelt, S. (2009). Dynamic neural representations of human visuomotor space. Radboud University Nijmegen, Nijmegen, The Netherlands.
11. Lommertzen, J. (2009). Visuomotor coupling at different levels of complexity. Radboud University Nijmegen, Nijmegen, The Netherlands.
12. Poljac, E. (2009). Dynamics of cognitive control in task switching: Looking beyond the switch cost. Radboud University Nijmegen, Nijmegen, The Netherlands.
13. Poser, B.A. (2009) Techniques for BOLD and blood volume weighted fMRI. Radboud University Nijmegen, Nijmegen, The Netherlands.
14. Baggio, G. (2009). Semantics and the electrophysiology of meaning. Tense, aspect, event structure. Radboud University Nijmegen, Nijmegen, The Netherlands.
15. van Wingen, G.A. (2009). Biological determinants of amygdala functioning. Radboud University Nijmegen Medical Centre, Nijmegen, The Netherlands.
16. Bakker, M. (2009). Supraspinal control of walking: lessons from motor imagery. Radboud University Nijmegen Medical Centre, Nijmegen, The Netherlands.
17. Aarts, E. (2009). Resisting temptation: the role of the anterior cingulate cortex in adjusting cognitive control. Radboud University Nijmegen, Nijmegen, The Netherlands.
18. Prinz, S. (2009). Waterbath stunning of chickens – Effects of electrical parameters on the electroencephalogram and physical reflexes of broilers. Radboud University Nijmegen, Nijmegen, The Netherlands.

19. Knippenberg, J.M.J. (2009). The N150 of the Auditory Evoked Potential from the rat amygdala: In search for its functional significance. Radboud University Nijmegen, Nijmegen, The Netherlands.
20. Dumont, G.J.H. (2009). Cognitive and physiological effects of 3,4-methylenedioxy-methamphetamine (MDMA or 'ecstasy') in combination with alcohol or cannabis in humans Radboud University Nijmegen, Nijmegen, The Netherlands.
21. Pijnacker, J. (2010). Defeasible inference in autism: a behavioral and electrophysiogical approach. Radboud Universiteit Nijmegen, The Netherlands.
22. de Vrijer, M. (2010). Multisensory integration in spatial orientation. Radboud University Nijmegen, Nijmegen, The Netherlands.